Doctoral Dissertation (Censored)
博士論文（要約）

Kinetically Controlled Stepwise Syntheses of a Heterometallic $Co^{II}Ni^{II}_3$ Complex and a Tetrahedral Chiral-at-Metal Zn^{II} Complex

（速度論的制御を伴った段階的手法による異種金属 $Co^{II}Ni^{II}_3$ 錯体および四面体型 chiral-at-metal Zn^{II} 錯体の合成）

A Dissertation Submitted for the Degree of Doctor of Philosophy
December 2019
令和元年 12 月博士（理学）申請

Department of Chemistry, Graduate School of Science,
The University of Tokyo
東京大学大学院理学系研究科
化学専攻

Kenichi Endo
遠藤　健一

Abstract

Introduction

Synthesis of metal complexes is usually based on direct reaction of metal sources and ligands. However, this one-step method is not always useful because kinetic control is difficult. In contrast, stepwise synthesis can provide a variety of structures with high selectivity through kinetically controlled pathways. This method has been widely employed for some inert metal complexes,[1] but rarely used for labile metal complexes. Herein, I report two new methods of highly selective syntheses of relatively labile metal complexes through kinetically controlled, stepwise reactions: (1) a heterometallic tetranuclear $Co^{II}Ni^{II}_3$ complex and (2) an enantiopure tetrahedral chiral-at-metal Zn^{II} complex with achiral ligands.

Heterometallic $Co^{II}Ni^{II}_3$ complex

Heterometallic multinuclear complexes have great potential to exhibit unique chemical and physical properties based on the cooperation of different metal ions.[2] However, most examples previously reported depend on one-step methods or are based only on 4d- or 5d-metal ions. In this work, a new strategy toward an otherwise difficult arrangement of different 3d-metal ions has been achieved by site-selective redox switching and transmetalation (Figure 1).

In my master course study, I have found that the porphyrin-based ligand **L1** can construct a tetranuclear complex, $[Zn^{II}_4\mathbf{L1}_3X_6]$ (X = solvent or counterion), by self-assembly with Zn^{II} ions. This complex possessed chemically inequivalent Zn^{II} sites, which prompted me to initiate the stepwise synthesis of heteronuclear 3d-metal complexes with this structural framework.

First, I introduced Co^{II} as a redox-active component to construct a tetranuclear complex, $[Co^{II}_4\mathbf{L1}_3X_6]$, by self-assembly of **L1** and Co^{II} ions. This complex contained two different Co^{II} centers, one $Co^{II}(bpy)_3$ and three $Co^{II}(bpy)_2X_2$ sites. Then, site-selective oxidation at the $Co^{II}(bpy)_3$ site was found possible by addition of 1 equiv. of oxidant. This site selectivity is due to the stronger coordination field provided by the three bpy ligands of the $Co^{II}(bpy)_3$ site. In the next step, the remaining $Co^{II}(bpy)_2X_2$ sites were site-selectively transmetalated by Ni^{II} ions. This is possible because the thermodynamic affinity of bpy to Ni^{II} is intermediate between Co^{III} and Co^{II}. Finally, site-selective reduction at the $Co^{III}(bpy)_3$ site afforded a $[Co^{II}Ni^{II}_3\mathbf{L1}_3X_6]$ complex. Each complex was well-characterized by ^{1}H NMR spectroscopy and ESI-MS, and some of them by single-crystal XRD and XPS.

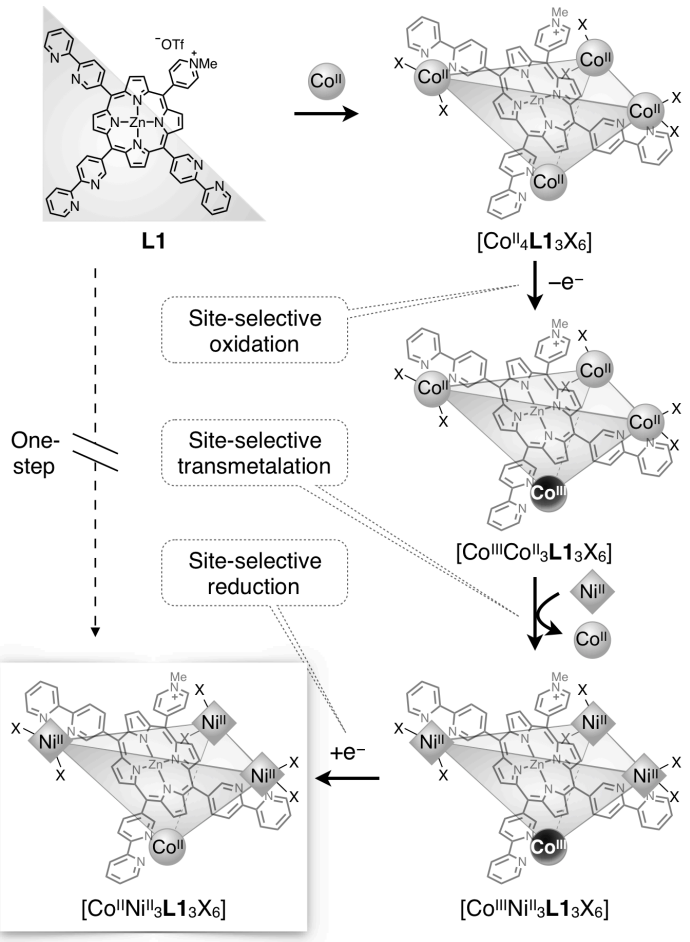

Figure 1. Synthetic scheme of heterometallic tetranuclear $Co^{II}Ni^{II}_3$ complex.

Notably, the last complex $[Co^{II}Ni^{II}_3\mathbf{L1}_3X_6]$ cannot be synthesized directly from **L1**, Co^{II}, and Ni^{II} because a $Ni^{II}(bpy)_3$ motif is thermodynamically favored. The synthesis of this complex is not possible without the kinetically controlled stepwise method developed in this work.

Tetrahedral chiral-at-metal Zn^{II} complex

A metal center of a metal complex can be a chirality center in some cases, which are called chiral-at-metal complexes. The usefulness of chiral-at-metal complexes has been demonstrated in enantioselective catalysis, chiroptical materials, and so on. Therefore, it is necessary to develop an excellent method to synthesize enantiopure chiral-at-metal complexes, desirably with a catalytic center. Historically, separation of enantiomers was initially employed, and it was a little later that diastereoselective synthesis with chiral ligands/counterions was developed as a more efficient method. At last, enantioselective synthesis with a transiently usable chiral reagent was invented, which is useful to obtain complexes free from chiral ligands/counterions (Figure 2).[3]

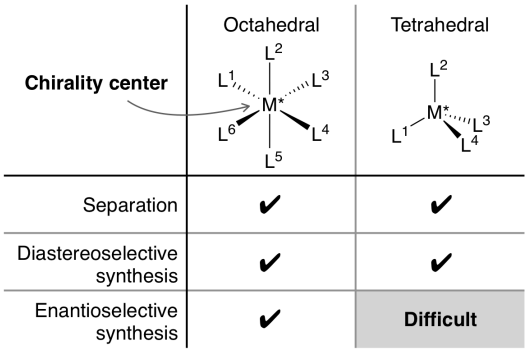

Figure 2. Preparation methods for enantiopure chiral-at-metal complex

Note that this development has been focused chiefly on octahedral, relatively inert metal complexes. Although tetrahedral complexes are common in coordination chemistry, enantioselective synthesis has been rarely reported for chiral-at-metal tetrahedral complexes. Therefore, it remains as a challenging task to develop their enantioselective synthetic methods for highly labile tetrahedral chiral-at-metal complexes. It is a key here to avoid fast racemization of the labile tetrahedral complexes.

Herein, I report enantioselective synthesis of a tetrahedral chiral-at-metal complex by kinetically suppressing racemization. In addition, the practical utility of the complex was demonstrated in application to enantioselective catalysis.

Design of a tetrahedral chiral-at-metal complex

In this study, I newly designed a tridentate ligand, **L2**, to suppress racemization while leaving one labile site for chirality induction and catalytic application (Figure 3). In the presence of a tridentate ligand, racemization pathways of a tetrahedral complex are limited to dissociation or planarization of the tridentate ligand. To block both pathways, I designed ligand **L2** with strong coordination ability by negatively charged, deprotonated nitrogen donors and with a rigid non-planar structure by steric crowding. In addition, wide bite angles are provided by the 6- and 7-membered chelate rings, in order to favor a tetrahedral geometry.

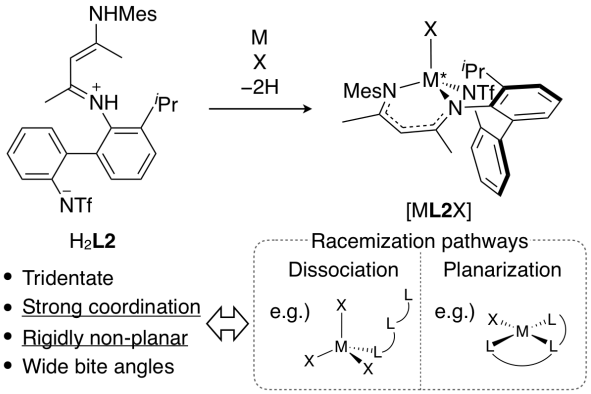

Figure 3. Design of a tridentate ligand **L2** to form a tetrahedral chiral-at-metal complex stable against racemization.

Enantioselective synthesis of a tetrahedral chiral-at-metal Zn^{II} complex

Ligand H_2**L2** was synthesized in 5 steps in 52% overall yield. Enantioselective synthesis of a tetrahedral metal complex using **L2** was conducted in three steps: (1) racemic complexation; (2) asymmetric induction with a chiral ligand; (3) removal of the chiral ligand. Zn^{II} was used as a metal ion and a weakly acidic monodentate ligand, (*S*)-dpp, was chosen as a chiral ligand.

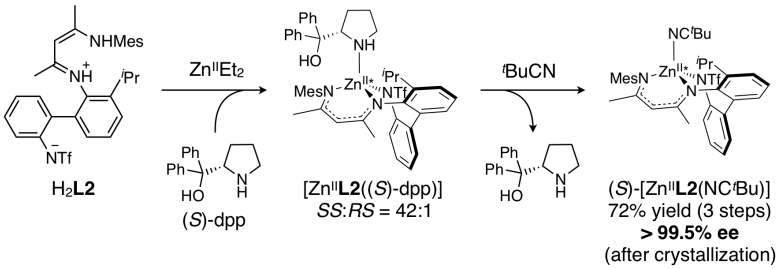

Figure 4. Enantioselective synthesis scheme of (*S*)-[Zn^{II}**L2**(NC^{t}Bu)].

First, complexation of the ligand H_2**L2** with $Zn^{II}Et_2$ was conducted to give racemic (*R**,*R**)-[Zn^{II}_2**L2**$_2$]. Then, (*S*)-dpp was added to give a diastereomeric mixture of [Zn^{II}**L2**((*S*)-dpp)] in the ratio of *SS*:*RS* = 42:1 (Figure 4). The structure of the *SS* isomer was revealed by ^{1}H-^{1}H NOESY NMR and single-crystal XRD. This isomer exhibited two NH-O hydrogen bonds and one OH-π interaction, which suggest that the high diastereoselectivity may arise from these intramolecular interactions in combination with steric repulsion.

Next, the diastereomeric mixture was treated with an excess amount of pivalonitrile (^{t}BuCN) to replace the (*S*)-dpp ligand. After crystallization in benzene/HMDSO, (*S*)-[Zn^{II}**L2**(NC^{t}Bu)] complex was successfully obtained in 72% yield with enantiopurity of over 99.5% ee. The structure of this complex and the *S* absolute configuration was confirmed by single-crystal XRD.

In this way, enantioselective synthesis of (*S*)-[Zn^{II}**L2**(NC^{t}Bu)] complex was achieved by the three-step sequence. This is the first example of enantioselective synthesis of a tetrahedral chiral-at-metal complex composed of achiral ligands using a chiral ligand as a chiral auxiliary.

Racemization kinetics of the Zn^{II}L2 complexes

The racemization rate of (*S*)-[Zn^{II}**L2**(NC^{t}Bu)] in solution state was examined using ^{19}F NMR (Figure 5). (*S*)-[Zn^{II}**L2**(NC^{t}Bu)] was dissolved in benzene-d_6, and then the solution was incubated at 24 °C or 70 °C for 0 h or 24 h, followed by addition of a chiral shift reagent. The ^{19}F NMR spectra showed slight racemization in the proportions of 0.02% at 24 °C and 0.35% at 70 °C after 24 h. This result shows exceptional kinetic stability of this complex.

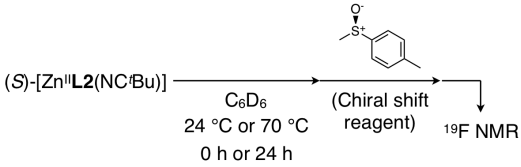

Figure 5. Measurement of the racemization rate for (*S*)-[Zn^{II}**L2**(NC^{t}Bu))].

Interestingly, the intermediate [Zn^{II}**L2**((*S*)-dpp)] diastereomers showed a contrastive behavior. When Zn^{II}Et$_2$ and (*S*)-dpp were added to H$_2$**L2** stepwise, the diastereomer ratio gradually changed from 1:1 to 22:1 during heating (Figure 6). A similar experiment with (*S*)-mdp, which have a methoxy group instead of a hydroxy group, showed no changes in the diastereomer ratio from 1:1. These results indicate that the weakly acidic hydroxy group of (*S*)-dpp accelerated stereoinversion temporarily and eventually enabled asymmetric induction.

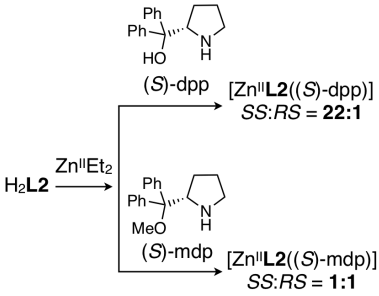

Figure 6. Effect of (*S*)-dpp on stereoinversion.

Application of the Zn^{II}L2 complex to enantioselective catalysis

Catalytic activity of (*S*)-[Zn^{II}**L2**(NC^{t}Bu)] was examined for oxa-Diels-Alder reaction, which is generally catalyzed by Lewis acids. Diene **8** was reacted with aldehyde **9** in the presence of 1 mol% (*S*)-[Zn^{II}**L2**(NC^{t}Bu)] (Figure 7). After acidic treatment, the product (*R*)-**10** was obtained in 78% yield and 88% ee. To examine the cause of enantioselectivity, a catalyst–substrate complex [Zn^{II}**L2**(**9**)] was prepared and analyzed by single-crystal XRD and ^{1}H-^{1}H NOESY NMR. These analyses indicated that the *Si*-face of aldehyde **9** was effectively shielded by the structural framework of Zn^{II}**L2**. The observed enantioselectivity can be well explained by the face-selective attack of diene **8**. This result demonstrates that a tetrahedral chiral-at-metal complex with achiral ligands is practically useful when the racemization rate is extremely slower than that of the reaction.

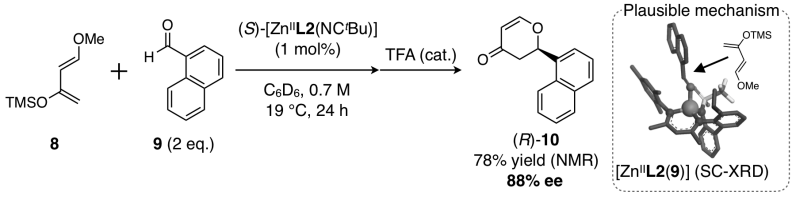

Figure 7. Enantioselective catalysis by (*S*)-[Zn^{II}**L2**(NC^{t}Bu)].

Conclusions

In this work, two metal complexes were synthesized using the kinetically controlled stepwise reactions. Firstly, a Co^{II}–Ni^{II} heterometallic complex was synthesized by site-selective redox switching and transmetalation. Secondly, an enantiopure tetrahedral Zn^{II} complex was synthesized using the rigid tridentate ligand. While both complexes are not accessible by the direct reactions of the ligands and metal ions, the stepwise methods shown here were effective with high selectivity. Notably, although both complexes contain labile metal ions, kinetic control was achieved by the appropriate designs of the systems. These results are expected to expand the structural variety and usability of metal complexes.

References

(1) MacDonnell, F. M.; Kim, M.-J.; Bodige, S. *Coord. Chem. Rev.* **1999**, *185–186*, 535–549. (2) Buchwalter, P.; Jacky, R.; Braunstein, P. *Chem. Rev.* **2015**, *115*, 28−126. (3) Meggers, E. *Chem. Eur. J.* **2010**, *16*, 752–758.

Contents

Abbreviations and symbols

a, b, c, α, β, γ	lattice constants
Abs.	absorbance
Ac	acetyl
ATR	attenuated total reflection
A.U.	arbitrary unit
bpy	2,2′-bipyridine
br	broad
Bu	butyl
calcd.	calculated
CCDC	Cambridge Crystallographic Data Centre
CD	circular dichroism
COSY	correlation spectroscopy
d	doublet
δ	chemical shift
D_{calc}	calculated density
de	diastereomeric excess
dr	diastereomer ratio
d-Fourier	differential Fourier
DMF	*N*,*N*-dimethylformamide
DMSO	dimethyl sulfoxide
ee	enantiomeric excess
eq.	equivalent
equiv.	equivalent
ESI	electrospray ionization
Et	ethyl
FT	Fourier transform
Fw	formula weight
g_{em}	dissymmetry factor for emission
GOF	goodness of fit
HMDSO	hexamethyldisiloxane
HPLC	high-performance liquid chromatography
HR	high resolution
i	*iso*-
IR	infrared
J	coupling constant
K_f	formation constant
l	cell length
L	ligand
λ	wavelength
m	multiplet

m	mass
M	metal
M	formula weight
μ	linear absorption coefficient
Me	methyl
Mes	mesityl
m.p.	melting point
MS	mass spectrometry
MS	molecular sieves
n	*normal*-
n	*normal*
NBS	*N*-bromosuccinimide
NIR	near infrared
NMR	nuclear magnetic resonance
NOE	nuclear Overhauser effect
NOESY	nuclear Overhauser effect correlated spectroscopy
ORTEP	Oak Ridge thermal-ellipsoid plot
p	*para*
p	decimal cologarithm of
Ph	phenyl
ppm	parts per million
Pr	propyl
θ	angle
Θ	angle
Θ	Weiss constant
ρ_{calc}	calculated density
R_1	reliability factor 1
R_{int}	internal consistency of equivalents
RT	room temperature
s	singlet
SC-XRD	single-crystal X-ray diffraction
t	triplet
t	*tert*-
T	temperature
T_C	Curie temperature
Tf	trifluoromethanesulfonyl
TFA	trifluoroacetic acid
THF	tetrahydrofuran
TMS	tetramethylsilane
TOF	time-of-flight
Ts	*p*-toluenesulfonyl
UV	ultraviolet

V	volume
vis	visible
wR_2	weighted reliability factor 2
XPS	X-ray photoelectron spectroscopy
XRD	X-ray diffraction
z	charge number
Z	number of formula units in the unit cell

1. General introduction

1-1. Selective synthesis of metal complexes

Metal complexes, comprised of metal atom(s) and coordinating ligand(s), reside in the cross section of organic and inorganic chemistry fields. Metal complexes exhibit many attractive chemical and physical properties based on the combination of the diverse properties of metal elements with the high designability of organic ligands. For example, metal complexes show unique assembled structures (host compounds, porous materials), physical properties (optical properties, magnetism, conductivity), and chemical reactivities (catalysis, photosensitization, enzyme mimicry).[1,2]

To synthesize a metal complex, typically, a direct one-step reaction between the inorganic part (metal source) and the organic part (ligands) of the target complex is employed (Fig. 1-1-1a). This process, called complexation, is usually rapid and under thermodynamic control because metal–ligand coordination bonds are labile. However, in some cases with heteroleptic, heterometallic, or isomeric complexes, the products can be a cumbersome mixture of multiple complexes (Fig. 1-1-1b). In such a case, development of a selective synthesis method is desired to spare the difficulty and labor of separation.

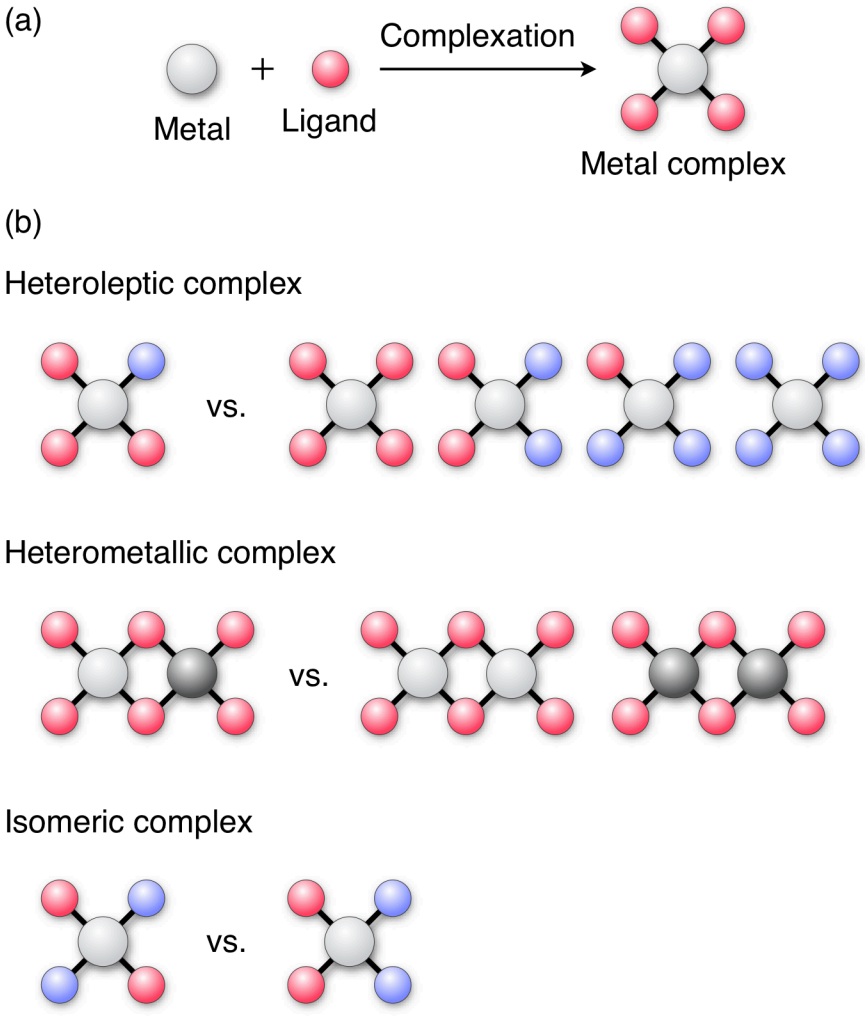

Figure 1-1-1. (a) Schematic diagram of typical metal complexation. (b) Examples of metal complexes whose synthesis can possibly produce multiple products.

One method to achieve selective synthesis is to modify the system so that the desired product will be thermodynamically more stable than the other possible products. Then, the desired complex can be selectively obtained by thermodynamically controlled one-step synthesis (Figure 1-1-2a). This can be realized by elaboration of organic ligands,[3,4] metals with complementary properties,[5] and/or specific interactions with counterions[6,7] or guest species[8] (Figure 1-1-2b). For example, selective syntheses of some heteroleptic,[3,4] heterometallic,[5] and isomeric[6,7] complexes based on this method are reported (Figure 1-1-2b). However, the requirement of thermodynamic stability poses limitations on the design of ligands and the choice of metals.

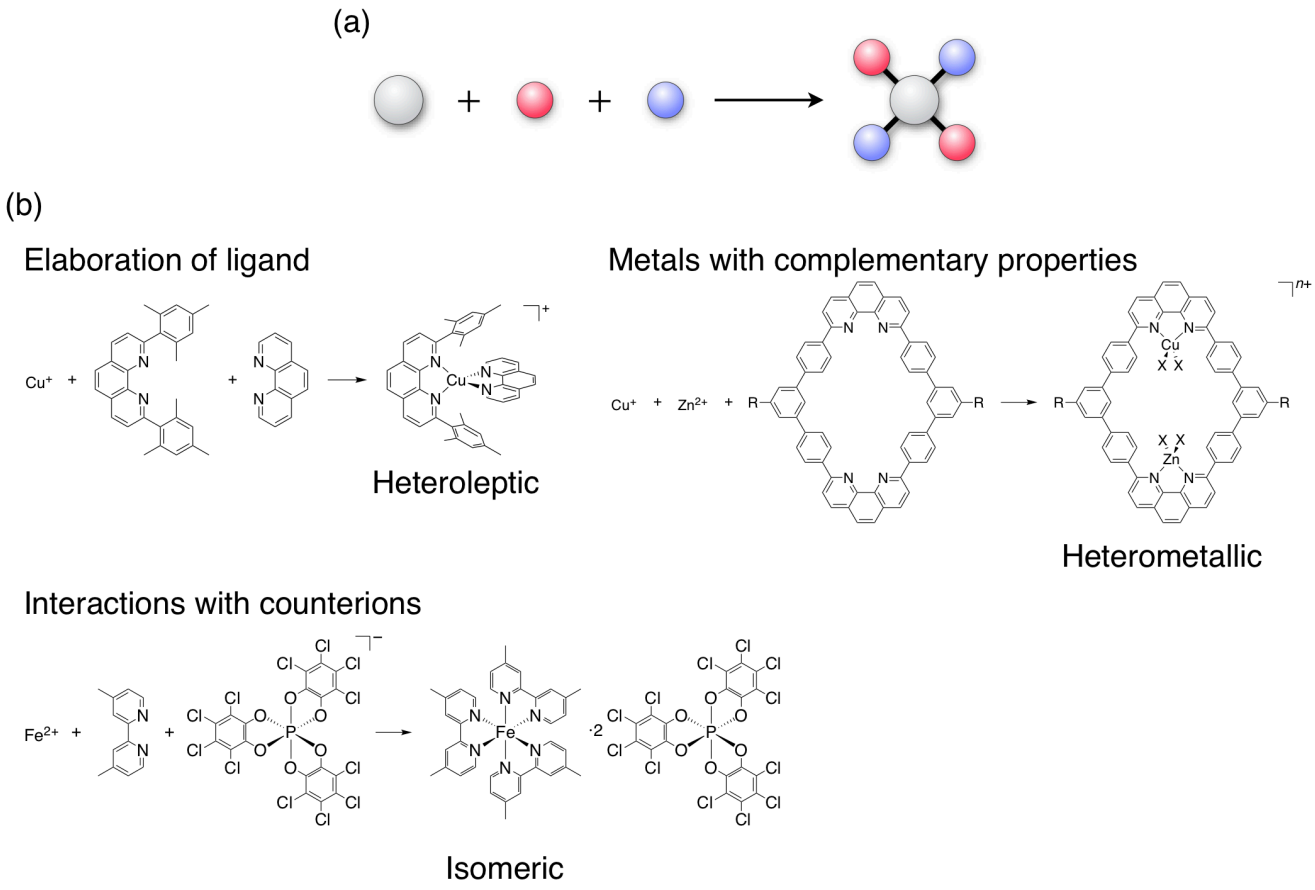

Figure 1-1-2. Thermodynamically controlled one-step synthesis of metal complexes. (a) Schematic representation. (b) Examples where selective syntheses of heteroleptic, heterometallic, and isomeric complexes were conducted based on elaboration of ligand,[4] metals with complementary properties (X = a solvent molecule or counterion),[5] and interactions with counterions,[7] respectively.

An alternative method is to divide the synthesis process into a few steps to enable kinetic control, just as organic synthesis does (Figure 1-1-3a).[9] This method includes sequential addition of different ligands[10] or metals,[11] post-modification of metal redox states or ligand structures after complexation,[12] and temporary introduction of auxiliary component followed by its removal[13,14] (Figure 1-1-3b). In every case, the initial steps are under thermodynamic control, but the final step is under kinetic control to give a different selectivity from thermodynamic control. Here, a selective reaction under kinetic control is easier than the one-step complexation because the final step will involve less changes in the structure of the complex and require milder conditions. For example, selective syntheses of the heteroleptic,[10] heterometallic,[11,12] and isomeric[13,14] complexes which cannot be selectively obtained by the thermodynamic one-step method have been reported (Figure 1-1-3b).

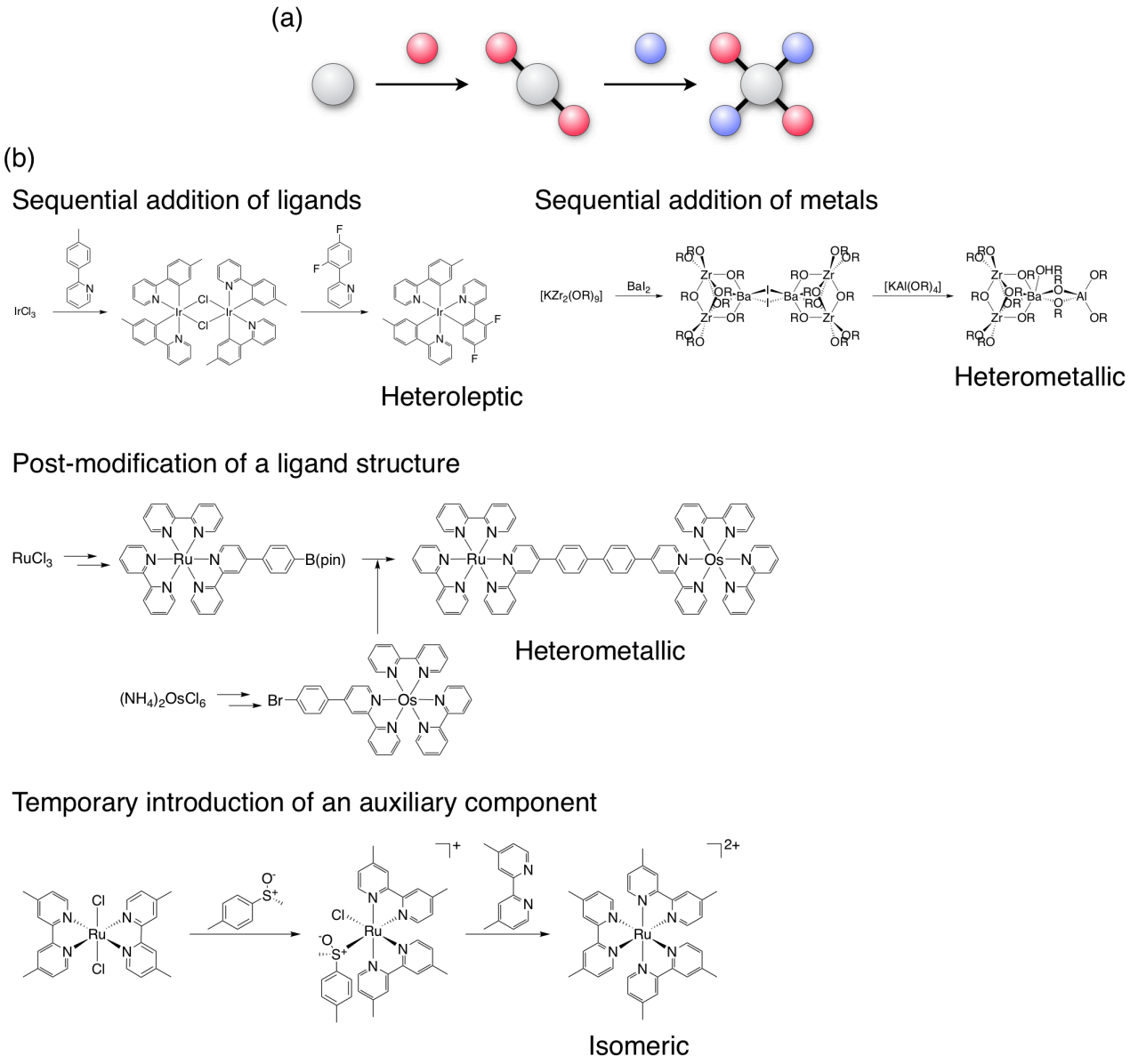

Figure 1-1-3. Kinetically controlled stepwise syntheses of metal complexes. (a) Schematic representation. (b) Examples based on sequential addition of ligands[10] or metals,[11] post-modification of a ligand structure,[12] and temporary introduction of an auxiliary component.[14]

1-2. Target scope of kinetically controlled stepwise synthesis

Despite its utility, the target scope of kinetically controlled stepwise synthesis has been severely limited. Previous examples are focused mainly on 4d or 5d metals (Figure 1-1-3b),[10,11,12,14] octahedral Cr^{III} [15] or Co^{III},[16] or non-Werner-type complexes[17] (Figure 1-2-1). This is because these complexes are relatively inert,[18] which makes kinetic control easier.

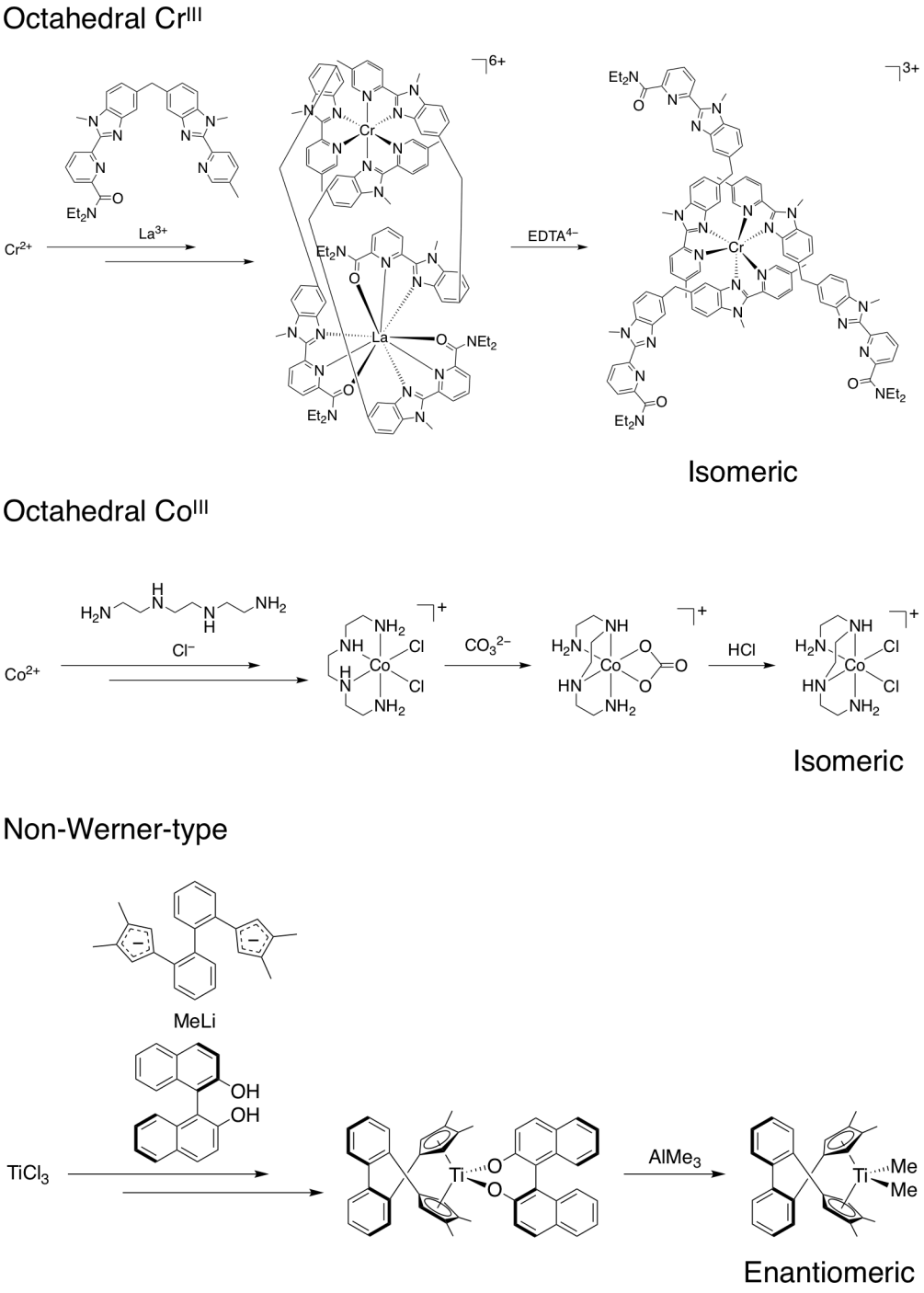

Figure 1-2-1. Examples of the kinetically controlled stepwise selective syntheses of octahedral Cr^{III} [15] and Co^{III} [16] and non-Werner-type[17] complexes.

Other kinds of metal complexes are usually more labile,[18] so kinetic control is more difficult. Only a limited number of examples have been reported: lanthanide complexes with octadentate ligands,[9,19] Cu^{I} complexes with bulky ligands,[20] and polynuclear complexes[21,22,23] (Figure 1-2-2).

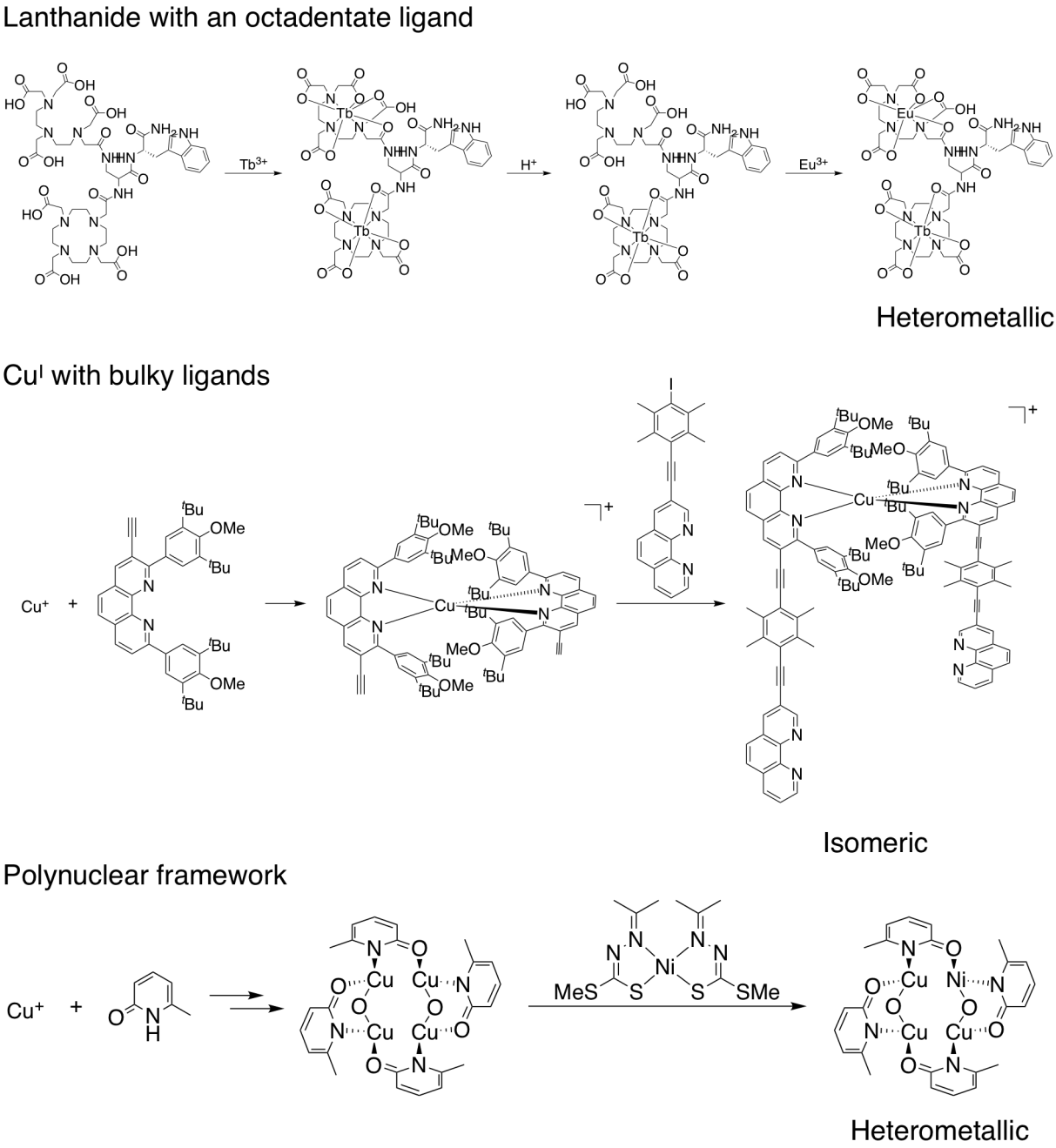

Figure 1-2-2. Examples of the kinetically controlled stepwise selective syntheses of Werner-type complexes of other metals based on lanthanide with an octadentate ligand,[19] Cu^{I} with bulky ligands,[20] and a polynuclear framework.[23]

Therefore, it is desired to expand the target scope of kinetically controlled stepwise synthesis for complexes of labile metal ions, by developing new methodologies and design principles. Such development will provide a greater freedom to the design of metal complexes, which can be used as functional chemicals.

1-3. Overview of this study

In this work, I aimed at development of kinetically controlled stepwise synthesis of complexes of labile metal ions in two distinct fields (Figure 1-3-1): (i) a heterometallic complex and (ii) a chiral-at-metal complex, which is a particular kind of an isomeric complex.

For the heterometallic complex, I propose "site-selective redox switching and transmetalation" as a new stepwise method and applied it to a labile Co^{II} and Ni^{II} complex. As a result, selective synthesis of the heterometallic complex $[Co^{II}Ni^{II}_3\mathbf{L1}_3X_6]$ (X = solvent molecule or counteranion) was achieved in four steps. This method showed kinetically controlled selectivity against a thermodynamic mixture of complexes such as $[Ni^{II}_4\mathbf{L1}_3X_6]$. This topic is discussed in Chapter 2.

For the chiral-at-metal complex, I propose the use of a strong and non-planar tridentate ligand in combination with acidic chiral ligand and applied it to a tetrahedral Zn^{II} complex, which is typically highly labile. As a result, selective synthesis of the chiral-at-metal complex (*S*)-[Zn**L2**(NC^{t}Bu)] was achieved in three steps. This strategy gave kinetically controlled selectivity against a thermodynamic mixture with (*R*)-[Zn**L2**(NC^{t}Bu)]. This topic is discussed in Chapter 3.

These ideas would be useful in preparation of new heterometallic or chiral-at-metal complexes which have been difficult to achieve. Such complexes can be expected for unique physical or chemical properties. As an example, enantioselective catalysis by the resultant complex is demonstrated in the latter topic.

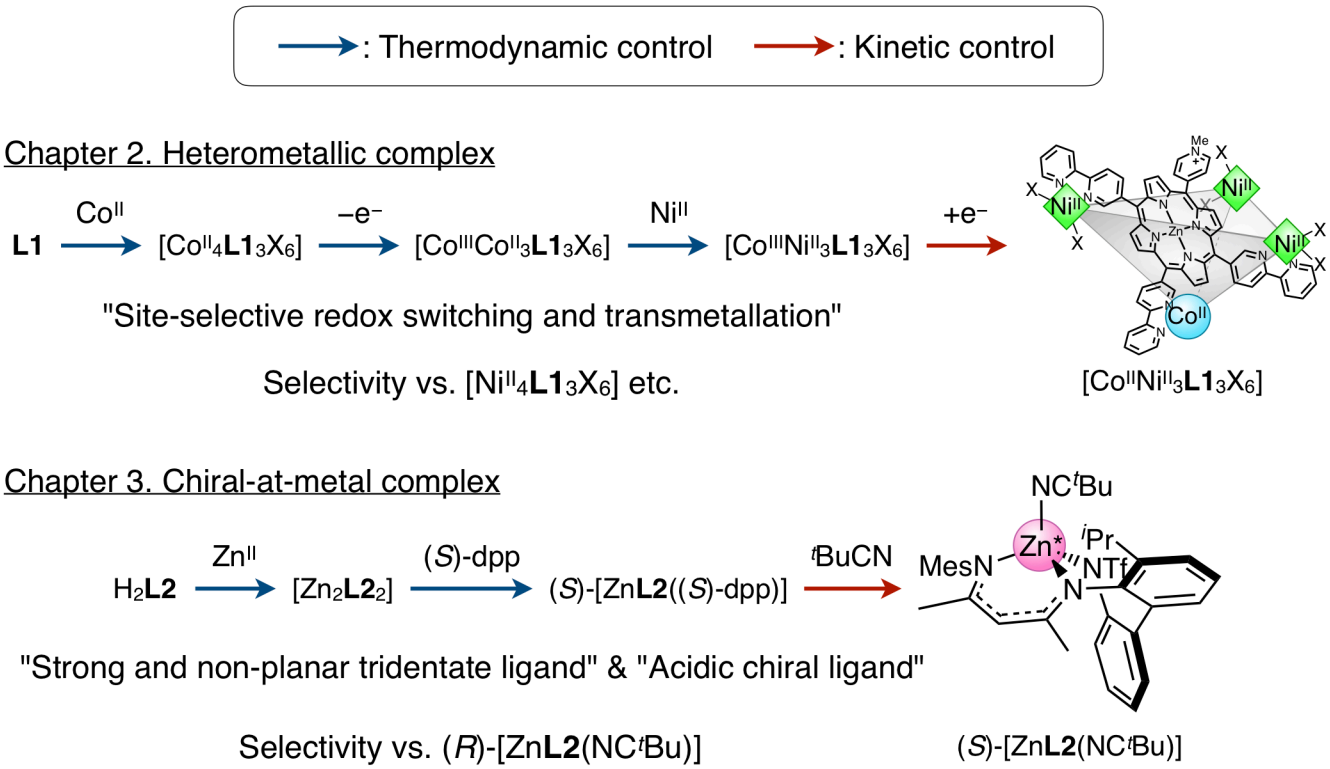

Figure 1-3-1. Summary of this study. For abbreviations, refer to each chapter.

1-4. References

1. Gispert, J. R. *Coordination Chemistry*; WILEY-VCH: Weinheim, 2008.
2. Hasegawa, Y., Ito, H. *錯体化学—基礎から応用まで*; Kodansha: Tokyo, 2014.
3. De, S.; Mahata, K.; Schmittel, M. *Chem. Soc. Rev.* **2010**, *39*, 1555–1575.
4. Schmittel, M.; Ganz, A. *Chem. Commun.* **1997**, 999–1000.
5. Kuritani, M.; Tashiro, S.; Shionoya, M. *Inorg. Chem.* **2012**, *51*, 1508−1515.
6. Lacour, J.; Moraleda, D. *Chem. Commun.* **2009**, 7073–7089.
7. Lacour, J.; Jodry, J. J.; Ginglinger, C.; Torche-Haldimann, S. *Angew. Chem., Int. Ed.* **1998**, *37*, 2379–2380.
8. Johnson, D. W.; Raymond, K. N. *Supramol. Chem.* **2001**, *13*, 639–659.
9. Sorensen, T. J.; Faulkner, S. *Acc. Chem. Res.* **2018**, *51*, 2493–2501.
10. Tamura, Y.; Hisamatsu, Y.; Kumar, S.; Itoh, T.; Sato, K.; Kuroda, R.; Aoki, S. *Inorg. Chem.* **2017**, *56*, 812–833.
11. Heidemann, T.; Mathur, S. *Inorg. Chem.* **2017**, *56*, 234–240.
12. Welter, S.; Salluce, N.; Belser, P.; Groeneveld, M.; De Cola, L. *Coord. Chem. Rev.* **2005**, *249*, 1360–1371.
13. Meggers, E. *Chem. Eur. J.* **2010**, *16*, 752–758.
14. Hesek, D.; Inoue, Y.; Ishida, H.; Everitt, S. R. L.; Drew, M. G. B. *Tetrahedron Lett.* **2000**, *41*, 2617–2620.
15. Cantuel, M.; Bernardinelli, G.; Muller, G.; Riehl, J. P.; Piguet, C. *Inorg. Chem.* **2004**, *43*, 1840–1849.
16. Sargeson, A. M.; Searle, G. H. *Inorg. Chem.* **1967**, *6*, 787–796.
17. Ringwald, M.; Stürmer, R.; Brintzinger, H. H. *J. Am. Chem. Soc.* **1999**, *121*, 1524–1527.
18. Richens, D. T. *Chem. Rev.* **2005**, *105*, 1961–2002.
19. Tremblay, M. S.; Sames, D. *Chem. Commun.* **2006**, 4116–4118.
20. Schmittel, M.; Mahata, K. *Chem. Commun.* **2008**, 2550–2552.
21. Carnes, M. E.; Collins, M. S.; Johnson, D. W. *Chem. Soc. Rev.* **2014**, *43*, 1825–1834.
22. Davies, G.; El-Sayed, M. A.; El-Toukhy, A. *Chem. Soc. Rev.* **1992**, *21*, 101–104.
23. Cai, G. Z.; Davies, G.; El-Sayed, M. A.; El-Toukhy, A.; Gilbert, T. R.; Onan, K. D. *Inorg. Chem.* **1986**, *25*, 1935–1940.

2. Heterometallic $Co^{II}Ni^{II}_3$ complex

2-1. Introduction

Heterometallic complexes are complexes containing several different metal elements. Such complexes are attractive because interactions between the metal atoms can lead to unique chemical and physical properties such as luminescence,[1,2,3,4,5] magnetism,[3,4,6,7] and catalysis[3,8,9,10] (Figure 2-1-1a–c). Heterometallic complexes are also seen in biological systems, especially in metalloenzymes (Figure 2-1-1d).[11,12]

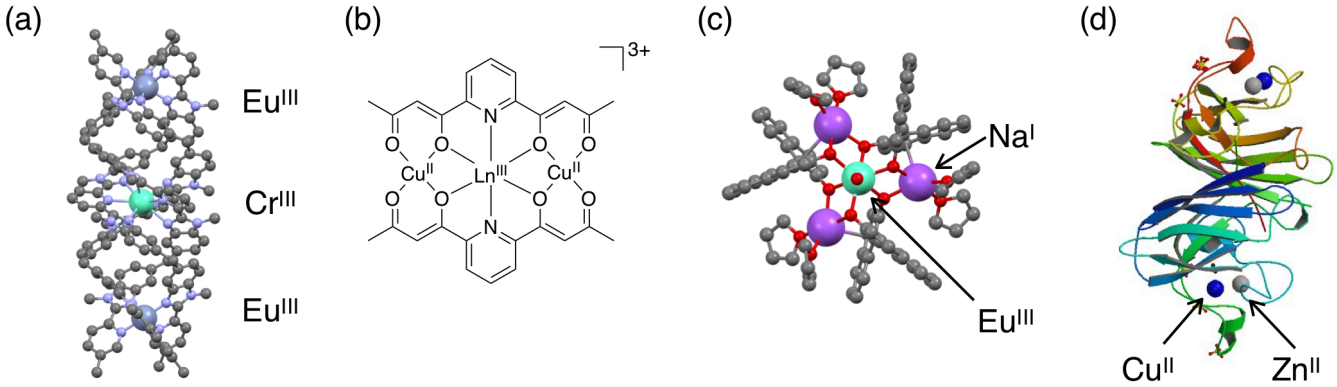

Figure 2-1-1. Examples of heterometallic complexes. (a–c) Heterometallic complexes which exhibit (a) luminescence,[5] (b) magnetism,[7] and (c) catalytic activity.[10] (d) Heterometallic enzyme, Cu-Zn human superoxide dismutase (PDB: 2C9V).[12]

To obtain a desired heterometallic complex, complexation between ligands and several different metal sources should be controlled.[13,14] If no care was taken, a complex with an undesired number of metal atoms or an isomer with an undesired positioning of the metal atoms can be generated (Figure 2-1-2a). Conventionally, thermodynamic control has been widely employed to achieve selective formation of the desired heterometallic complex (Figure 2-1-2b). A typical strategy is to use ligands and metals with orthogonal affinities based on their hard/soft characters.[15] In some other cases, difference between metals in the preferred coordination number/geometry[16] or ionic charge[17] is utilized.

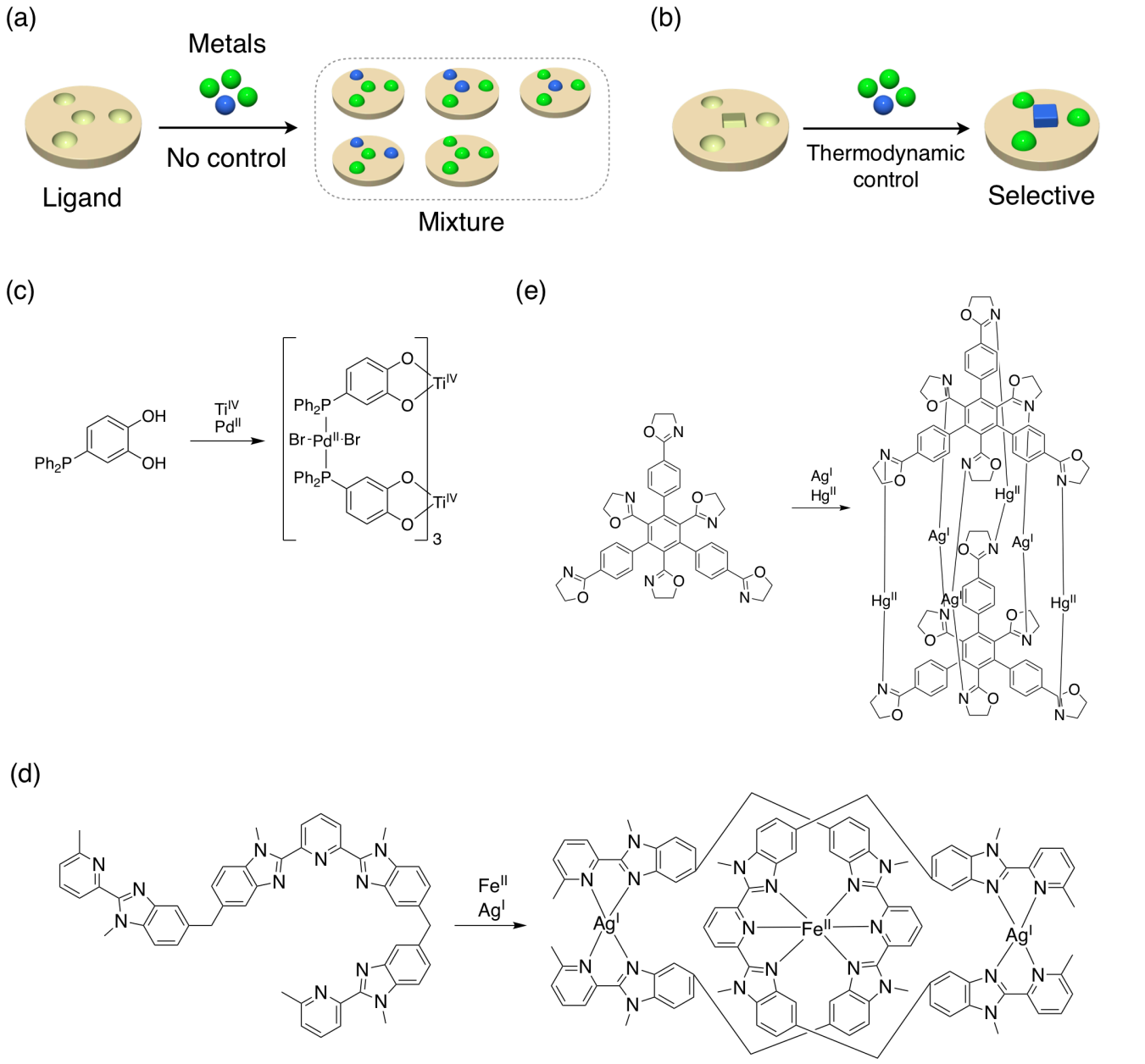

Figure 2-1-2. Synthesis of heterometallic complexes. (a,b) Typical schemes of (a) non-selective synthesis without any control and (b) selective synthesis under thermodynamic control. (c–e) Examples of selective syntheses under thermodynamic control based on (c) hard/soft ligands and metals,[15] (d) different preferred coordination numbers/geometry,[16] and (e) different ionic charges.[17]

However, the selective synthesis based on thermodynamic control sometimes fails, especially when the metals have similar thermodynamic properties, for example, in the cases of some transition metals or lanthanides. As discussed in Chapter 1, stepwise kinetic control is a good solution in such a case. As for the syntheses of heterometallic complexes, sequential addition of metals to each coordination site of a hetero-ditopic ligand is frequently used, which is called a metalloligand approach (Figure 2-1-3a).[18,19,20] On the other hand, site-selective transmetalation of a preformed homometallic complex is emerging in recent years as an alternative strategy to achieve kinetic control, especially when the metalloligand approach is not applicable (Figure 2-1-3b).[21,22,23,24,25,26] Still, it is sometimes difficult to kinetically differentiate the metal sites in homometallic complexes, resulting in a low yield or selectivity.[27,28,29] Therefore, it is desirable to develop a method of precisely controlling the transmetalation process for the synthesis of a heterometallic complex with high selectivity.

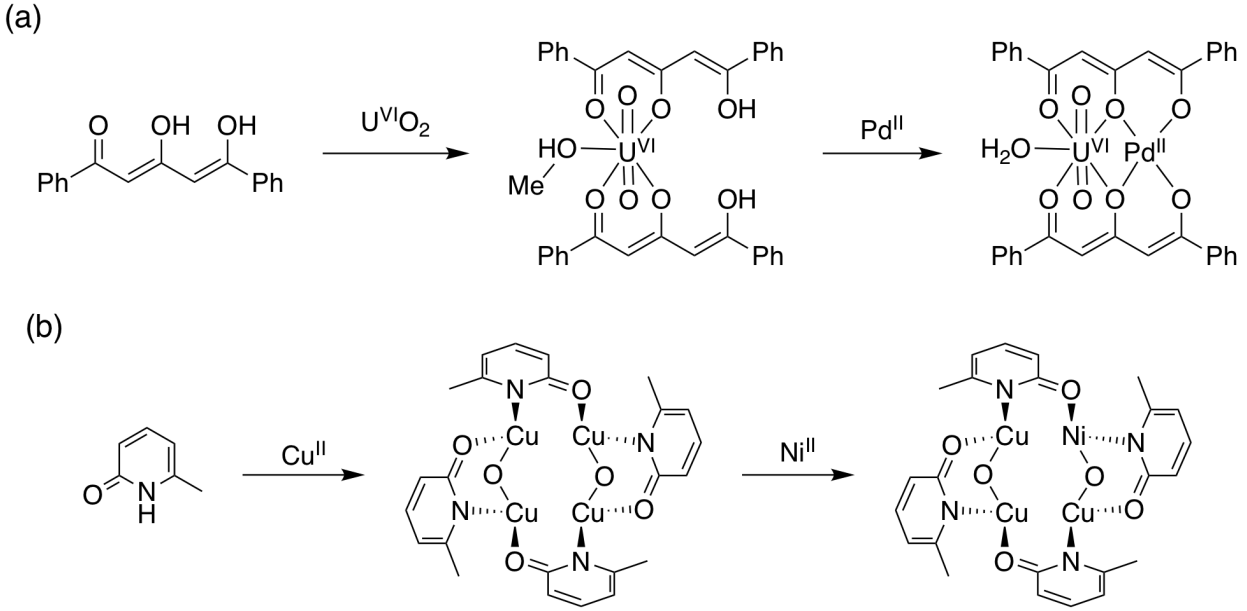

Figure 2-1-3. Examples of syntheses of heterometallic complexes under kinetic control adopting (a) a metalloligand approach[20] and (b) a transmetalation approach.[22]

In this work, I employed redox switching of metal centers because it is well known to affect the properties of metal centers.[30,31] From this viewpoint, I propose a stepwise strategy combining site-selective redox switching and transmetallation for kinetically controlled, highly selective synthesis of heterometallic complexes (Figure 2-1-4). In this method, a ligand with inequivalent coordination sites, a redox-active metal, and another metal are used. Firstly, a homometallic complex of the redox-active metal is constructed by normal complexation with the ligands. Secondly, some of the chemically inequivalent metal centers are site-selectively oxidized. Thirdly, the non-oxidized metal centers are site-selectively transmetalated with another metal. Finally, the oxidized metal center(s) are reduced back to their original states. Among these four steps, the early three steps can be conducted under thermodynamic control. The last step needs to be conducted under kinetic control to give the desired complex selectively, and this can be guaranteed by kinetic stability of the polynuclear framework and by a relatively mild condition required for reduction.

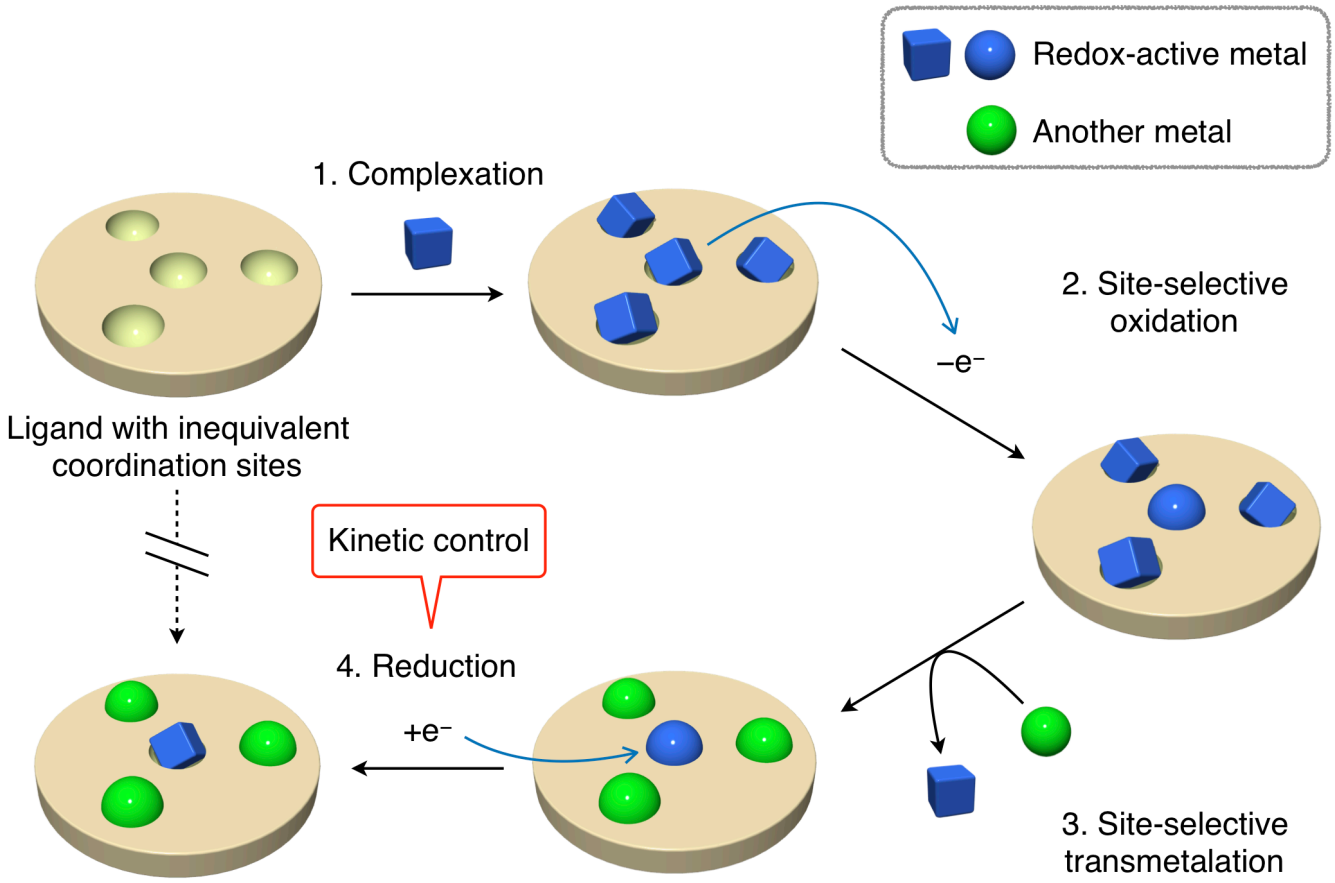

Figure 2-1-4. Schematic of the strategy proposed in this research for highly selective synthesis of heterometallic complexes.

The effectiveness of this strategy was demonstrated in the synthesis of a Co^{II}–Ni^{II} heterometallic complex (Figure 2-1-5). I employed ligand **L1** as a ligand with inequivalent coordination sites, $Co^{II/III}$ as a redox-active metal, and Ni^{II} as another metal. Starting from ligand **L1**, the homometallic complex $[Co^{II}_4\mathbf{L1}_3X_6]$ (**1-Co^{II}_4**; X = a coordinated solvent molecule or counteranion), the site-selectively oxidized complex $[Co^{III}Co^{II}_3\mathbf{L1}_3X_6]$ (**2-$Co^{III}Co^{II}_3$**), the site-selectively transmetalated complex $[Co^{III}Ni^{II}_3\mathbf{L1}_3X_6]$ (**3-$Co^{III}Ni^{II}_3$**), and the final, reduced complex $[Co^{II}Ni^{II}_3\mathbf{L1}_3X_6]$ (**4-$Co^{II}Ni^{II}_3$**) were successfully prepared stepwise with high selectivities and characterized well.

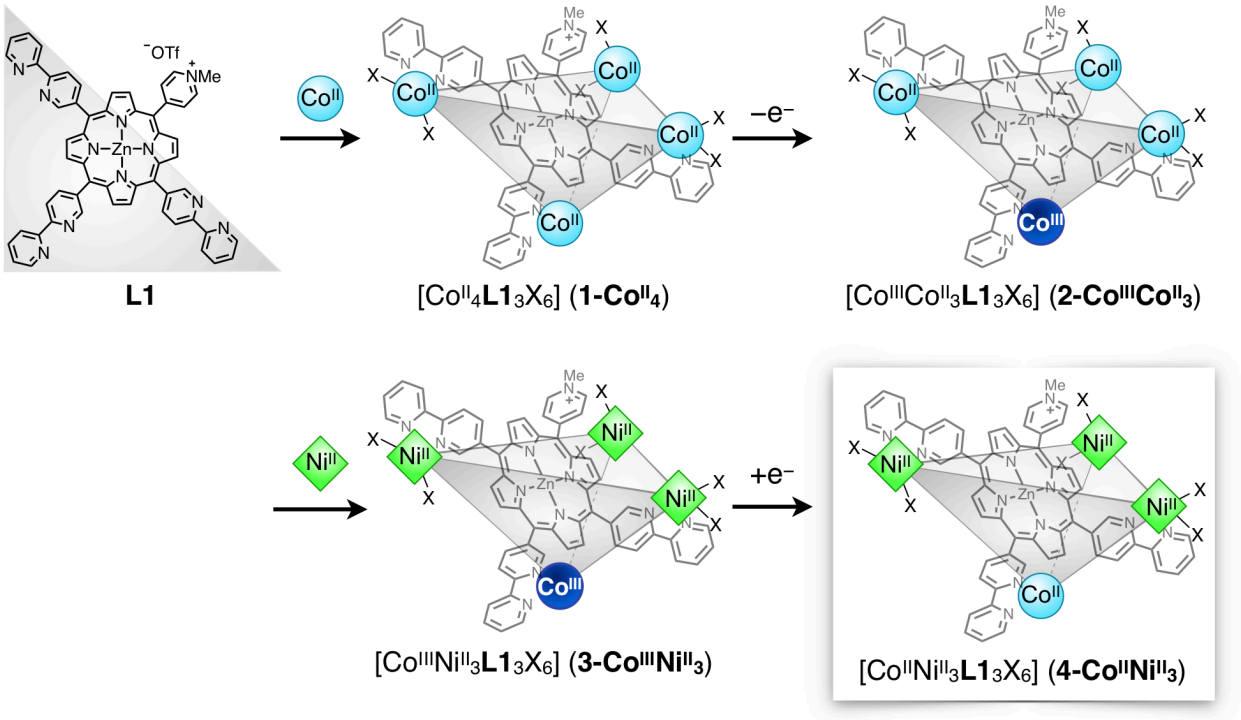

Figure 2-1-5. Synthetic scheme of a Co^{II}–Ni^{II} heterometallic complex, $[Co^{II}Ni^{II}_3\mathbf{L1}_3X_6]$ (**4-$Co^{II}Ni^{II}_3$**), demonstrated in this research using the aforementioned strategy.

2-2. Step 1: Complexation with a redox-active metal

As a ligand with inequivalent coordination sites, I employed ligand **L1**, which I previously synthesized in my master-course study (Figure 2-2-1).[32] I found therein that ligand **L1** can self-assemble with Zn^{II} ions to form an unsymmetrical tetranuclear complex, $[Zn^{II}_4\mathbf{L1}_3X_6]$ (X = a coordinated solvent molecule or counteranion). In this complex, two kinds of chemically inequivalent metal centers were arranged by the inequivalent coordination sites of **L1**: $Zn^{II}(bpy)_3$ and $Zn^{II}(bpy)_2X_2$ (bpy = 2,2'-bipyridine) (Figure 2-2-1b). This structure seemed suitable to perform site-selective oxidation.

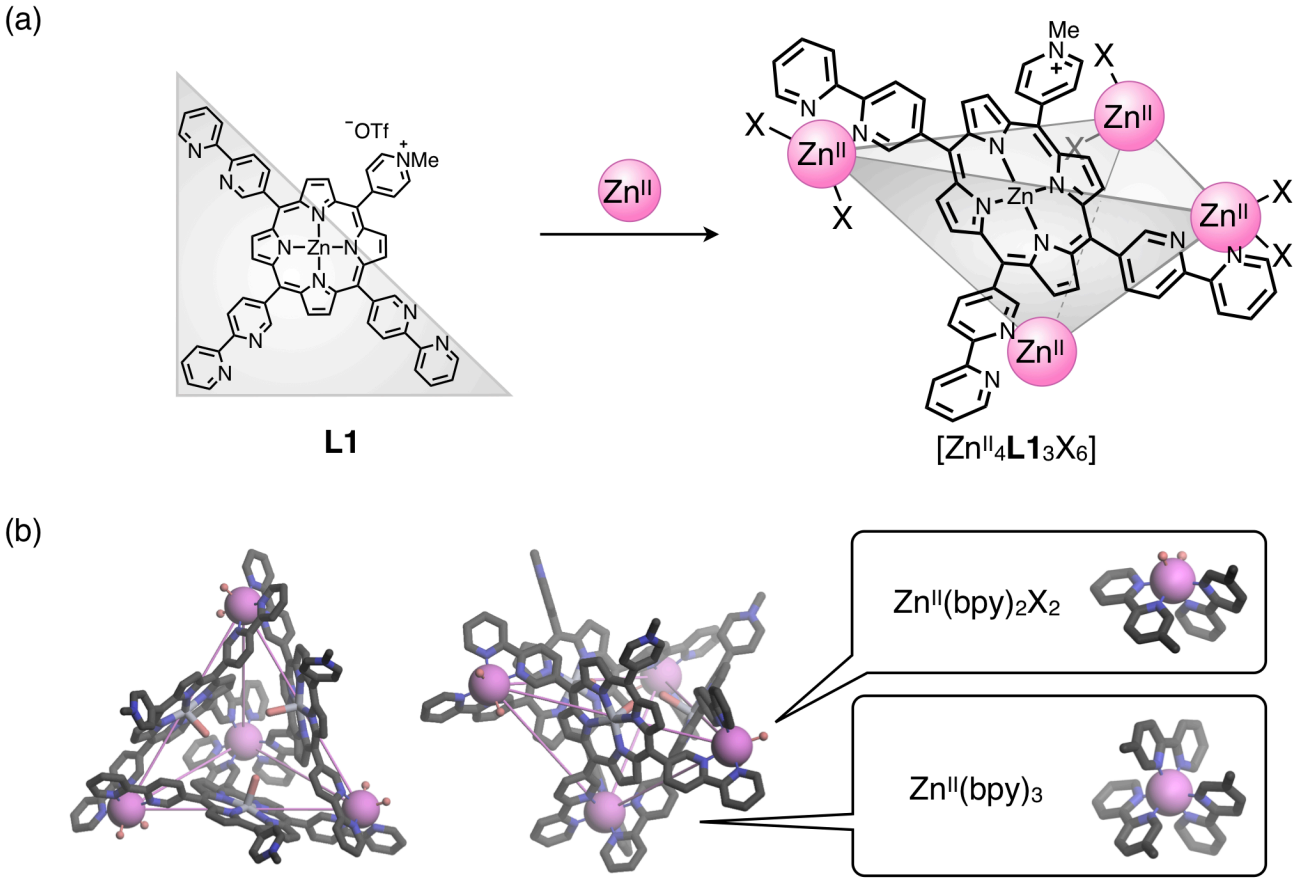

Figure 2-2-1. Ligand **L1** and complex $[Zn^{II}_4\mathbf{L1}_3X_6]$ (X = a coordinated solvent molecule or counteranion) developed in my master-course study.[32] (a) Reaction scheme of self-assembly of **L1** with Zn^{II} into $[Zn^{II}_4\mathbf{L1}_3X_6]$. (b) Molecular structure of $[Zn^{II}_4\mathbf{L1}_3X_6]$ from top and side views. Insets show the partial structures around the chemically inequivalent metal centers, $Zn^{II}(bpy)_3$ and $Zn^{II}(bpy)_2X_2$.

As a redox-active metal, $Co^{II/III}$ was chosen because it is well-known that the labile nature of Co^{II} dramatically changes into an inert nature when it was oxidized to Co^{III}.[30,31] Therefore, as the first step, complexation of **L1** with Co^{II} was conducted. Treatment of **L1**·OTf with $Co(OTf)_2$ (1.33 eq.) in CD_3CN/D_2O = 19:1 at 70 °C successfully afforded complex $[Co^{II}_4\mathbf{L1}_3X_6]$ (**1-Co$^{II}_4$**) as the major product in 65% yield (estimated from ^1H NMR) (Figure 2-2-2a). A coordinated solvent molecule or counteranion denoted by X could not be determined in solution state due to the fast exchange. The yield was calculated as a sum of every species with different Xs.

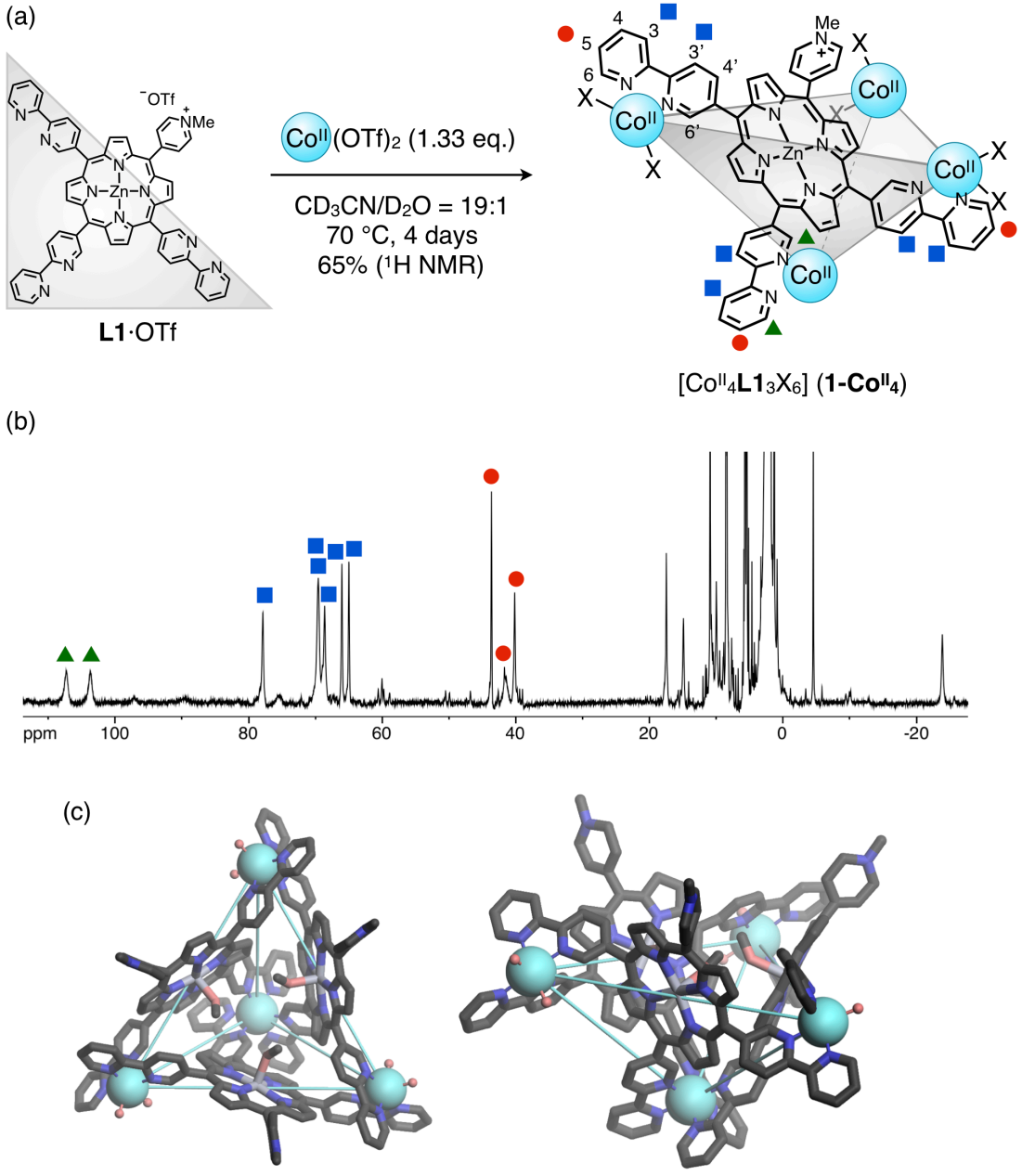

Figure 2-2-2. Preparation and characterization of complex $[Co^{II}_4\mathbf{L1}_3X_6]$ (**1-Co$^{II}_4$**). (a) Reaction scheme. The numbering of positions is shown in one of the bpy moieties. (b) Paramagnetic ^1H NMR spectrum (CD_3CN/D_2O = 19:1, 343 K, 500 MHz). (c) Single-crystal XRD structure of a MeOH adduct in top and side views. Hydrogen atoms, disorder, non-coordinated anions, and solvent molecules are omitted for clarity. Color code: Co^{II}, cyan; Zn, grey; C, black; N, blue; O, red. Lines are drawn between Co centers to guide the eye.

The paramagnetic ^{1}H NMR spectrum at 343 K showed three sets of signals with the 1:1:1 integral ratio in the 30–110 ppm region, which can be assigned to three bpy moieties of one molecule of **L1** coordinated to paramagnetic Co^{II} ions (Figure 2-2-2b). Each signal was assigned to 6,6'-, 3,3'-, and 5-positions of bpy, respectively, comparing the spectrum at 300 K with the literature of $[Co^{II}(bpy)_3]^{2+}$,[33,34] because the through-bond proximity to paramagnetic metal atom is known to dominate downfield shifting.[35,36,37] Some signals of hydrogens at the 5-, 6-, and 6'-positions were broadened to different degrees, probably due to the dynamic exchange of X. The two chemically equivalent bpy moieties in **L1** became inequivalent because the connection to the $Co^{II}(bpy)_3$ moiety (C_3 symmetry) lowers the symmetry of **L1** (C_{2v}) to C_1. In the diamagnetic region, the signal of methyl protons was assigned by its characteristic high intensity derived from 3 protons and relatively non-shifted chemical shift around 5 ppm. The presence of only one set of signals for **L1** is consistent with the C_3-symmetric structure of **1-Co$^{II}_4$**. The ESI-MS measurement predominantly showed a series of signals for $[Co^{II}_4\mathbf{L1}_3(OTf)_{11-n}]^{n+}$. The single-crystal XRD analysis showed the detailed molecular structure of **1-Co$^{II}_4$** (Figure 2-2-2c). **1-Co$^{II}_4$** had a triangular-pyramidal framework formed by inequivalent Co^{II} centers, analogous to the aforementioned $[Zn^{II}_4\mathbf{L1}_3X_6]$. The apex site was constituted by a $Co^{II}(bpy)_3$ motif, while the other basal sites were constituted by a $Co^{II}(bpy)_2X_2$ motif.

In this way, the first step, construction of homometallic complex with a redox-active metal at chemically inequivalent sites, was accomplished. As all attempts to obtain pure **1-Co$^{II}_4$** in a preparative scale were not successful, the sample was used for the next step without purification and the isolated yield could not be calculated. For similar reasons, the following complexes were also used without purification unless otherwise noted and only NMR yields were calculated as a sum of every species with different Xs.

2-3. Step 2: Site-selective oxidation

Next, site-selective oxidation of chemically inequivalent metal centers was conducted. In **1-Co$^{II}_4$**, the $Co^{II}(bpy)_3$ site is expected to be more easily oxidized than $Co^{II}(bpy)_2X_2$ sites in thermodynamic equilibrium because the electron donation from bpy ligands should lower the redox potential of $Co^{III/II}$. Attempts to electrochemically determine the redox potential of each Co^{II} site of **1-Co$^{II}_4$** failed because of high irreversibility of these redox couples and interference of redox reaction at the porphyrin core of **L1** at high potentials. Nonetheless, the literature values of the standard redox potentials of $[Co^{III/II}(OH_2)_6]$ (+1.92 V)[38] and $[Co^{III/II}(bpy)_3]$ (+0.32 V)[39] supported the hypothesis of electron donation from the bpy moiety.

As an initial screening, various oxidants were tested to site-selectively oxidize the $Co^{II}(bpy)_3$ site of **1-Co$^{II}_4$**. H_2O_2 showed extensive decomposition probably due to too strong oxidization power. DDQ indicated simultaneous oxidation at the $Co^{II}(bpy)_2X_2$ site with coordination of OH^- formed by the basicity of reduced species. $AgNO_3$ and 1,8-naphthoquinone showed no redox reactions probably due to a thermodynamic or kinetic reason. Finally, a stoichiometric amount of cerium(IV) ammonium nitrate was found to be effective for site-selective oxidation.

Accordingly, **1-Co$^{II}_4$** was treated with cerium(IV) ammonium nitrate (0.333 eq. to **L1**) in CD_3CN/D_2O = 19:1 at room temperature to afford $[Co^{III}Co^{II}_3\mathbf{L1}_3X_6]$ (**2-Co^{III}Co$^{II}_3$**), where only the $Co^{II}(bpy)_3$ site was oxidized to $Co^{III}(bpy)_3$ (Figure 2-3-1a). A paramagnetic ^{1}H NMR spectrum of the product showed that one set of bpy signals shifted from the paramagnetic region (30–110 ppm) to the diamagnetic region (7–11 ppm), while the other two sets of bpy signals remained in the paramagnetic region (Figure 2-3-1b). Oxidation at the $Co^{II}(bpy)_3$ site can only explain such shift of one bpy signal sets maintaining the symmetry of the framework. The ESI-MS measurement predominantly showed the signal series of $[Co^{III}Co^{II}_3\mathbf{L1}_3(NO_3)(OTf)_{11-n}]^{n+}$. The single-crystal XRD analysis showed that the framework of **1-Co$^{II}_4$** was maintained (Figure 2-3-1c). In comparison with **1-Co$^{II}_4$**, the average Co–N bond distance at the $Co(bpy)_3$ site was significantly shorter (2.002(4) Å vs. 2.046(6)Å), while that at the $Co(bpy)_2X_2$ sites was similar (2.106(6) Å vs. 2.122(6) Å). In literature, Co–N bond distances are known to be shorter in $[Co^{III}(bpy)_3]$ than in $[Co^{II}(bpy)_3]$ (1.938 Å vs. 2.128 Å as median values in Cambridge Structural Database[40]). Thus, this contraction of bond distances suggests that only the $Co^{II}(bpy)_3$ site was oxidized.

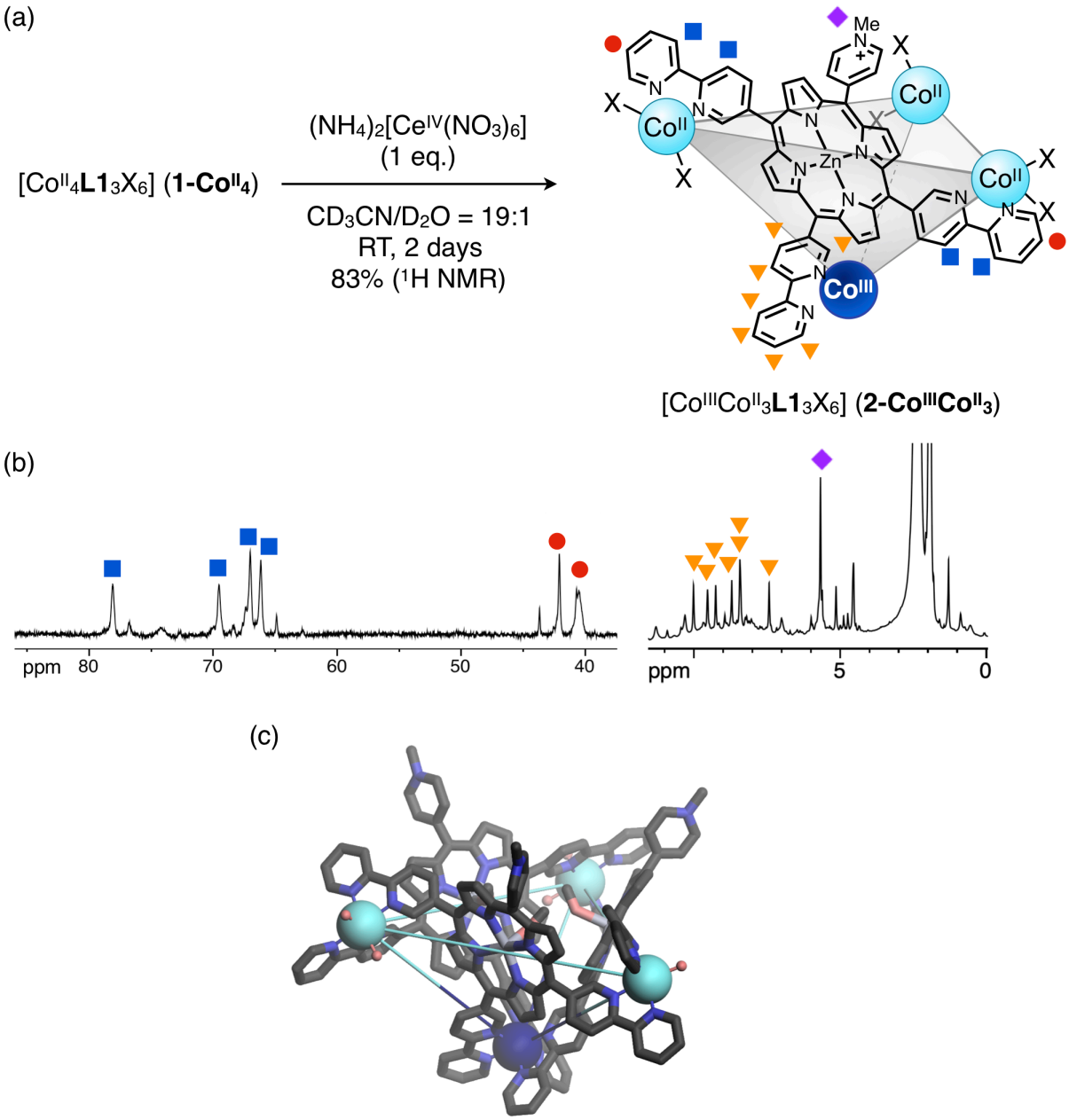

Figure 2-3-1. Preparation and characterization of complex [$Co^{III}Co^{II}_3$**L1**$_3X_6$] (**2-$Co^{III}Co^{II}_3$**). (a) Reaction scheme. (b) Paramagnetic ^{1}H NMR spectrum (CD_3CN/D_2O = 19:1, 343 K, 500 MHz). (c) Single-crystal XRD structure of a MeOH adduct. Hydrogen atoms, disorder, non-coordinated anions, and solvent molecules are omitted for clarity. Color code: Co^{III}, dark blue; Co^{II}, cyan; Zn, grey; C, black; N, blue; O, red. Lines are drawn between Co centers to guide the eye.

In this way, oxidation of **1-Co^{II}_4** into **2-$Co^{III}Co^{II}_3$** was site-selectively completed. The yield was 83% as estimated from ^{1}H NMR. Although 14% of **1-Co^{II}_4** remained, the reaction yield was not improved even when an additional amount of the oxidant was added. It seems that there was an equilibrium with other oxidized species. When a large excess of the oxidant was used, a complex mixture was generated presumably via oxidation at the $Co^{II}(bpy)_2X_2$ sites. As shown later, the remaining **1-Co^{II}_4** was found to be converted similarly to **2-$Co^{III}Co^{II}$**. Therefore, the sample was used for the next step without further treatment.

2-4. Step 3: Site-selective transmetalation

Next, site-selective transmetalation at the unoxidized $Co^{II}(bpy)_2X_2$ sites was conducted. In **2-$Co^{III}Co^{II}_3$**, the $Co^{III}(bpy)_3$ site is expected to be more stable against transmetalation than the $Co^{II}(bpy)_2X_2$ sites. From a thermodynamic point of view, the affinity of bpy to Co^{III} is much higher than that to Co^{II} as can be seen in the formation constant of $[Co(bpy)_3]$ complexes ($10^{43.0}$ for Co^{III} vs. $10^{15.9}$ for Co^{II} in H_2O, as calculated from the redox potential of $[Co^{III/II}(OH_2)_6]$[38] and $[Co^{III/II}(bpy)_3]$[39] and the formation constant of $[Co^{II}(bpy)_3]$[41]). From a kinetic point of view, octahedral Co^{III} complexes are known to be kinetically much more inert than Co^{II} ones,[30,31] and the $Co(bpy)_3$ site has more bridging to the other Co centers than the $Co(bpy)_2X_2$ sites. I selected Ni^{II} as another metal to introduce because the thermodynamic affinity of bpy to Ni^{II} is intermediate between Co^{III} and Co^{II} (the formation constant of $[Ni(bpy)_3]$ is $10^{20.2}$ in H_2O).[41] Accordingly, **2-$Co^{III}Co^{II}_3$** was treated with $Ni(OTf)_2$ (2 eq. to **L1**) in CD_3CN/D_2O = 19:1 at 70 °C to afford $[Co^{III}Ni^{II}_3\mathbf{L1}_3X_6]$ (**3-$Co^{III}Ni^{II}_3$**) (Figure 2-4-1a).

The paramagnetic ^1H NMR spectrum showed the disappearance of the $Co^{II}(bpy)_2X_2$ signals and appearance of new broad signals with different chemical shifts, typical for Ni^{II}–bpy complexes (Figure 2-4-1b).[34] In the diamagnetic region, the signal of methyl group of **L1** initially changed into a complicated pattern, and then converged to one signal (Figure 2-4-1c). These results indicate that all the three $Co^{II}(bpy)_2X_2$ sites were stepwise transmetalated with Ni^{II}. The ESI-MS measurement showed the signal series of $[Co^{III}Ni^{II}_3\mathbf{L}_3(NO_3)(OTf)_{11-n}]^{n+}$, supporting that transmetalation did not occur at the $Co^{III}(bpy)_3$ site. The XPS measurement after removal of free metal ions by reprecipitation showed that the atomic ratio of Co:Ni was 1:3.1. The single-crystal XRD analysis showed that the framework of **2-$Co^{III}Co^{II}_3$** was maintained (Figure 2-4-1d). The average Co–N bond distance at the $Co^{III}(bpy)_3$ site was 1.936(3) Å, and the average Ni–N bond distance at the $Ni^{II}(bpy)_2X_2$ sites was 2.056(4) Å. These values agree well with typical values of Co^{III} (1.938 Å) and Ni^{II} (2.086 Å), but not with Co^{II} (2.128 Å as median values of $[M(bpy)_3]$ in Cambridge Structural Database).[40] This crystal was obtained as an adduct of chloride ions, which probably came from decomposition of $CDCl_3$ used for crystallization.[42]

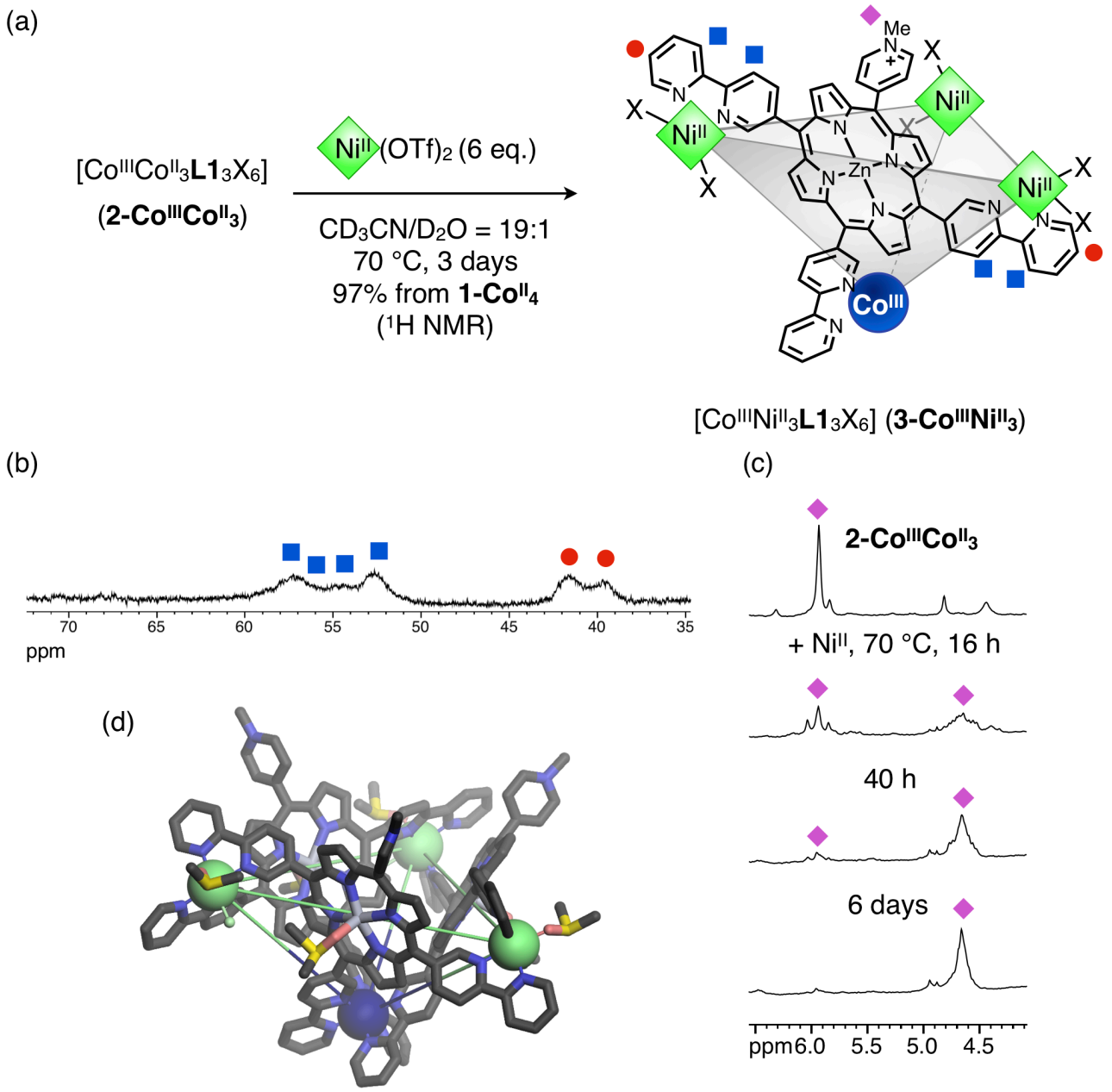

Figure 2-4-1. Preparation and characterization of complex $[Co^{III}Ni^{II}_3\mathbf{L1}_3X_6]$ (**3-Co^{III}Ni$^{II}_3$**). (a) Reaction scheme. (b) Paramagnetic ^{1}H NMR spectrum (CD_3CN/D_2O = 19:1, 343 K, 500 MHz). (c) Time-course ^{1}H NMR spectra (CD_3CN/D_2O = 19:1, 300 K, 500 MHz). (d) Single-crystal XRD structure of an adduct with DMSO and chloride. Hydrogen atoms, disorder, non-coordinated anions, and solvent molecules are omitted for clarity. Color code: Co^{III}, dark blue; Ni^{II}, yellow-green; Zn, grey; Cl, light yellow-green; C, black; N, blue; O, red. Lines are drawn between the Co and Ni centers to guide the eye.

In this way, transmetalation of **2-Co^{III}Co$^{II}_3$** into **3-Co^{III}Ni$^{II}_3$** was site-selectively completed. The yield was 97% from **1-Co$^{II}_4$** as estimated from ^{1}H NMR. This yield indicates the remaining **1-Co$^{II}_4$** (14%) in the sample of **2-Co^{III}Co$^{II}_3$** was also converted to **3-Co^{III}Ni$^{II}_3$**, probably via oxidation by other oxidized species.

2-5. Step 4: Reduction

As the final step, reduction of the initially oxidized metal center was conducted. Since the thermodynamic affinity of bpy to Ni^{II} is higher than Co^{II}, the reduction product of **3-$Co^{III}Co^{II}_3$** would be thermodynamically unstable against metal exchange between the $Co^{II}(bpy)_3$ site and the $Ni^{II}(bpy)_2X_2$ sites. Nonetheless, considering the kinetic stability of the polynuclear framework consisting of multiple coordination bonds, it may be possible to conduct reduction under kinetic control without causing metal exchange. From this viewpoint, **3-$Co^{III}Co^{II}_3$** was treated with ^{n}Bu$_4$N·I (1.5 eq. to **L1**) in CD_3CN/D_2O = 19:1 at 70 °C to afford $[Co^{II}Ni^{II}_3$**L1**$_3X_6]$ (**4-$Co^{II}Ni^{II}_3$**) (Figure 2-5-1a). ^{n}Bu$_4$N·I was chosen as a reductant because it is known to be effective for similar complexes.[31]

The paramagnetic ^{1}H NMR spectrum showed the re-appearance of one set of sharp Co^{II}–bpy signals, while the signals of the $Ni^{II}(bpy)_2X_2$ sites were unchanged (Figure 2-5-1b). In the diamagnetic region, the methyl signal of **3-$Co^{III}Co^{II}_3$** disappeared and a new signal appeared. This result indicates that the Co^{III} center was reduced to Co^{II} without affecting the other parts of the structure. The ESI-MS measurement showed a series of signals for $[Co^{II}Ni^{II}_3$**L1**$_3(NO_3)_2(OTf)_{9-n}]^{n+}$. The UV-Vis absorption spectrum of **4-$Co^{I}Ni^{II}_3$** was similar to that of **1-Co^{II}_4** but markedly different from those of **2-$Co^{III}Co^{II}_3$** and **3-$Co^{III}Ni^{II}_3$**, suggesting the absence of Co^{III} character (Figure 2-5-1c).

In this way, reduction of **3-$Co^{III}Ni^{II}_3$** to **4-$Co^{II}Ni^{II}_3$** was successfully confirmed. However, the yield in an initial attempt was 48% as estimated from ^{1}H NMR. This result suggests that the reaction was not completely under kinetic control, and that decomposition of the product occurred in part. To prevent possible decomposition, the sample of **3-$Co^{III}Ni^{II}_3$** was partially purified by reprecipitation from $MeCN/H_2O$ = 1:2 with NH_4PF_6 (50 eq. to **L1**), and the amount of the reductant was decreased to 0.417 eq. to **L1**. In this case, the yield was improved to 95% as estimated from ^{1}H NMR, which means reduction surely proceeded under kinetic control.

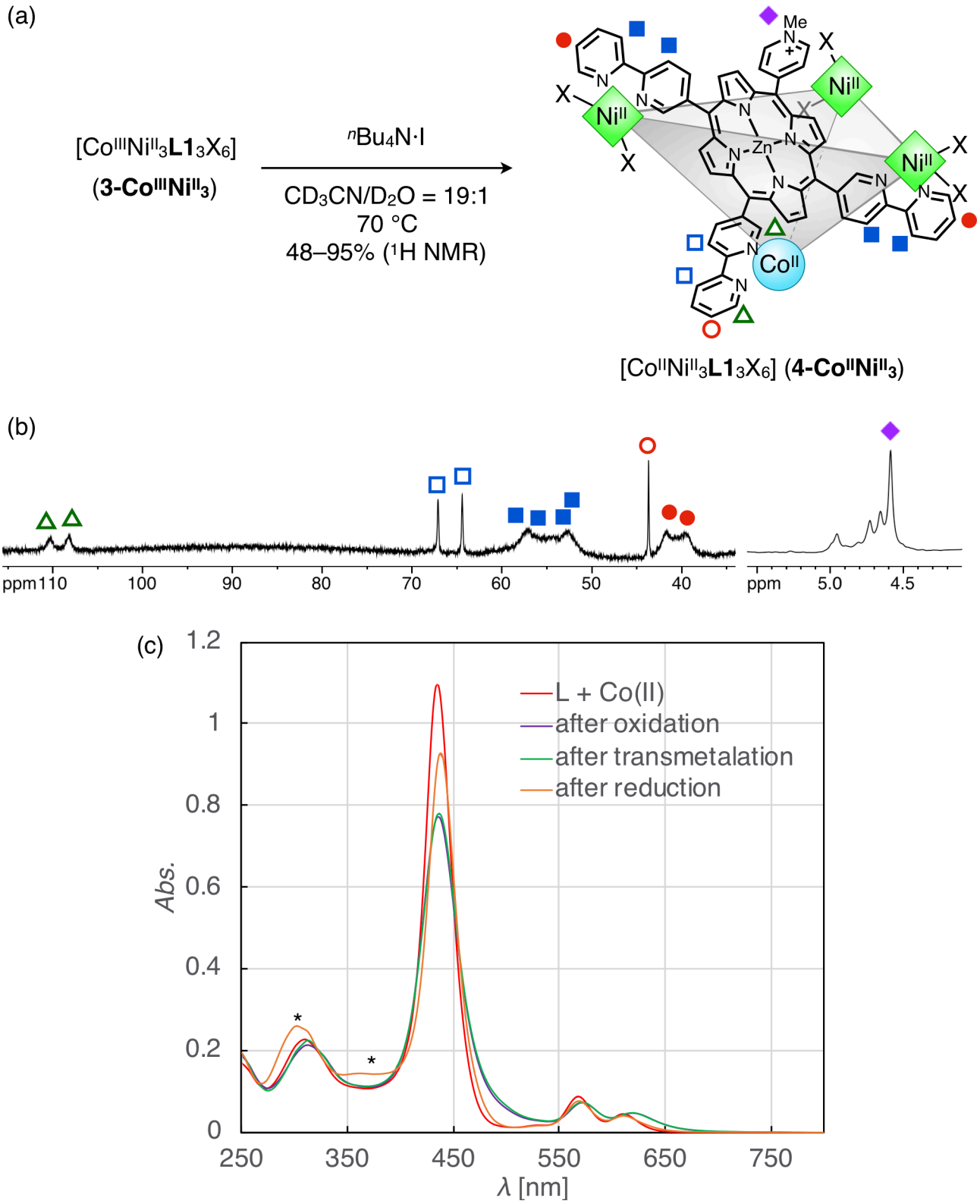

Figure 2-5-1. Preparation and characterization of complex $[Co^{II}Ni^{II}_3\mathbf{L1}_3X_6]$ (**4-Co^{II}Ni$^{II}_3$**). (a) Reaction scheme. (b) Paramagnetic ^{1}H NMR spectrum (CD_3CN/D_2O = 19:1, 343 K, 500 MHz). (c) UV-Vis absorption spectra (MeCN, 298 K, l = 0.10 cm). Each sample prepared in CD_3CN/D_2O = 19:1 was diluted to 25 times with CH_3CN. The total concentration of **L** was 40 μM. The asterisks denote the absorption bands of triiodide ion.

Overall, the heterometallic complex **4-Co^{II}Ni$^{II}_3$** was selectively obtained in 92% yield from **1-Co$^{II}_4$** via stepwise site-selective redox switching and transmetalation.

Surprisingly, **4-Co^{II}Ni$^{II}_3$** prepared by the modified procedure showed no sign of decomposition when heated at 70 °C in CD_3CN/D_2O = 20:1 for 21 h, or even in CD_3CN/D_2O/DMSO-d_6 = 20:1:2 for 24 h (Figure 2-5-2). This high kinetic stability would come from the polynuclear framework consisting of multiple coordination bonds.

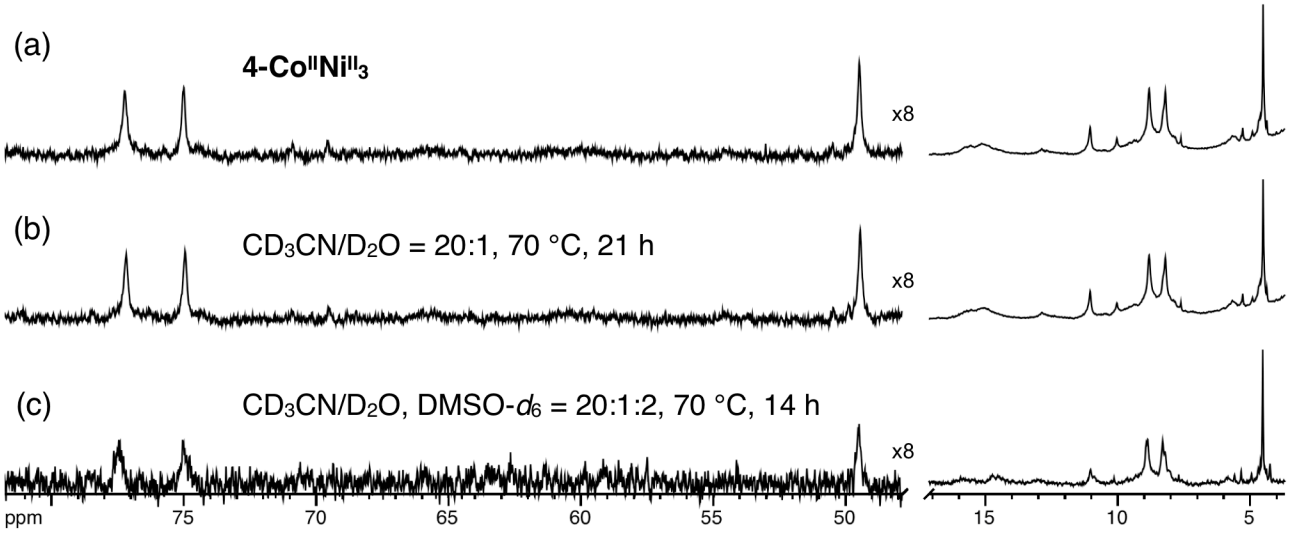

Figure 2-5-2. Stability test of **4-Co^{II}Ni$^{II}_3$**. Paramagnetic ^{1}H NMR spectrum ((a,b) CD_3CN/D_2O = 20:1; (c) CD_3CN/D_2O/DMSO-d_6 = 20:1:2, 300 K, 500 MHz).

2-6. Comparison with other strategies

To confirm the effectiveness of the strategy used here, I conducted three control experiments using other strategies.

Firstly, the one-step strategy was examined. **L1**·OTf was treated with $Co^{II}(OTf)_2$ (0.33 eq.) and $Ni^{II}(OTf)_2$ (1 eq.) simultaneously in CD_3CN/D_2O = 19:1 at 70 °C (Figure 2-6-1a). The paramagnetic ^1H NMR spectrum showed only signals of Ni^{II}–bpy but no discernable signals of Co^{II}–bpy (Figure 2-6-1b). In the region of methyl protons, many weak signals were observed. This result indicates non-selective formation of Ni^{II}-containing complexes. This failure would be caused by the higher thermodynamic stability of a $Ni^{II}(bpy)_3$ motif than $Co^{II}(bpy)_3$. The one-step strategy could not provide the kinetic control necessary to afford **4-$Co^{II}Ni^{II}_3$** selectively.

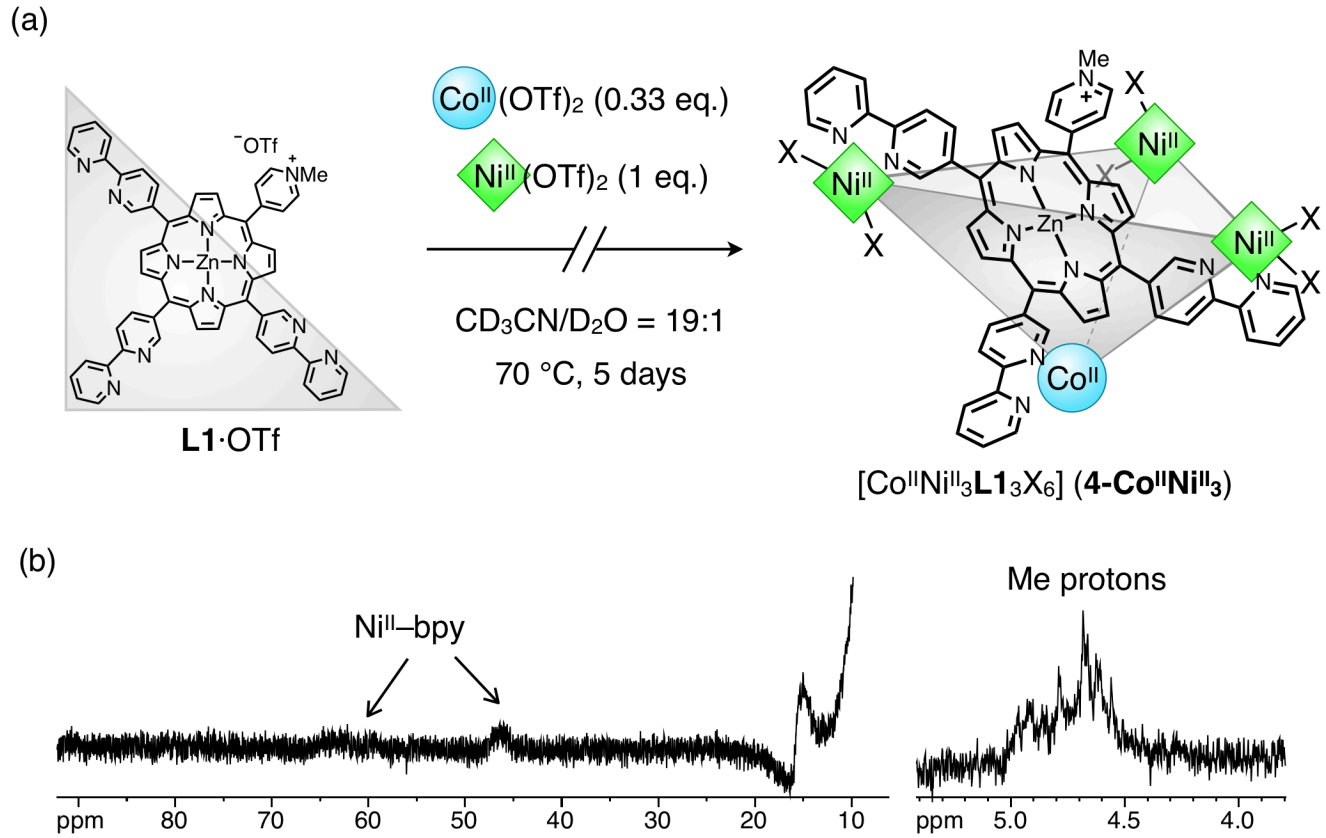

Figure 2-6-1. Control experiment of the one-step strategy. (a) Reaction scheme. (b) Paramagnetic ^1H NMR spectrum (CD_3CN/D_2O = 19:1, 300 K, 500 MHz).

Secondly, the transmetalation strategy without redox switching was examined. **1-Co$^{II}_4$** was treated with $Ni(OTf)_2$ (2 eq. to **L1**) in CD_3CN/D_2O = 19:1 at 70 °C (Figure 2-6-2a). Similarly to the previous experiment, the paramagnetic ^1H NMR spectrum showed only signals of Ni^{II}–bpy but no discernable signals of Co^{II}–bpy (Figure 2-6-2b). In the region of methyl protons, some weak signals were observed. This result indicates transmetalation at the $Co^{II}(bpy)_3$ site and non-selective formation of Ni^{II}-containing complexes. This failure would be caused by the insufficient kinetic control. The transmetalation condition was harsher than that of reduction, because a longer reaction time was necessary, and because a high concentration of free metal ions was present in solution. Although the transmetalation strategy works in some cases,[21–26] combination with redox switching was necessary in the case of **4-Co^{II}Ni$^{II}_3$**.

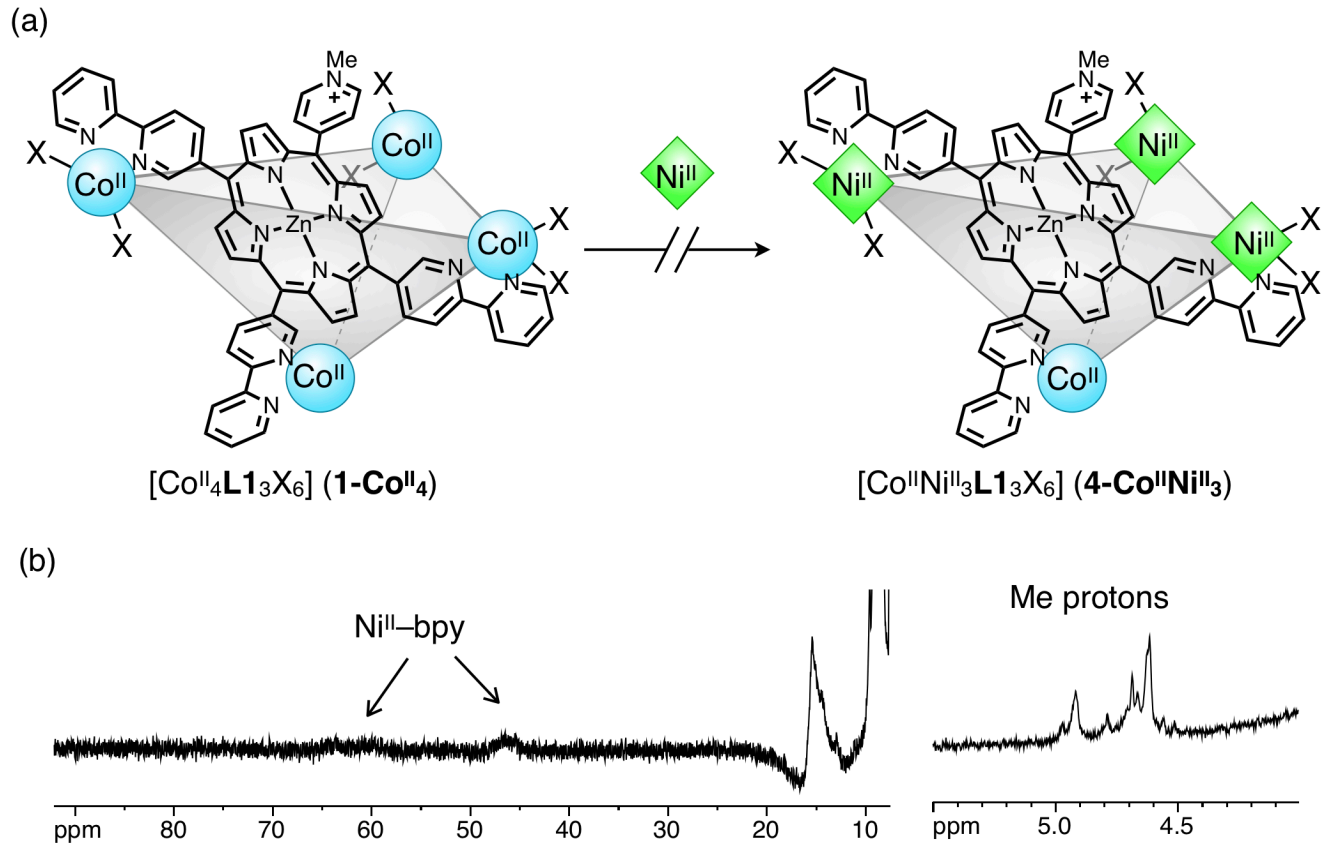

Figure 2-6-2. Control experiment of the transmetalation strategy without redox switching. (a) Reaction scheme. (b) Paramagnetic ^1H NMR spectrum (CD_3CN/D_2O = 19:1, 300 K, 500 MHz).

Thirdly, the redox-switching strategy without transmetalation was examined. Since **3-Co^{III}Ni$^{II}_3$** is expected to be thermodynamically stable, direct synthesis of **3-Co^{III}Ni$^{II}_3$** from **L1** and subsequent reduction might be another route to **4-Co^{II}Ni$^{II}_3$**. Accordingly, **L1**·OTf was treated with Co^{II}(OTf)$_2$ (0.33 eq.) and Ni^{II}(OTf)$_2$ (1 eq.) in CD_3CN/D_2O = 19:1 at 70 °C, and then $(NH_4)_2[Ce^{IV}(NO_3)_6]$ (0.33 eq.) was added to the reaction mixture at 70 °C (Figure 2-6-3a). In-situ oxidation of Co^{II} was employed here because preparation of Co^{III}(OTf)$_3$ is not known. The ^{1}H NMR spectrum showed many weak signals, indicating non-selective formation of some complexes (Figure 2-6-3b). This failure would be caused either by the high kinetic barrier to ligand exchange at a Co^{III} center or by the thermodynamic instability of **3-Co^{III}Ni$^{II}_3$** due to the smaller size of Co^{III} than that of Co^{II}. It seems that redox switching and introduction of another metal should be separately conducted to avoid complexity.

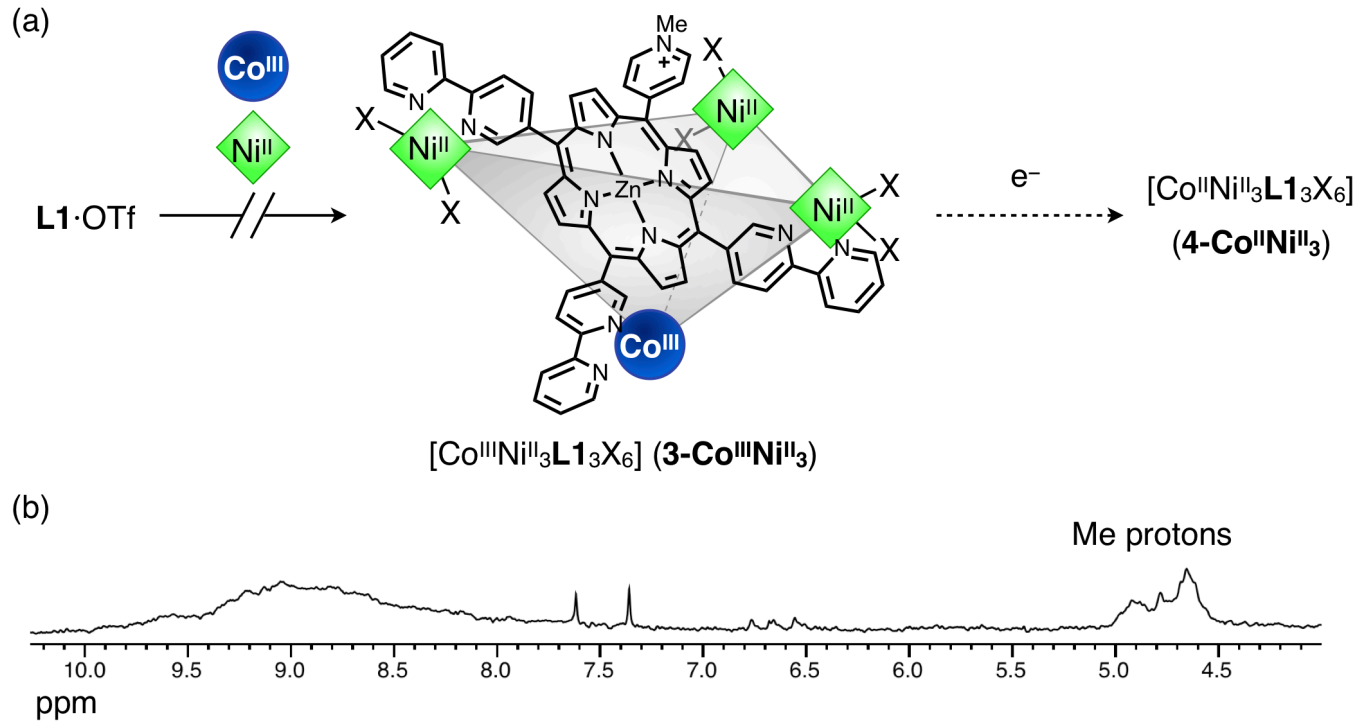

Figure 2-6-3. Control experiment of the redox switching strategy without transmetalation. (a) Reaction scheme. (b) ^{1}H NMR spectrum (CD_3CN/D_2O = 19:1, 300 K, 500 MHz).

2-7. Conclusions

In this chapter, I have proposed a novel kinetically controlled, stepwise strategy for highly selective synthesis of heterometallic complexes. This strategy uses a redox-active metal and a ligand with inequivalent coordination sites and consists of four steps: complexation with a redox-active metal, site-selective oxidation, site-selective transmetalation, and reduction. In this strategy, the early three steps proceed under thermodynamic control, and the fourth step needs kinetic control. This kinetic control can be provided by the relatively mild condition of reduction and the high kinetic stability of polynuclear framework consisting of multiple coordination bonds.

The effectiveness of this strategy was demonstrated in the synthesis of a new heterometallic complex, **4-$Co^{II}Ni^{II}_3$**. In this synthesis, $Co^{II/III}$ worked as a redox-active metal whose affinity to ligand was dramatically increased upon oxidation. Tris-bipyridine ligand **L1** was employed to construct an [M_4**L1**$_3X_6$] framework with inequivalent metal sites. Ligand **L1** was treated with Co^{II} to yield **1-Co^{II}_4**, and then it was site-selectively oxidized to give **2-$Co^{III}Co^{II}_3$**, and it was site-selectively transmetalated to give **3-$Co^{III}Ni^{II}_3$**, and finally it was reduced to give **4-$Co^{II}Ni^{II}_3$** selectively. In contrast, this complex could not be selectively obtained either by the conventional one-step strategy or by the simple transmetalation. Therefore, this "site-selective redox switching and transmetalation" strategy is an excellent way to construct novel heterometallic complexes, which can exhibit functions specific to the combination of metals.

As an extension of this strategy, it may be possible to synthesize a hetero-trimetallic complex. As discussed in section 2-4, the introduction of Ni^{II} ions were observed in a stepwise manner. This may allow introduction of less Ni^{II} ions and subsequent transmetalation with another metal ion. Meanwhile, complex **4-$Co^{II}Ni^{II}_3$** may be useful as a catalyst by binding a substrate at the Ni^{II} site and providing electron transfer from the Co^{II} site.

2-8. Experimental section

Materials and methods

Unless otherwise noted, solvents and reagents were purchased from TCI Co., Ltd., FUJIFILM Wako Pure Chemical Corporation Ltd., Kanto Chemical Co., and Sigma-Aldrich Co., and used without further purification.

Elemental analysis was conducted in the Microanalytical Laboratory, Department of Chemistry, School of Science, the University of Tokyo.

^{1}H, ^{13}C, ^{19}F, and 2D NMR spectra were recorded on a Bruker AVANCE III-500 (500 MHz) spectrometer. Wide-sweep paramagnetic NMR spectra were recorded with a spectral width (SW) of 200 ppm, a transmitter frequency offset (O1P) of 50.00 ppm and a line width of 10.0 Hz unless otherwise noted. NMR yield estimation using an internal standard was conducted in a normal measurement method for the diamagnetic region. Tetramethylsilane was used as an internal standard (δ 0 ppm) for ^{1}H and ^{13}C NMR measurements when $CDCl_3$ was used as a solvent. A residual solvent signal was used for the calibration of ^{1}H NMR measurements when CD_3CN (δ 1.94 ppm), DMSO-d_6 (δ 2.50 ppm), or mixed solvents with them were used as a solvent. No corrections were conducted for ^{19}F NMR measurements. Abbreviations: s, singlet; d, doublet; t: triplet; br, broad; m, multiplet.

ESI-TOF MS data were recorded on a Micromass LCT Premier XE mass spectrometer. Unless otherwise noted, experimental conditions were as follows (Ion mode, positive; Desolvation temperature, 150 °C; Source temperature, 80 °C).

UV–vis spectra were recorded on a JASCO V-770 UV–vis–NIR spectrophotometer. The experimental conditions were as follows (0.10 cm glass cell; λ = 250–800 nm; scanning rate, 100 nm/min; data acquisition intervals, 0.5 nm).

Single-crystal X-ray crystallographic analyses were performed using a Rigaku XtaLAB PRO MM007DW PILATUS diffractometer, and obtained data were processed by using CrysAlisPro 1.171.39.7e (Rigaku OD, 2015) software and analyzed by Olex^2 1.2.10 (OlexSys Ltd., 2018) software[43] and SHELXL-2017/1 software.[44] Crystallographic data in this chapter can be obtained free of charge from the Cambridge Crystallographic Data Centre (http://www.ccdc.cam.ac.uk/data_request/cif).

XPS spectra were recorded using an Ulvac-Phi PHI 5000 VersaProbe III spectrometer and an Al Kα X-ray source ($h\nu$ = 1486.6 eV).

Synthesis of compounds

Synthetic route to L1·OTf·3H$_2$O

L1·OTf·3H$_2$O was synthesized via the route below according to my master thesis (Scheme 2-8-1).[32]

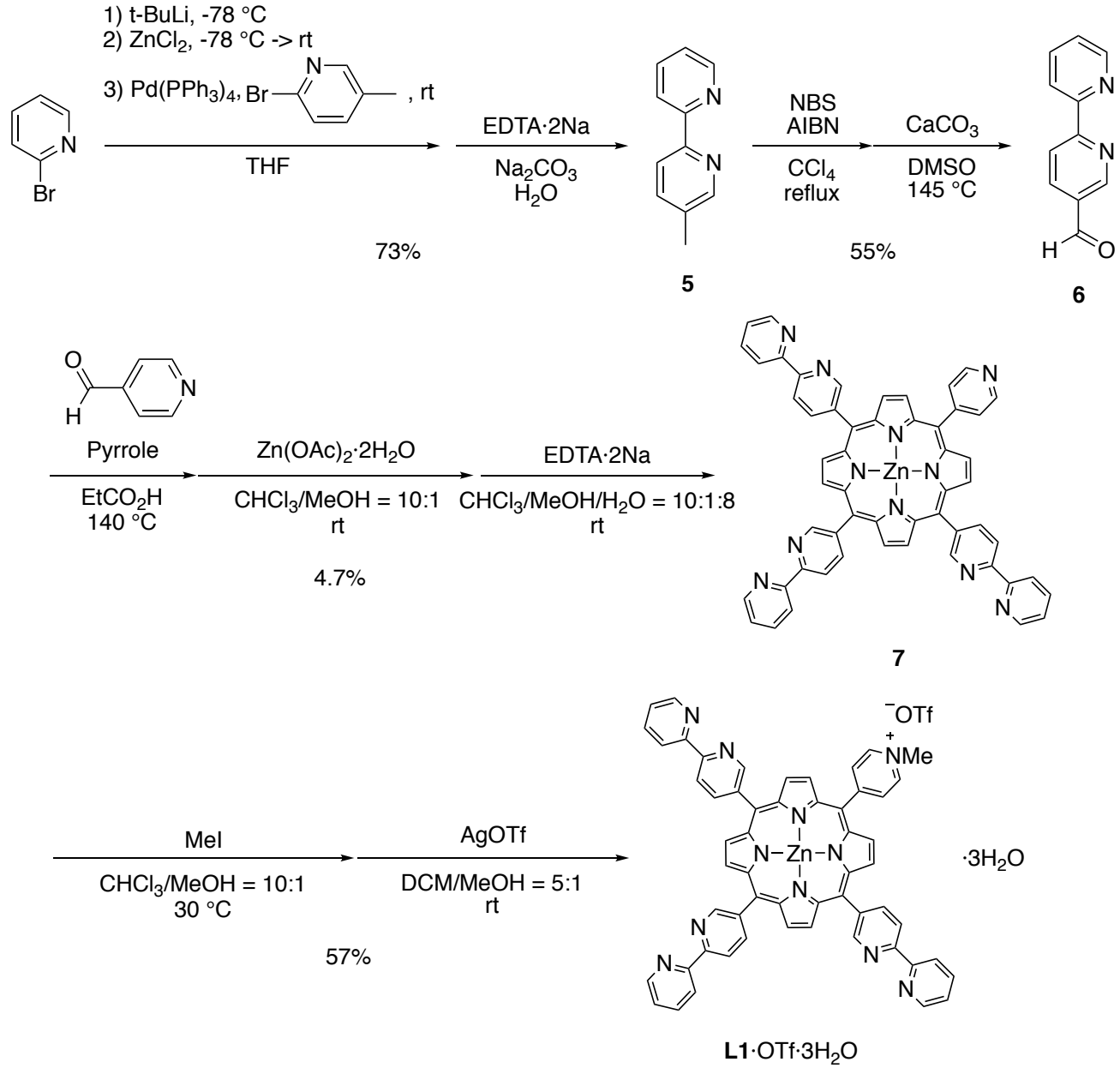

Scheme 2-8-1. Synthetic route of **L1**·OTf·3H$_2$O.

5-Methyl-2,2'-bipyridine (5)

This compound was prepared according to a previous report.[45] The ^{1}H NMR data of the compound were identical with those reported.[45]

^{1}H NMR ($CDCl_3$, 300 K, 500 MHz): δ 8.66 (ddd, J = 4.8, 1.8, 0.9 Hz, 1H), 8.50 (dt, J = 2.2, 0.7 Hz, 1H), 8.36 (dt, J = 8.0, 1.1 Hz, 1H), 8.28 (dd, J = 8.1, 0.3 Hz, 1H), 7.79 (ddd, J = 8.0, 7.5, 1.8 Hz, 1H), 7.62 (dd, J = 8.1, 1.7 Hz, 1H), 7.27 (ddd, J = 7.4, 4.9, 1.2 Hz, 1H), 2.38 (s, 1H) ppm.

5-Formyl-2,2'-bipyridine (6)

This compound was prepared by a procedure modified from a previous report.[45] A three-necked 1 L flask was equipped with a reflux condenser and a magnetic stirring bar, and to the flask were added 5-methyl-2,2'-bipyridine (**5**) (7.50 g, 44.1 mmol, 1 eq), NBS (19.6 g, 110 mmol, 2.49 eq) and CCl_4 (600 mL). The mixture was degassed and bubbled with Ar gas. To the mixture was added AIBN (0.867 g, 5.28 mmol, 12.0 mol%). The reaction mixture was degassed, and the flask was replaced with Ar gas. The reaction mixture was stirred and heated at reflux for 6 h. The resulting precipitate was removed with suction and washed with CCl_4. The filtrate and wash liquid were combined and evaporated to afford a brown solid. The solid was dissolved in CH_2Cl_2 (200 mL) and the solution was washed with Na_2CO_3 aqueous solution (pH 9, 200 mL × 2). The organic layer was evaporated to afford a brown solid. The solid was dissolved in Et_2O (100 mL) and the solution was filtered through SiO_2 short-path column with suction. The filtrate was evaporated to afford a yellow solid (12.5 g) containing 5-bromomethyl-2,2'-bipyridine, 5-dibromomethyl-2,2'-bipyridine as a desired intermediate and 5-tribromomethyl-2,2'-bipyridine.

A 1 L three-necked flask was equipped with a reflux condenser and a magnetic stirring bar, and to the flask were added the resultant solid (12.5 g), DMSO (370 mL) and $CaCO_3$ (15.6 g, 155 mmol, 2.1 eq to Br atom). The reaction mixture was degassed and bubbled with Ar gas. The reaction mixture was stirred at 145 °C for 4.5 h. To the reaction mixture was added H_2O (1.85 L) and Et_2O (400 mL). The mixture was filtered with suction and washed with Et_2O. The organic layer of the filtrate was separated. The aqueous layer was extracted with Et_2O (400 mL × 4). The organic layers were combined, evaporated and the resultant solid was dissolved in Et_2O (150 mL). The solution was washed with brine, dried over Na_2SO_4 and evaporated to afford a pale-yellow solid containing 5-formyl-2,2'-bipyridine (**6**) as a main product. Recrystallization of the solid from hot *n*-hexane gave **6** as a pale-yellow solid (4.43 g, 24.0 mmol, 55%). The ^{1}H NMR data were identical with those reported.[45]

^{1}H NMR ($CDCl_3$, 300 K, 500 MHz): δ 10.18 (s, 1H), 9.13 (dd, J = 2.1, 0.8 Hz, 1H), 8.73 (ddd, J = 4.8, 1.8, 0.9 Hz, 1H), 8.62 (dd, J = 8.2, 0.6 Hz, 1H), 8.52 (dt, J = 8.0, 1.1 Hz, 1H), 8.29 (dd, J = 8.2, 2.1 Hz, 1H), 7.87 (ddd, J = 7.9, 7.6, 1.8 Hz, 1H), 7.39 (ddd, J = 7.5, 4.8, 1.2 Hz, 1H) ppm.

5,10,15-Tri([2,2'-bipyridin]-5-yl)-20-(pyridin-4-yl)porphyrinatozinc(II) (7)

Pyrrole and 4-pyridinecarboxaldehyde were distilled under reduced pressure before use. A 500 mL round-bottom flask was equipped with a reflux condenser and a magnetic stirring bar. To the flask were added **6** (2.772 g, 15.0 mmol, 2 eq) and $EtCO_2H$ (91 mL). The mixture was heated up to 140 °C, and then to the solution were added 4-pyridinecarboxaldehyde (0.708 mL, 7.52 mmol, 1.00 eq) and pyrrole (1.59 mL, 22.9 mmol, 3.05 eq). The mixture was stirred at 140 °C for 45 min under aerobic and dark conditions, and then cooled to room temperature. H_2O (182 mL) was added and the mixture was stood for 5 h. The precipitate was collected with suction, washed with H_2O and then CH_3OH, and dried in vacuo to give a purple solid (0.697 g) as a crude mixture of porphyrin derivatives.

A 2 L round-bottom flask was equipped with a magnetic stirring bar. To the flask were added the aforementioned mixture of porphyrin derivatives (0.697 g, 0.798 mmol as porphyrins, 1 eq), $CHCl_3$ (520 mL), CH_3OH (52 mL) and $Zn(OAc)_2 \cdot 2H_2O$ (1.493 g, 6.78 mmol, 8.5 eq to porphyrins). The mixture was stirred at room temperature for 4.5 h under dark conditions. To the flask was added a 50 mM EDTA·2Na aqueous solution (400 mL, 20 mmol), and the mixture was stirred for 30 min. The organic layer was separated, washed with a 50 mM EDTA·2Na aqueous solution (400 mL) and H_2O (400 mL × 2), dried over Na_2SO_4 and evaporated. The obtained solid was adsorbed onto neutral Al_2O_3 (4 g) by evaporation of a THF solution, and purified by neutral Al_2O_3 column chromatography (Merck 40–230 mesh, ϕ = 4 cm, H = 12 cm, THF/*n*-hexane/pyridine = 100:50:1 to 100:33:2, 100:17:2, 100:0:2). The late fractions were checked by ESI-MS to ensure exclusion of bis(4-pyridyl)porphyrin derivatives. The obtained solid was reprecipitated from $CHCl_3/CH_3OH$ = 10:1 adding acetone. The obtained solid was triturated in refluxing $CHCl_3$/acetone = 3:5 for 23 h. The resultant solid was dried in vacuo to afford **7** as a purple solid (215 mg, 0.236 mmol, 4.7%).

^{1}H NMR (DMSO-d_6, 300 K, 500 MHz): δ 9.51 (s, 1H), 9.42 (s, 2H), 9.01 (d, J = 4.5 Hz, 2H), 8.98 (d, J = 4.5 Hz, 2H), 8.84–8.79 (m, 6H), 8.72–8.67 (m, 6H), 8.60 (br, 2H), 7.99–7.92 (m, 3H), 7.50 (br, 2H), 7.45–7.40 (m, 3H), 6.32 (br, 2H) ppm.

^{13}C NMR (DMSO-d_6, 300 K, 126 MHz): δ 155.3, 154.5, 152.7, 150.5, 149.7, 149.7, 149.6, 149.6, 148.8, 148.0, 142.0, 138.6, 137.7, 132.3, 132.2, 132.2, 132.1, 129.4, 124.6, 121.0, 118.9, 118.1, 117.1, 117.0 ppm.

mp: > 400 °C.

HR-ESI-MS (positive, $CHCl_3/CH_3OH/HCO_2H$ = 10:1:1, Capillary voltage: 1500 V, Sample cone voltage: 80 V): $[\mathbf{7} \cdot H]^+$ ($C_{55}H_{34}N_{11}Zn$) *m/z* 912.224 (required, 912.228).

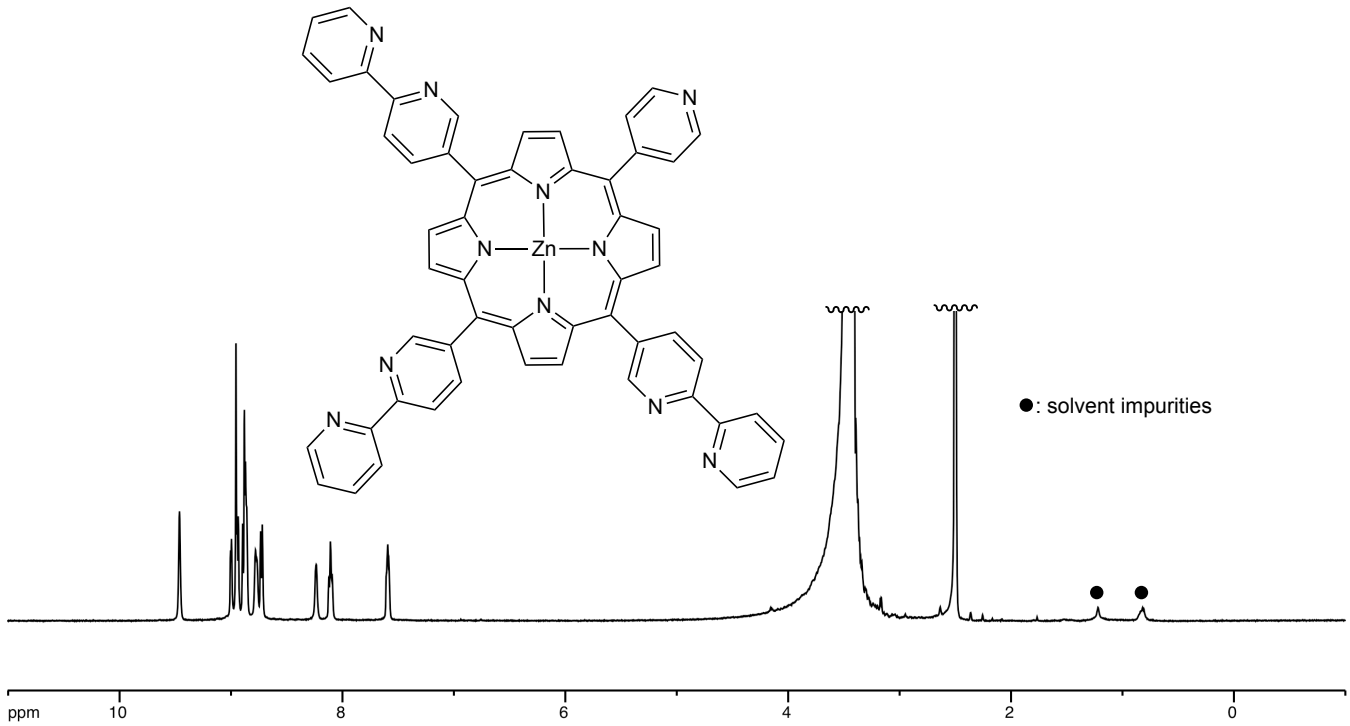

Figure 2-8-1. ^{1}H NMR spectrum of **7** (DMSO-d_6, 300 K, 500 MHz).

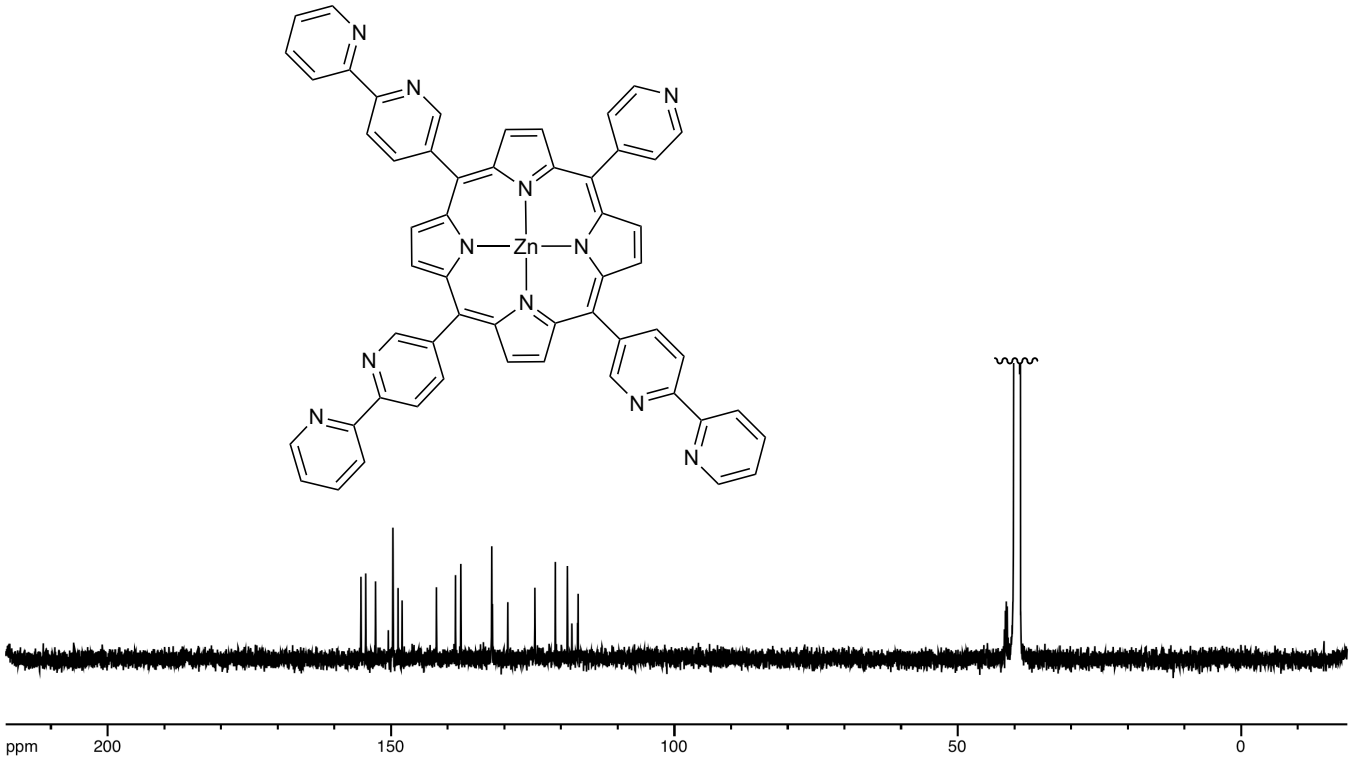

Figure 2-8-2. ^{13}C{^{1}H} NMR spectrum of **7** (DMSO-d_6, 300 K, 126 MHz)

1-Methyl-4-(10,15,20-tri([2,2'-bipyridin]-5-yl)porphyrinatozinc(II)-5-yl)pyridin-1-ium trifluoromethanesulfonate trihydrate (L1·OTf·3H_2O)

The solid compound **7** (0.215 g, 0.236 mmol, 1 eq) was evaporated from its $CHCl_3/CH_3OH$ = 10:1 solution to convert it into a film-like morphology for fast dissolution. A 30 mL pressure tube was equipped with a magnetic stirring bar. To the tube were added the aforementioned film-like solid of **7** (0.215 g, 0.236 mmol, 1 eq) dissolved in $CHCl_3/CH_3OH$ = 10:1 (20 mL) and MeI (1.47 mL, 23.6 mmol, 100 eq). The tube was sealed and heated at 30 °C for 24 h under dark conditions. The resultant solution was evaporated to dryness. The obtained solid was adsorbed onto neutral Al_2O_3 (1.25 g) by evaporation of a CH_2Cl_2/CH_3OH = 10:1 solution and purified by neutral Al_2O_3 column chromatography (Merck 40–230 mesh, ϕ = 4 cm, H = 12.5 cm, CH_2Cl_2/CH_3OH = 30:1 to 10:1 gradient). The resultant solid was dried in vacuo to afford crude **L1**·I as a green-purple solid (0.162 g, 0.153 mmol, 65%).

A 200 mL round-bottom flask was equipped with a magnetic stirring bar. To the flask were added the aforementioned solid of **L1**·I (0.162 g, 0.153 mmol, 1 eq), CH_2Cl_2/CH_3OH = 5:1 (53 mL), and AgOTf (44.5 mg, 0.173 mmol, 1.13 eq). The mixture was stirred at room temperature for 18 h under dark conditions. The resultant suspension was evaporated to give a dark solid. The obtained solid was extracted with CH_2Cl_2/CH_3OH = 5:1 (10 mL) by filtration and recrystallized by vapor diffusion of Et_2O. The solid was collected by suction and washed with Et_2O/CH_3OH = 10:1 and then Et_2O. This extraction-recrystallization sequence was repeated once again. The obtained solid was extracted again by centrifugation to strictly exclude any insoluble particles and recrystallized again. The resultant solid was dried in vacuo at 100 °C for 24 h to afford **L1**·OTf·3H_2O as a purple solid (0.154 g, 0.136 mmol, 57% from **7**).

^{1}H NMR ($CDCl_3/CD_3OD$ = 1:1, 300 K, 500 MHz): δ 9.49 (s, 3H), 9.27 (d, J = 6.4 Hz, 2H), 9.08 (d, J = 4.7 Hz, 2H), 9.03 (d, J = 4.7 Hz, 2H), 9.02 (d , J = 4.7 Hz, 2H), 8.96 (d, J = 4.7 Hz, 2H), 8.89 (d, J = 6.5 Hz, 2H), 8.85 (t, J = 4.3 Hz, 3H), 8.80 (d, J = 8.0 Hz, 3H), 8.77 (d, J = 7.9 Hz, 3H), 8.67 (d, J = 7.8 Hz, 3H), 8.11–8.07 (m, 3H), 7.59–7.56 (m, 3H), 4.78 (s, 3H) ppm.

^{13}C NMR ($CDCl_3/CD_3OD$ = 1:1, 300 K, 126 MHz): δ162.0, 156.3, 156.3, 155.7, 155.7 153.46, 153.43, 151.5, 151.01, 150.84, 149.91, 149.89, 148.8, 143.5, 142.8, 142.8, 139.54, 139.52, 138.4, 138.4, 133.82, 133.63, 133.1, 132.8, 131.1, 125.02, 125.01, 122.6, 122.6, 120.24, 120.21, 119.3, 118.3, 113.3, 48.4 ppm. The resonance from the carbon of TfO^- anion was not observed, probably due to the slow relaxation and splitting by coupling with the ^{19}F nuclei.

^{19}F NMR ($CDCl_3/CD_3OD$ = 1:1, 300 K, 471 MHz): δ -79.2 ppm.

m.p.: > 400 °C.

IR: 574.683 (CF_3), 637.358, 717.39, 750.174, 790.671, 862.989, 993.16, 1029.8, 1066.44, 1157.08 (CF_3), 1206.26, 1222.65 (CF_3), 1254.47, 1339.32, 1367.28, 1433.82, 1457.92, 1525.42, 1546.63, 1571.7,

1587.13, 1636.3 (H_2O), 3053.73 (C-H), 3378.67 (broad, H_2O) cm^{-1}.

HR-ESI-MS (positive, CH_2Cl_2/CH_3OH = 1:5, Capillary voltage: 250 V, Sample cone voltage: 80 V): [**L1**]$^+$ ($C_{56}H_{36}N_{11}Zn^+$) *m/z* 926.245 (required, 926.244).

HR-ESI-MS (negative, CH_2Cl_2/CH_3OH = 1:5, Capillary voltage: 100 V, Sample cone voltage: 60 V): [OTf]$^-$ ($CF_3O_3S^-$) *m/z* 148.951 (required, 148.953).

Elemental analysis (calcd., found for $C_{57}H_{42}F_3N_{11}O_6SZn$ [**L**·OTf·3H_2O]): C (60.51, 60.77), H (3.74, 3.72), N (13.62, 13.61).

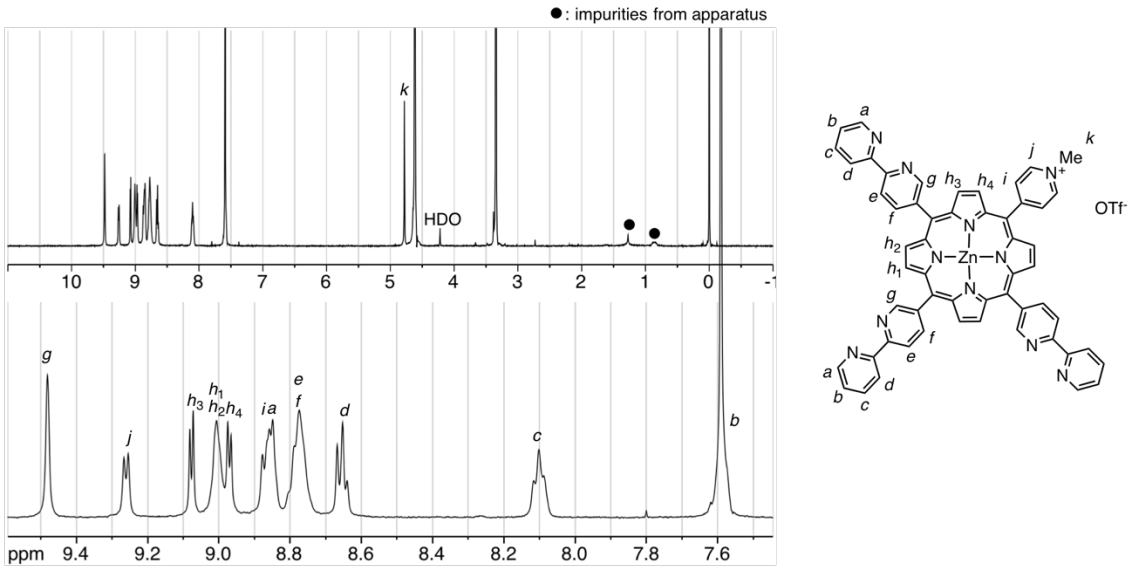

Figure 2-8-3. ^{1}H NMR spectrum of **L1**·OTf·3H_2O ($CDCl_3/CD_3OD$ = 1:1, 300 K, 500 MHz)

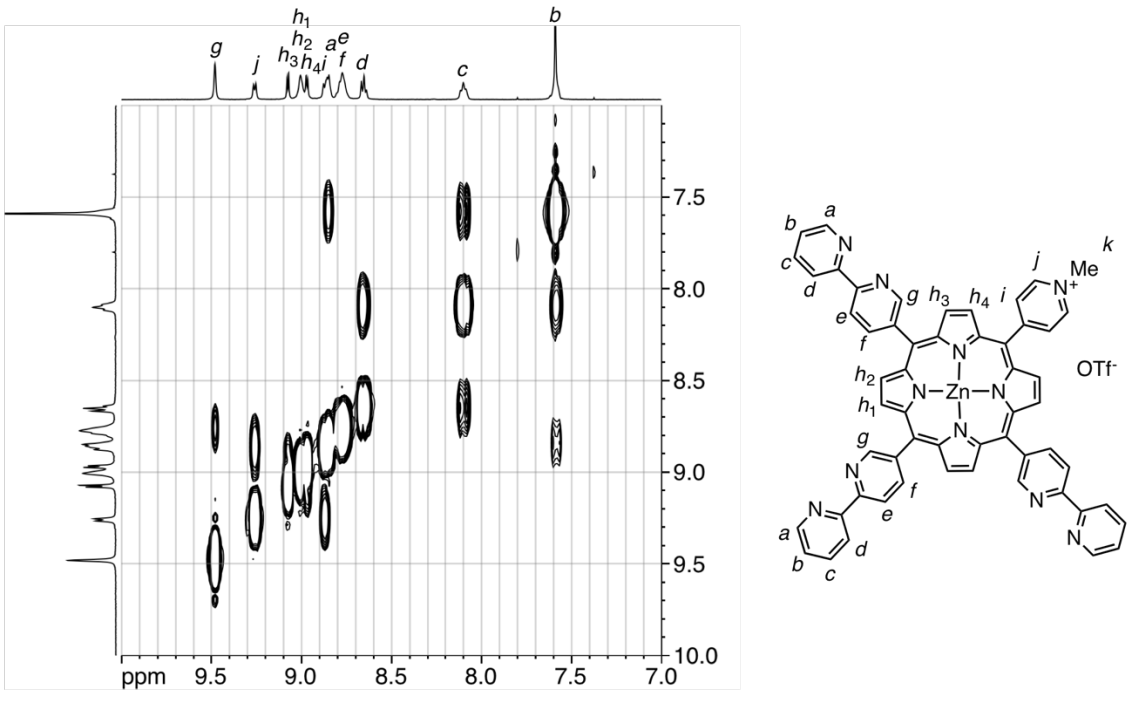

Figure 2-8-4. ^{1}H-^{1}H COSY NMR spectrum of **L**·OTf·3H_2O ($CDCl_3/CD_3OD$ = 1:1, 300 K, 500 MHz)

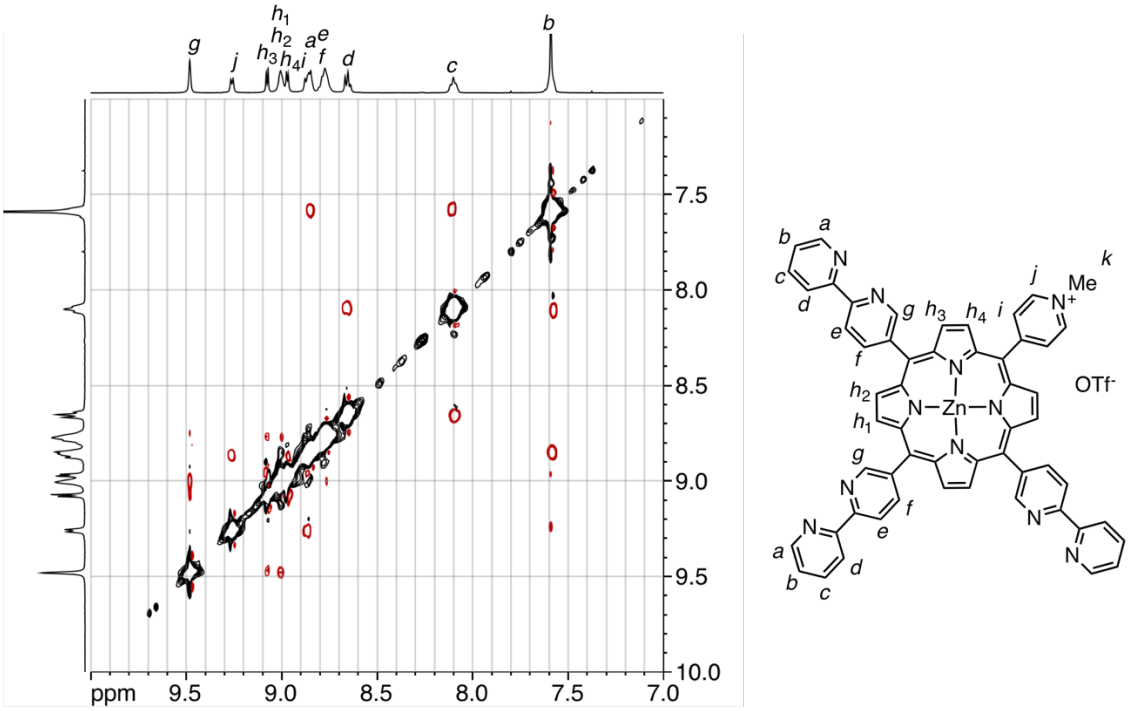

Figure 2-8-5. ^{1}H-^{1}H ROESY NMR spectrum of **L**·OTf·3H_2O ($CDCl_3$/CD_3OD = 1:1, 300 K, 500 MHz)

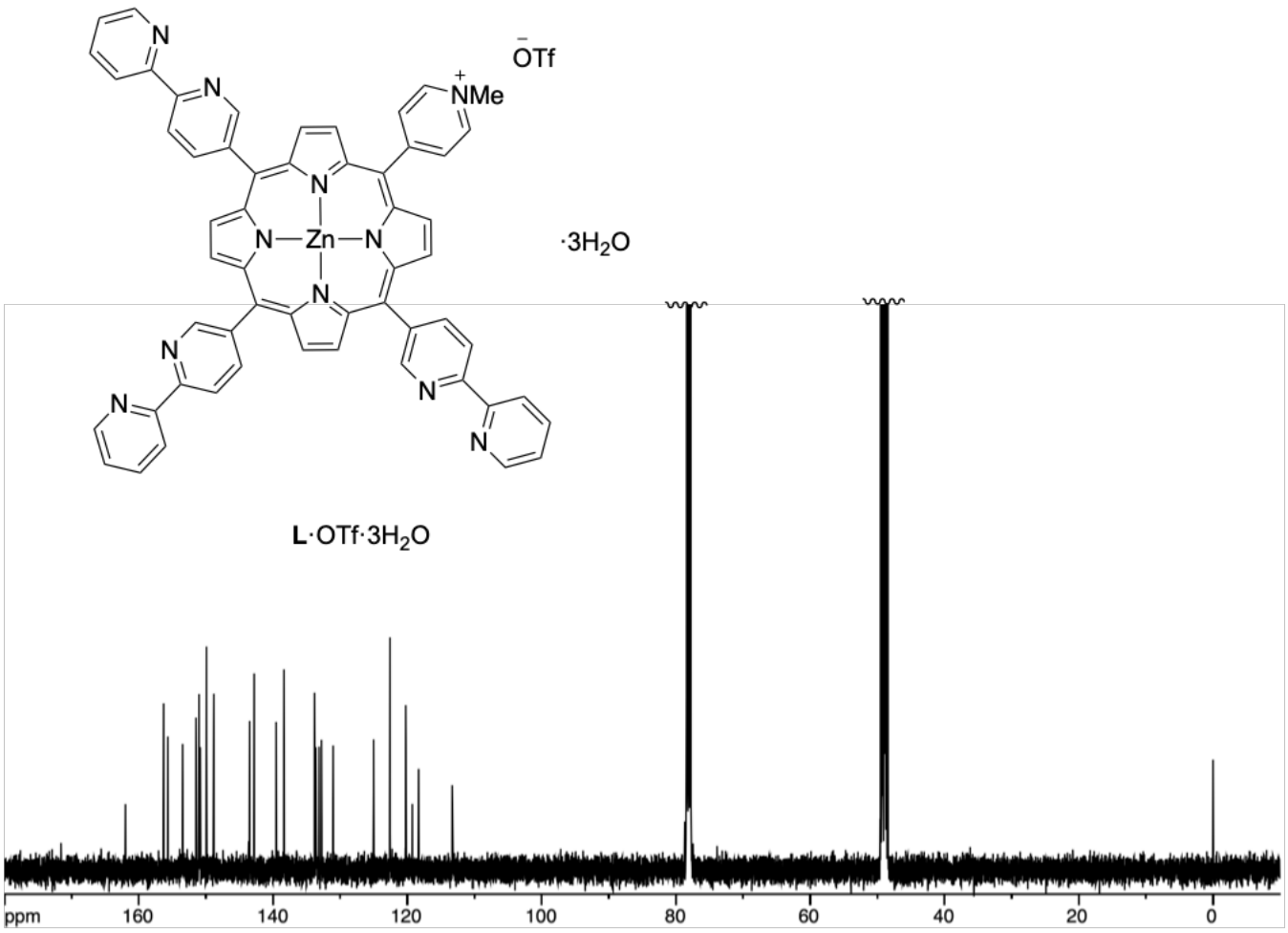

Figure 2-8-6. ^{13}C{^{1}H} NMR spectrum of **L1**·OTf·3H_2O ($CDCl_3$/CD_3OD = 1:1, 300 K, 126 MHz)

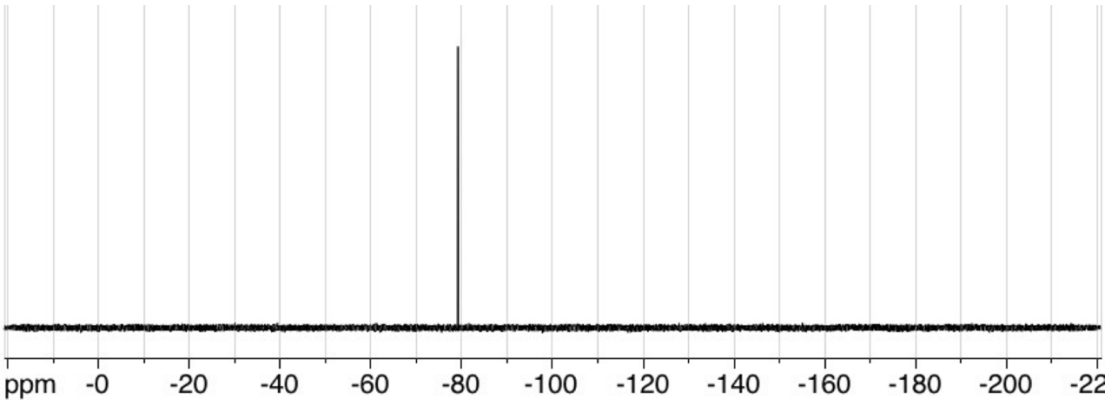

Figure 2-8-7. ^{19}F NMR spectrum of **L1**·OTf·3H_2O ($CDCl_3$/CD_3OD = 1:1, 300 K, 471 MHz)

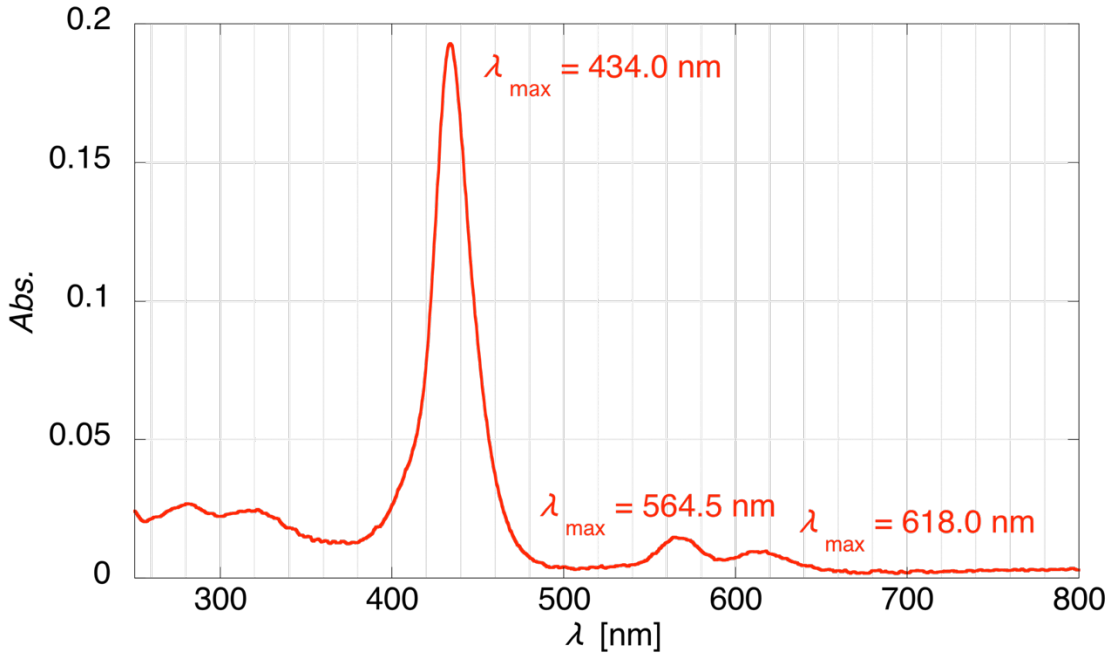

Figure 2-8-8. UV–vis absorption spectrum of **L1**·OTf·3H_2O (CH_3CN, 1.0 μM, 293 K, l = 1.0 cm).

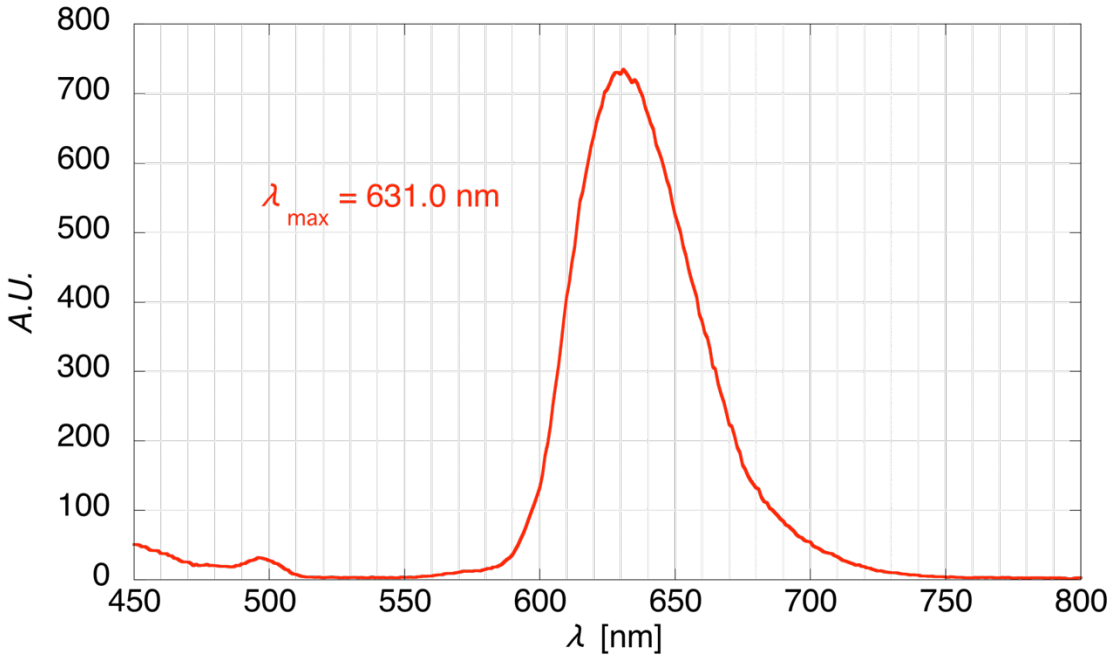

Figure 2-8-9. UV–vis emission spectrum of **L1**·OTf·3H_2O (CH_3CN, 1.0 μM, 293 K, l = 1.0 cm, λ_{ex} = 434 nm). The solvent used for the measurement was air-saturated.

$Co^{II}(OTf)_2 \cdot 6H_2O$

This compound was prepared according to a reported procedure.[37] The product purity was confirmed by elemental analysis.

Elemental analysis (calcd., found for $C_2H_{12}CoF_6O_{12}S_2$ [$Co(OTf)_2 \cdot 6H_2O$]): C (5.16, 5.16), H (2.60, 2.63), N (0.00, 0.00).

1-Co^{II}_4

To an NMR tube were added a suspension of **L1**·OTf·3H_2O (0.500 μmol, 1 eq) in CD_3CN (100 μL), D_2O (25.0 μL), a solution of $Co(OTf)_2 \cdot 6H_2O$ in CD_3CN (30.0 μL, 0.667 μmol, 22.2 mM, 1.33 eq) and CD_3CN (345 μL). The mixture was heated at 70 °C for 4 days.

The yield was estimated to be 65% using *p*-dimethoxybenzene as an internal standard in ^1H NMR.

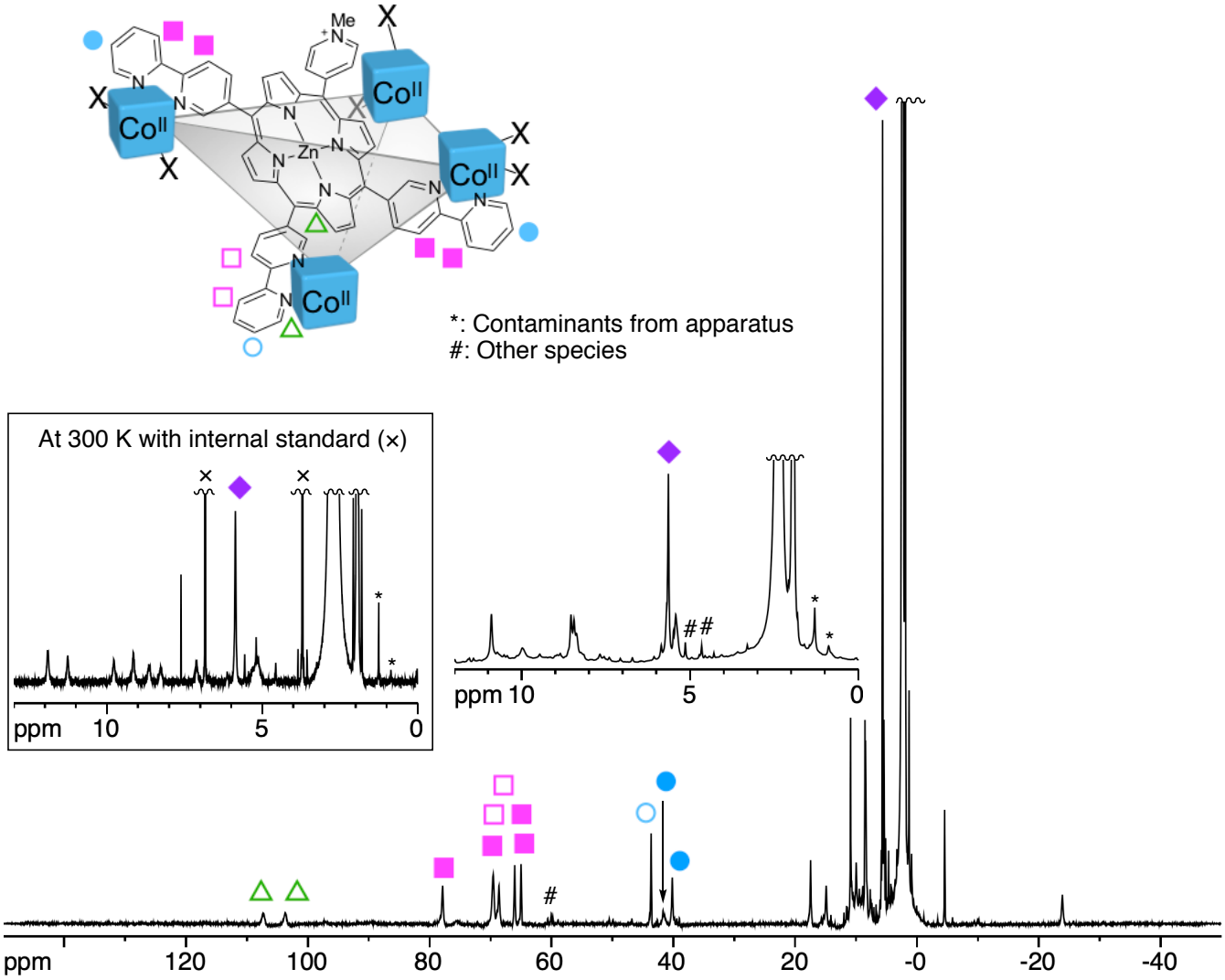

Figure 2-8-10. Paramagnetic ^1H NMR spectrum of the resultant solution containing **1-Co^{II}_4** (CD_3CN/D_2O = 19:1, 300 K, 500 MHz). The right inset shows a magnified diamagnetic region. The left inset shows the normal measurement at 300 K with *p*-dimethoxybenzene as an internal standard for the yield determination.

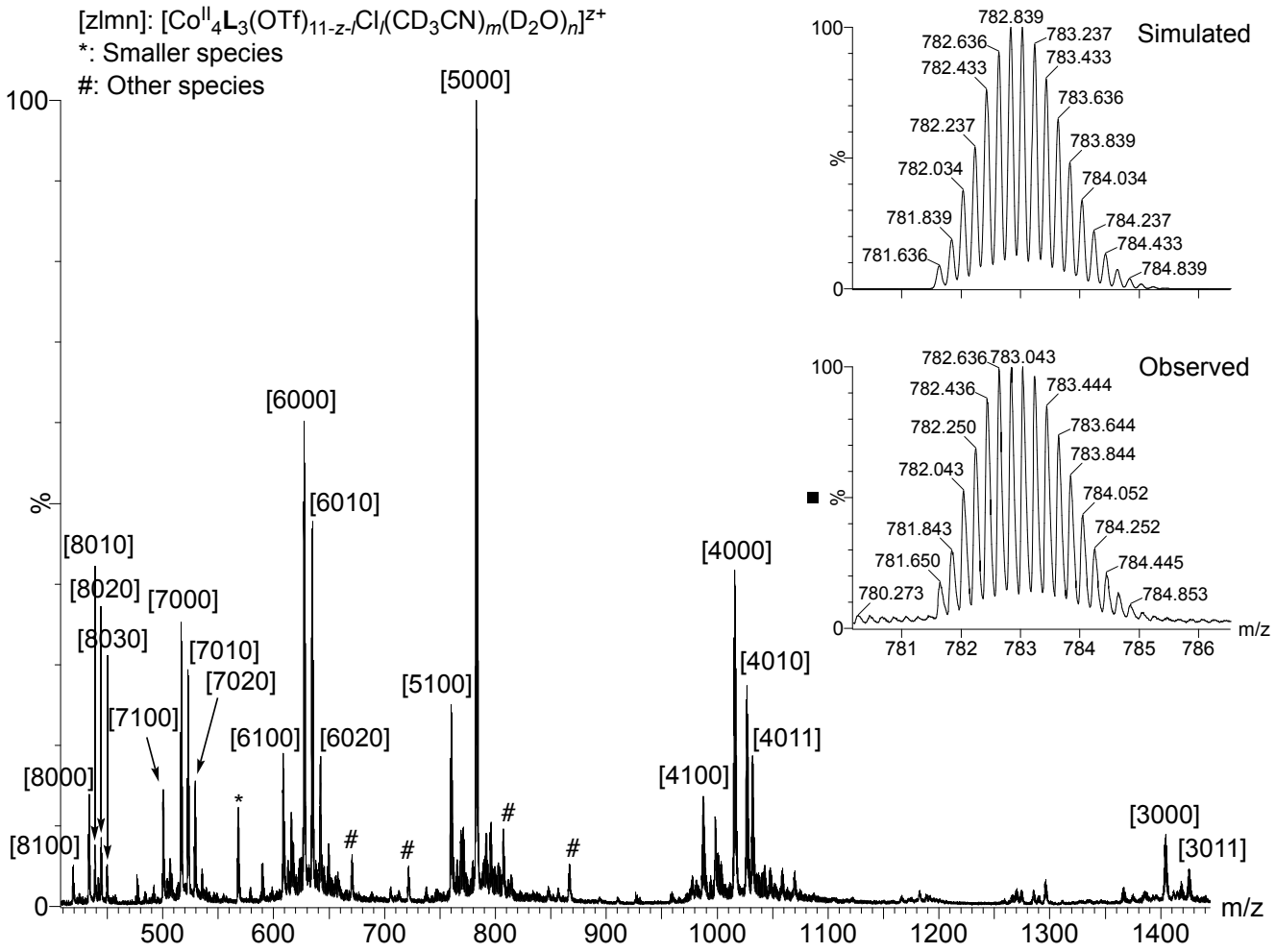

Figure 2-8-11. ESI-MS spectrum of the resultant solution containing **1-Co$^{II}_4$** (CD_3CN/D_2O = 19:1, positive, Capillary voltage: 1200 V, Sample cone voltage: 80 V). The chloride ions are supposed to come from the ESI-MS apparatus. The smaller species may be a product of fragmentation under the measurement condition. Inset shows comparison of simulated and observed isotope patterns for the signal of $[Co^{II}_4\mathbf{L1}_3(OTf)_6]^{5+}$.

2-$Co^{III}Co^{II}_3$

To a solution of **1-Co^{II}_4** prepared in the above-mentioned procedure was added a solution of $(NH_4)_2[Ce(NO_3)_6]$ in CD_3CN (10.0 μL, 0.167 μmol, 16.7 mM, 0.333 eq to **L1**). The mixture was kept at room temperature for 2 days.

The yield from **1-Co^{II}_4** was estimated to be 83% using *p*-dimethoxybenzene as an internal standard in ^1H NMR. The amount of remaining **1-Co^{II}_4** was also estimated to be 14% in the same manner.

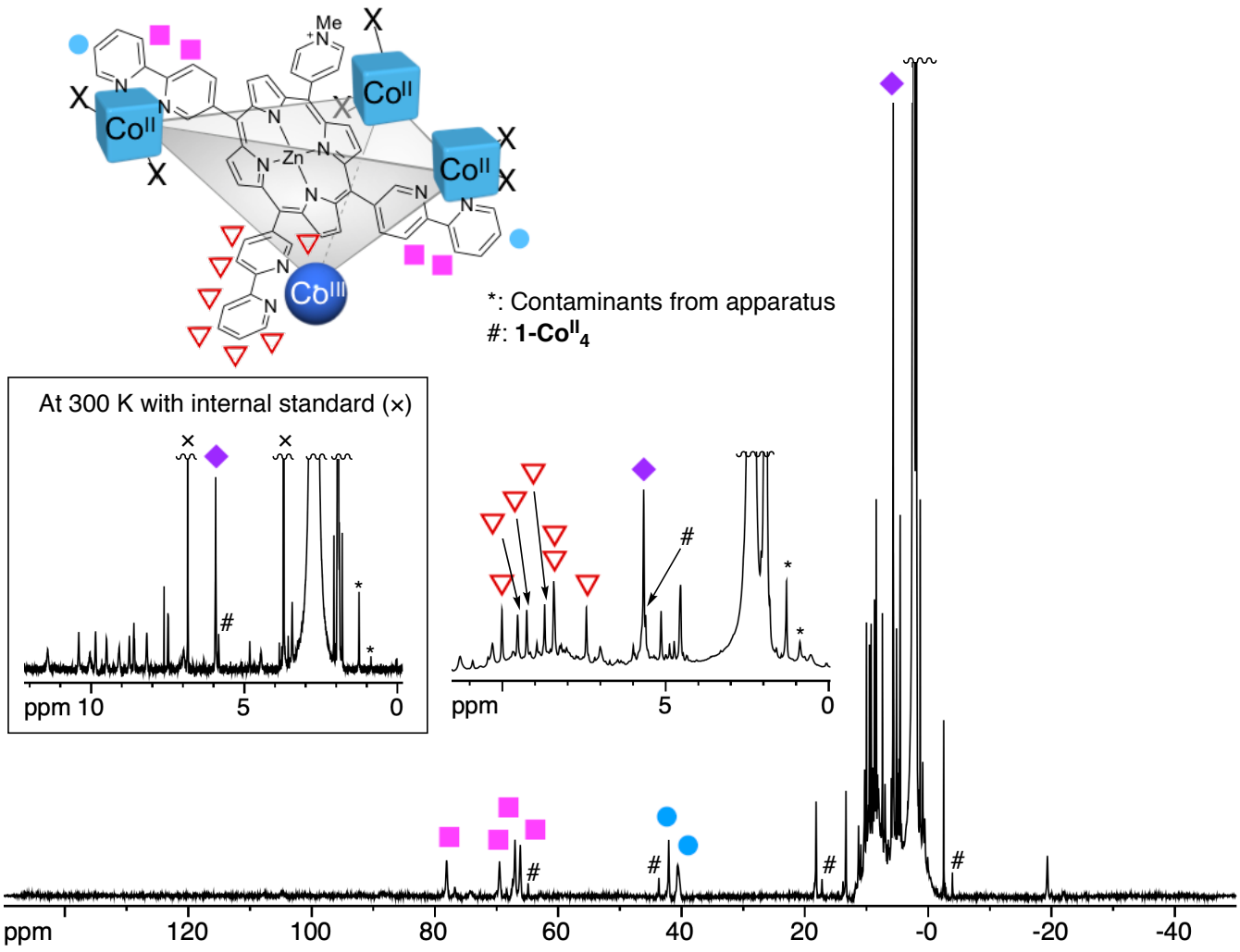

Figure 2-8-12. Paramagnetic ^1H NMR spectrum of the resultant solution containing **2-$Co^{III}Co^{II}_3$** (CD_3CN/D_2O = 19:1, 300 K, 500 MHz). The right inset shows a magnified diamagnetic region. The left inset shows the normal measurement at 300 K with *p*-dimethoxybenzene as an internal standard for the yield determination.

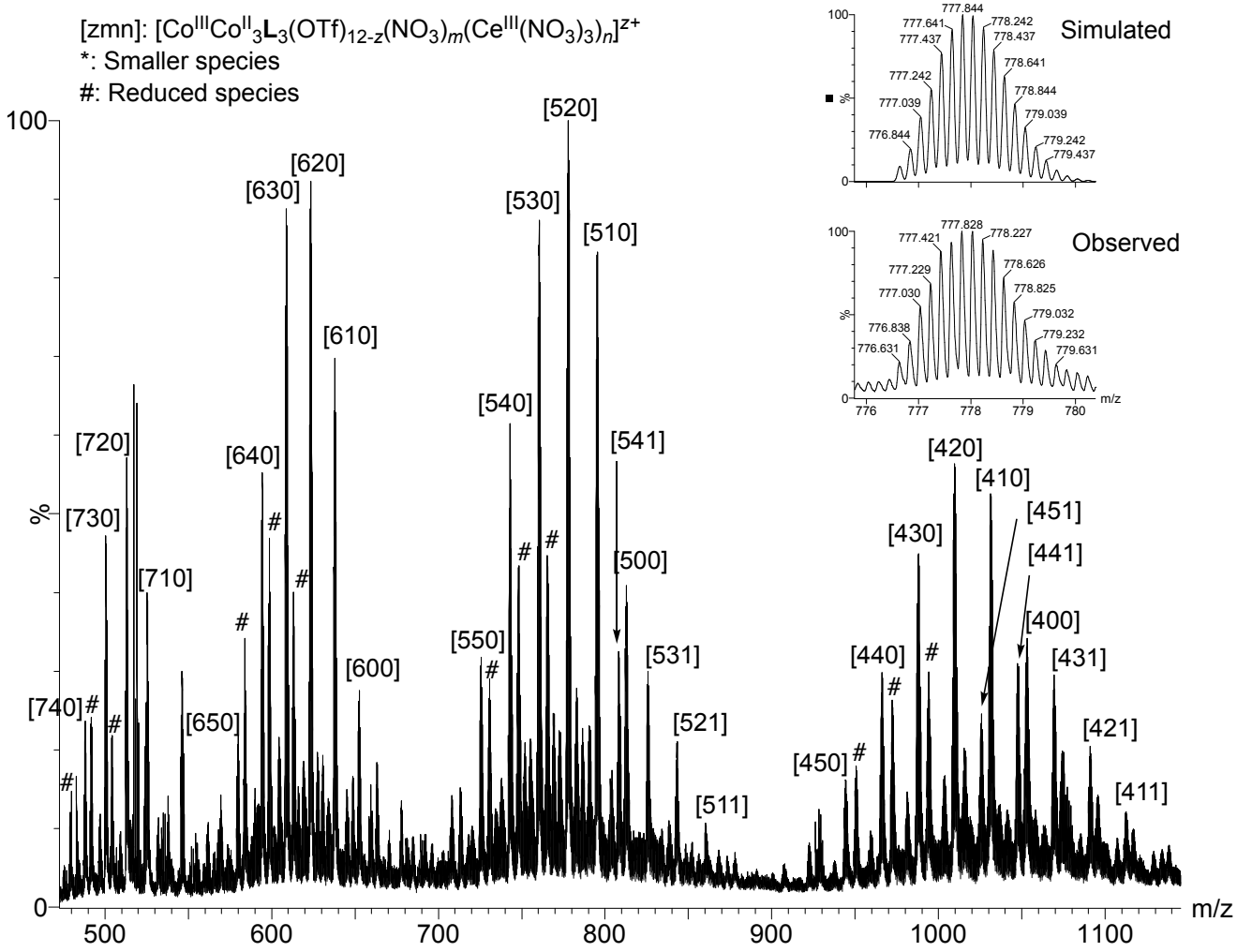

Figure 2-8-13. ESI-MS spectrum of the resultant solution containing **2-Co^{III}Co$^{II}_3$** (CD_3CN/D_2O = 19:1, positive, Capillary voltage: 3000 V, Sample cone voltage: 60 V). The reduced species may be a product of reduction under the measurement condition.[46] Inset shows the comparison of simulated and observed isotope patterns for the signal of $[Co^{III}Co^{II}_3\mathbf{L1}_3(NO_3)_2(OTf)_5]^{5+}$.

3-$Co^{III}Ni^{II}_3$

To a solution of **2-$Co^{III}Co^{II}_3$** prepared in the above-mentioned procedure was added a solution of $Ni(OTf)_2$ in CD_3CN/D_2O = 9:1 (20.0 μL, 1.00 μmol, 50.0 mM, 2.00 eq to **L1**). The mixture was heated at 70 °C for 3 days.

The yield from **1-Co^{II}_4** was estimated to be 97% in two steps using *p*-dimethoxybenzene as an internal standard in ^{1}H NMR.

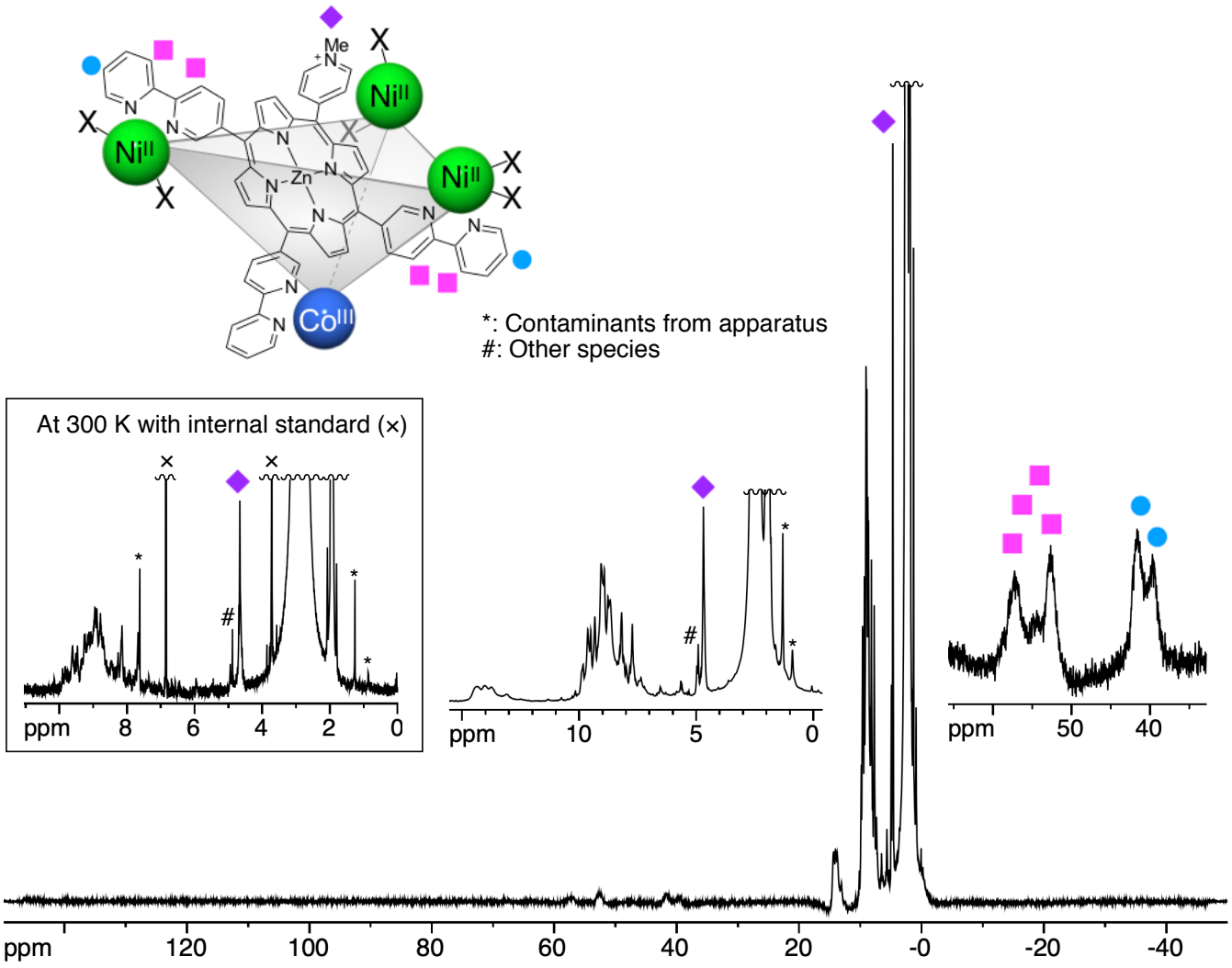

Figure 2-8-14. Paramagnetic ^{1}H NMR spectrum of the resultant solution containing **3-$Co^{III}Ni^{II}_3$** (CD_3CN/D_2O = 19:1, 343 K, 500 MHz). The right inset shows a magnified paramagnetic region with weakened baseline correction to clarify the broadened signals. The middle inset shows a magnified diamagnetic region. The left inset shows the normal measurement at 300 K with *p*-dimethoxybenzene as an internal standard for the yield determination.

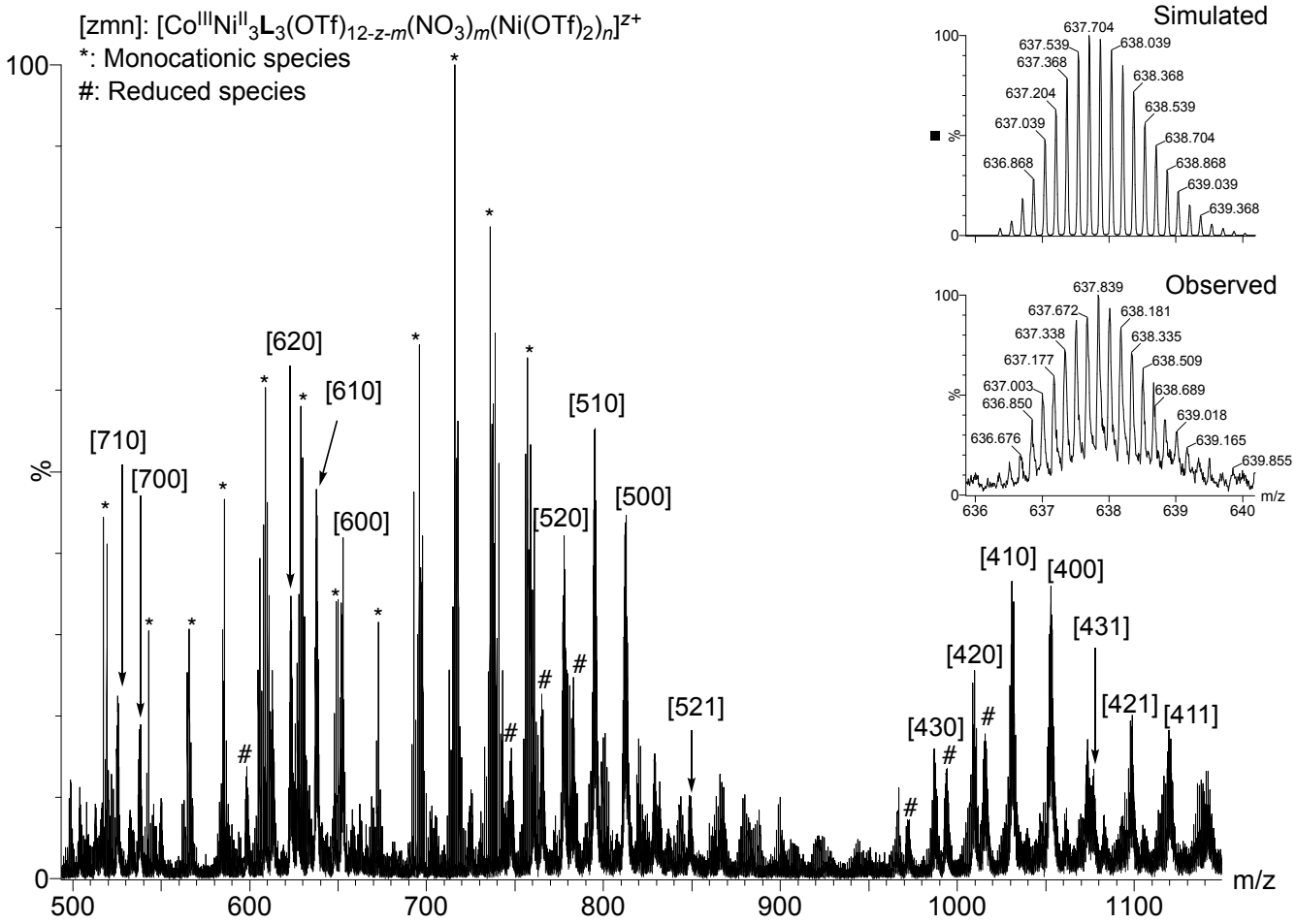

Figure 2-8-15. ESI-MS spectrum of the resultant solution containing **3-Co^{III}Ni$^{II}_3$** (CD_3CN/D_2O = 19:1, positive, Capillary voltage: 3000 V, Sample cone voltage: 60 V). The monocationic species are supposed to come from excess Ni^{II} and byproducts Co^{II} and Ce^{III}. The reduced species may be a product of reduction under the measurement condition.[46] Inset shows the comparison of simulated and observed isotope patterns for the signal of $[Co^{III}Ni^{II}_3\mathbf{L1}_3(NO_3)(OTf)_5]^{6+}$.

For XPS measurement and improved synthesis of **4-Co^{II}Ni$^{II}_3$**, the following procedure was added: The resultant solution was evaporated to dryness. The obtained solid was re-dissolved in a mixed solvent of CH_3CN (150 μL) and H_2O (50 μL). To the solution was added an aqueous solution of NH_4PF_6 (250 μL, 25.0 μmol, 100 mM, 50.0 eq to **L1**). The formed precipitate was collected and washed with H_2O (800 μL x 2) by centrifugation. The solid was dissolved in dry CH_3CN (500 μL) and all the volatiles were removed under reduced pressure.

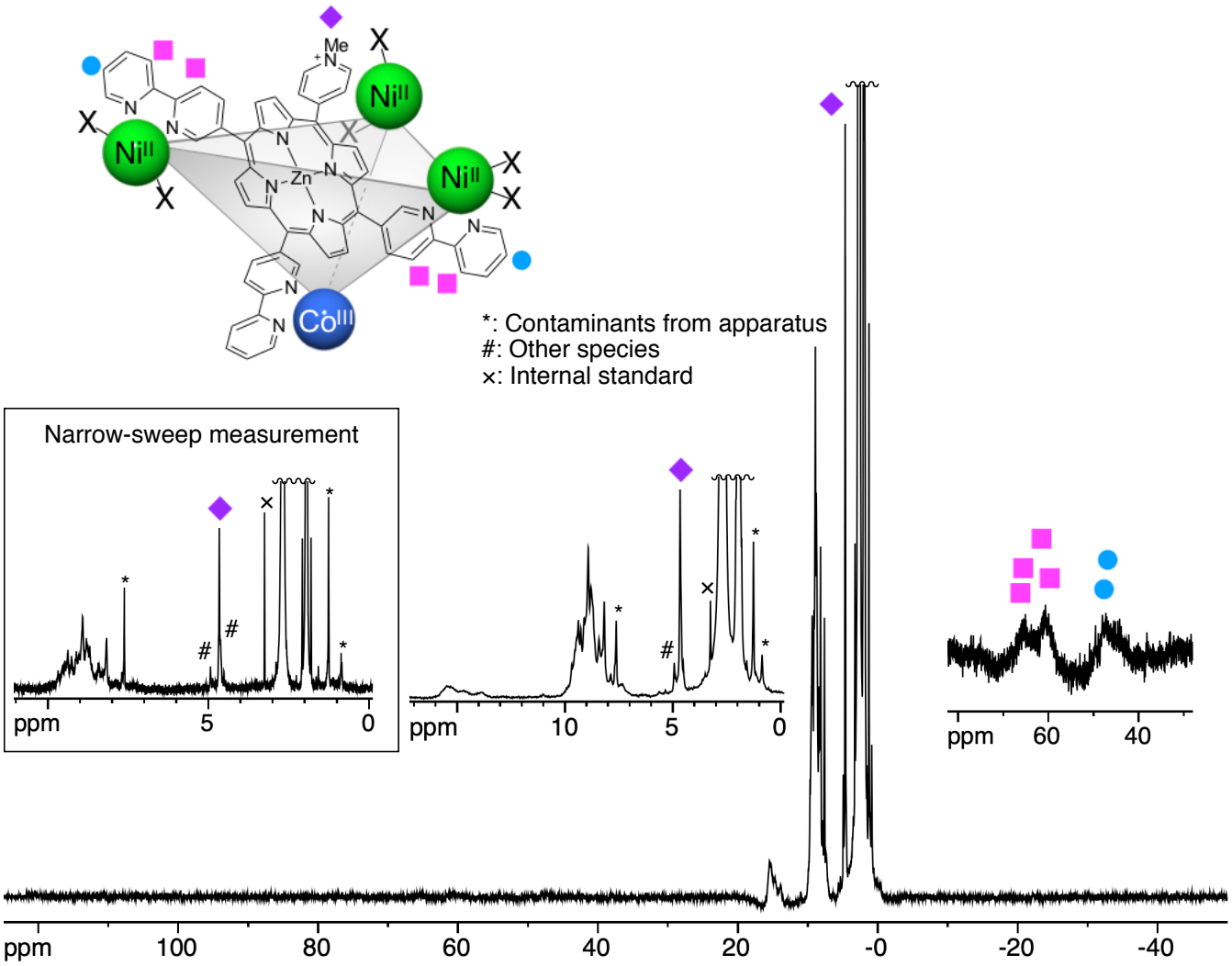

Figure 2-8-16. Paramagnetic ^{1}H NMR spectrum of the resultant solid containing **3-Co^{III}Ni$^{II}_3$** (CD_3CN/D_2O = 20:1, 300 K, 500 MHz). MeOH was added as an internal standard for the yield determination of **4-Co^{II}Ni$^{II}_3$**. The right inset shows a magnified paramagnetic region with weakened baseline correction to clarify the broadened signals. The middle inset shows a magnified diamagnetic region. The left inset shows the normal measurement for the yield determination of **4-Co^{II}Ni$^{II}_3$**.

[zlmn]: $[Co^{III}Ni^{II}_3\mathbf{L}_3(PF_6)_{12-z-l}F_l(CH_3CN)_m(Z)_n]^{z+}$ (Z = Unknown compound with mass 80 Da)
*: Other species
#: Reduced species

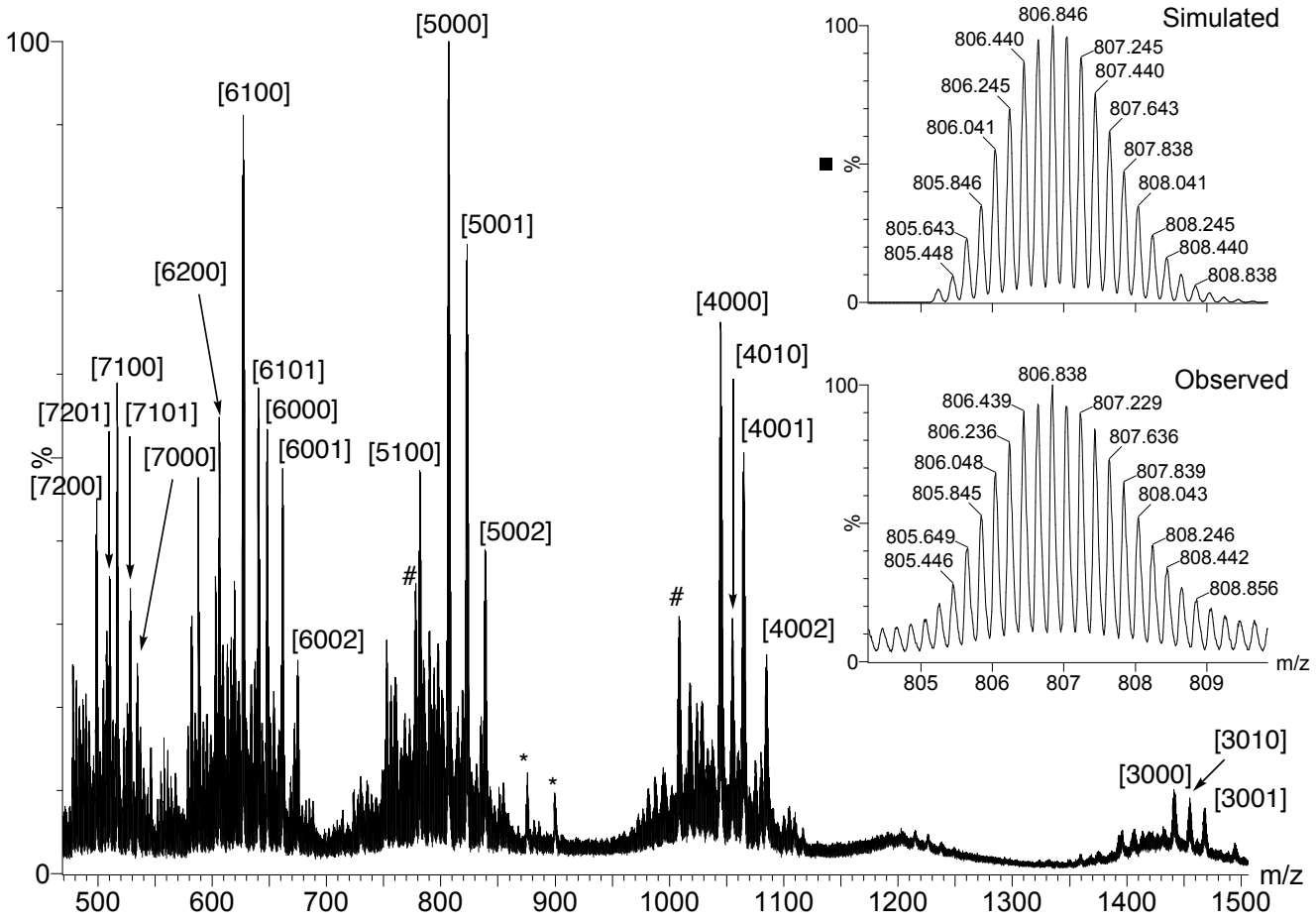

Figure 2-8-17. ESI-MS spectrum of the resultant solid containing **3-$Co^{III}Ni^{II}_3$** (CH_3CN, positive, Capillary voltage: 3000 V, Sample cone voltage: 80 V). The unknown compound Z is supposed to come from the ESI-MS apparatus. The fluoride ions are supposed to be a decomposition product of PF_6^- under the measurement condition. The reduced species may be a product of reduction under the measurement condition.[46] The right inset shows the comparison of simulated and observed isotope patterns for the signal of $[Co^{III}Ni^{II}_3\mathbf{L1}_3(PF_6)_7]^{5+}$.

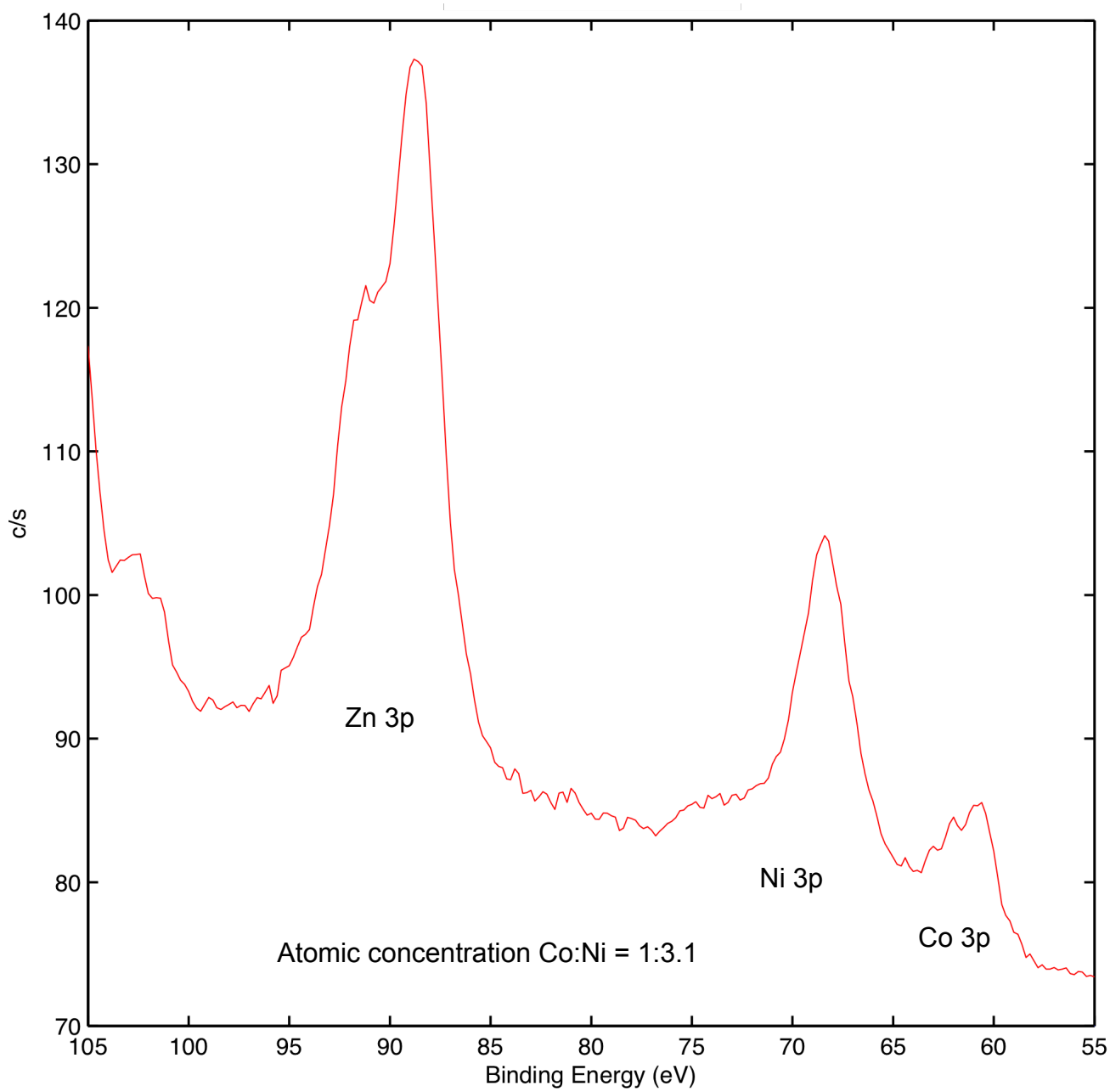

Figure 2-8-18. Core-level XPS spectrum of the resultant solid containing **3-$Co^{III}Ni^{II}_3$**

4-$Co^{II}Ni^{II}_3$

Initial attempt: To a solution of **3-$Co^{III}Ni^{II}_3$** prepared in the above-mentioned procedure was added a solution of $^{n}Bu_4N{\cdot}I$ in CD_3CN (37.5 μL, 0.750 μmol, 20.0 mM, 1.50 eq to **L1**). The mixture was heated at 70 °C for 8 h. The yield from **3-$Co^{III}Ni^{II}_3$** was estimated to be 48% using *p*-dimethoxybenzene as an internal standard in ^{1}H NMR.

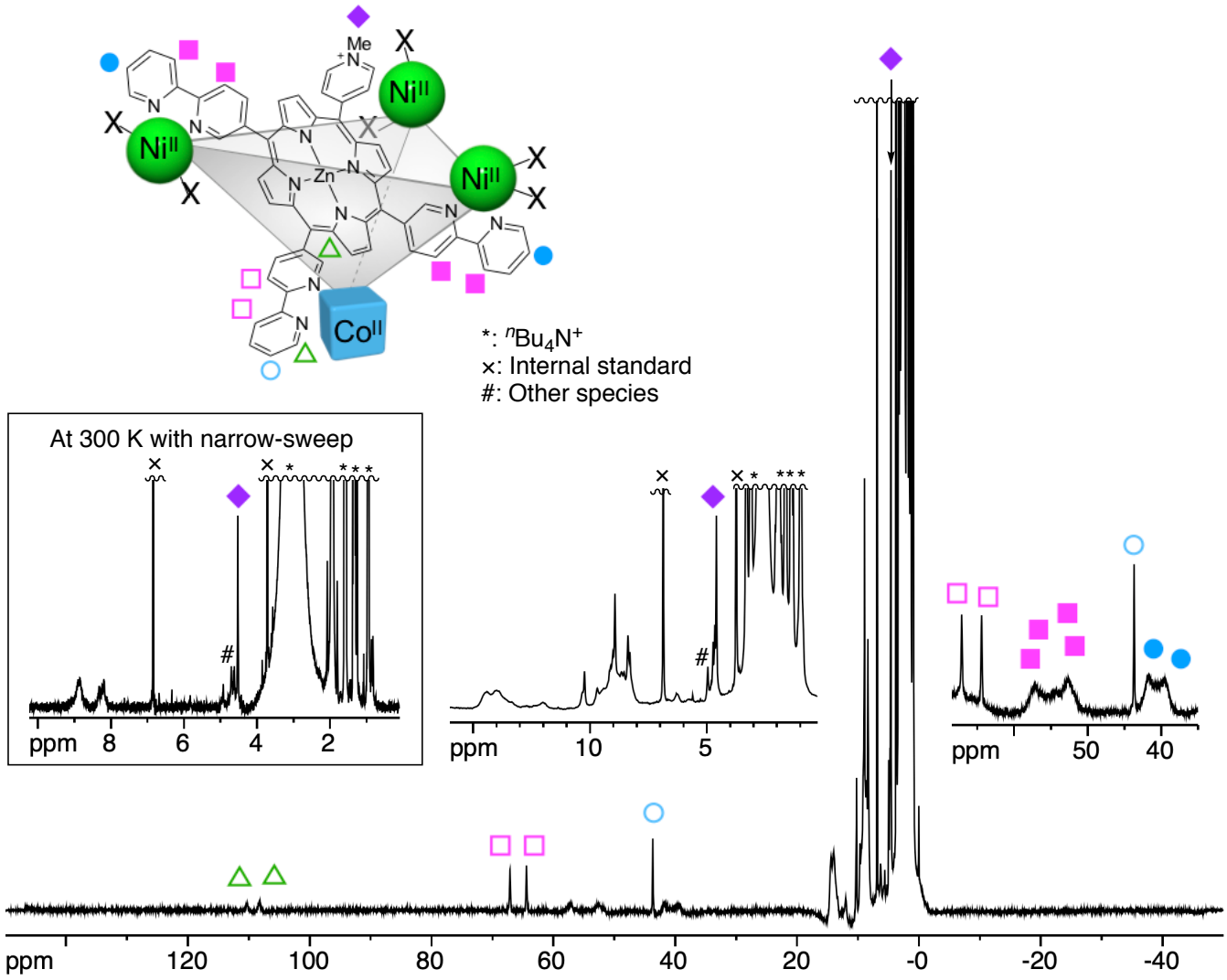

Figure 2-8-19. Paramagnetic ^{1}H NMR spectrum of the resultant solution containing **4-$Co^{II}Ni^{II}_3$** (CD_3CN/D_2O = 19:1, 343 K, 500 MHz). The right inset shows a magnified paramagnetic region with weakened baseline correction to clarify the broadened signals. The middle inset shows a magnified diamagnetic region. The left inset shows the normal measurement for the yield determination.

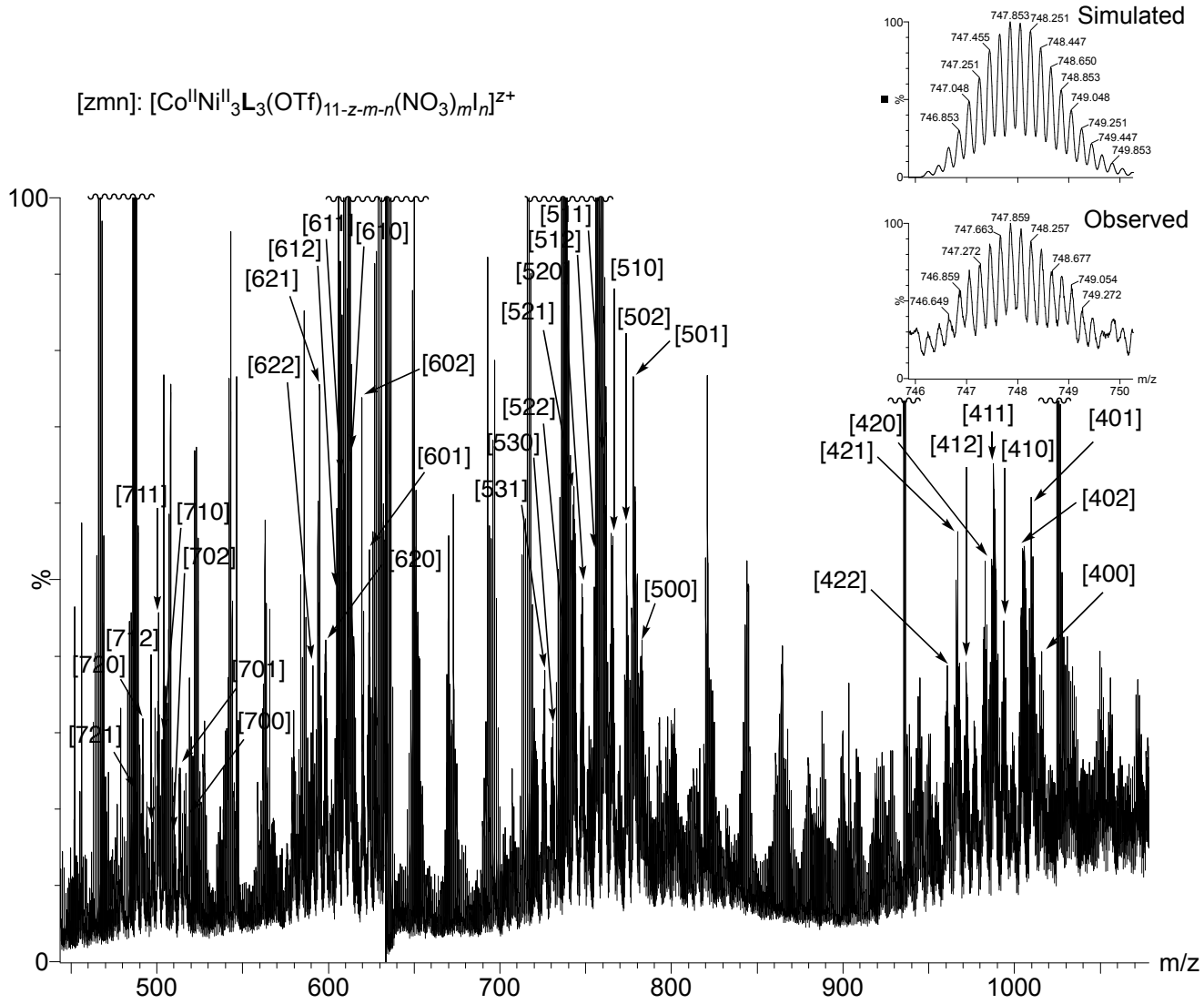

Figure 2-8-20. ESI-MS spectrum of the resultant solution containing **4-Co^{II}Ni$^{II}_3$** (CD_3CN/D_2O = 19:1, positive, Capillary voltage: 3000 V, Sample cone voltage: 80 V). Numerous monocationic species were observed, presumably because of the excess Ni^{II} and byproducts $^{n}Bu_4N^+$, Co^{II}, and Ce^{III}. The right inset shows the comparison of simulated and observed isotope patterns for the signal of $[Co^{II}Ni^{II}_3\mathbf{L1}_3(NO_3)_2(OTf)_4]^{5+}$.

Improved procedure: The purified sample of **3-Co^{III}Ni$^{II}_3$** prepared in the above-mentioned procedure was dissolved in a mixed solvent of CD_3CN (500 μL) and H_2O (25.0 μL). To the solution was added a solution of ^{n}Bu$_4$N·I in CD_3CN (12.5 μL, 0.625 μmol, 50.0 mM, 0.417 eq to the initial amount of **L1**). The reaction mixture was heated at 70 °C for 2 days. The yield from **3-Co^{III}Ni$^{II}_3$** was estimated to be 95% using CH_3OH as an internal standard in ^{1}H NMR.

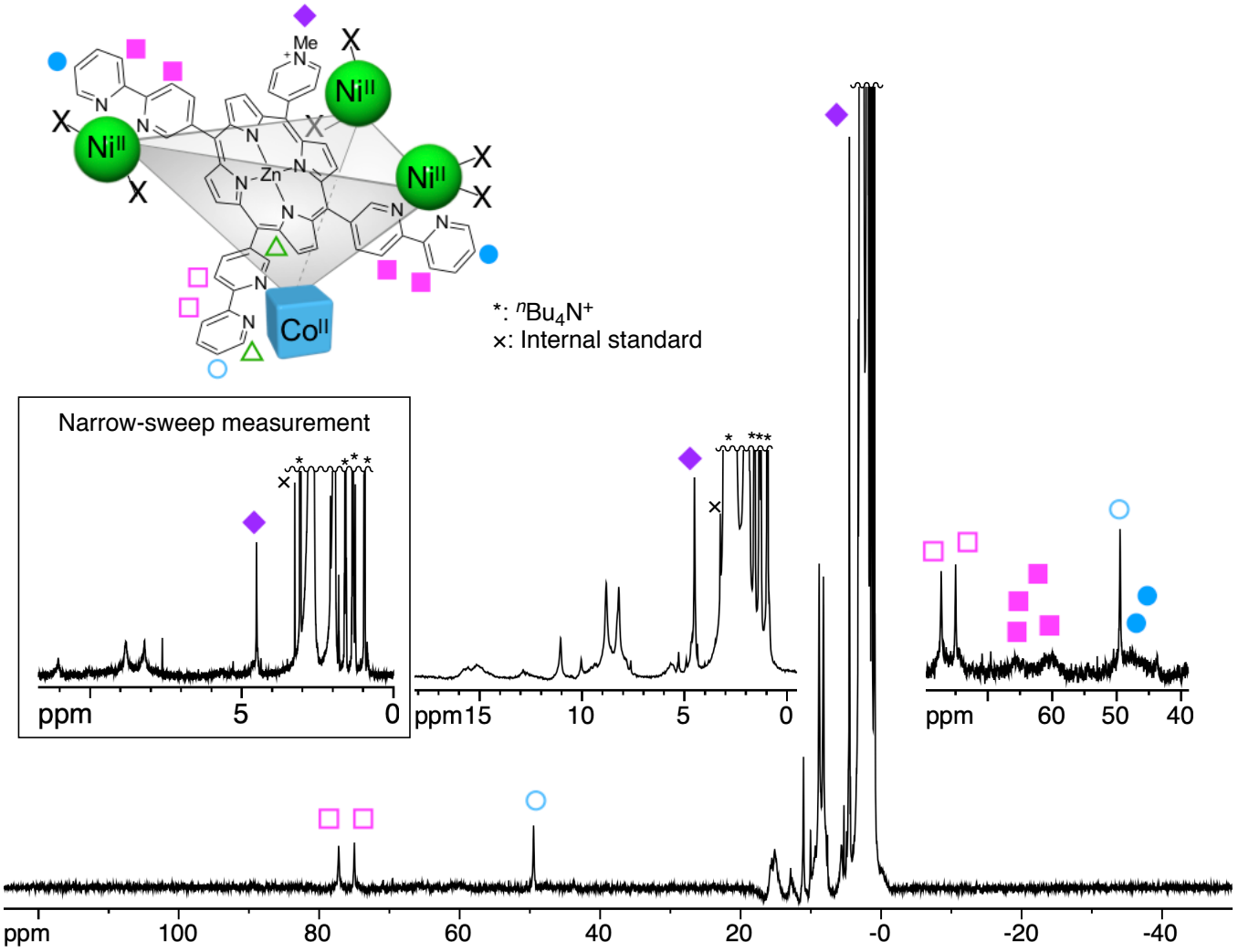

Figure 2-8-21. Paramagnetic ^{1}H NMR spectrum of the resultant solution containing **4-Co^{II}Ni$^{II}_3$** in the improved procedure (CD_3CN/D_2O = 20:1, 300 K, 500 MHz). The right inset shows a magnified paramagnetic region with weakened baseline correction to clarify the broadened signals. The middle inset shows a magnified diamagnetic region. The left inset shows the normal measurement for the yield determination.

[zlmno]: $[Co^{II}Ni^{II}{}_3\mathbf{L}_3(PF_6)_{11-z-l-m}F_lI_m(CD_3CN)_n(^nBu_4N{\cdot}NO_3)_o]^{z+}$-$d_1$

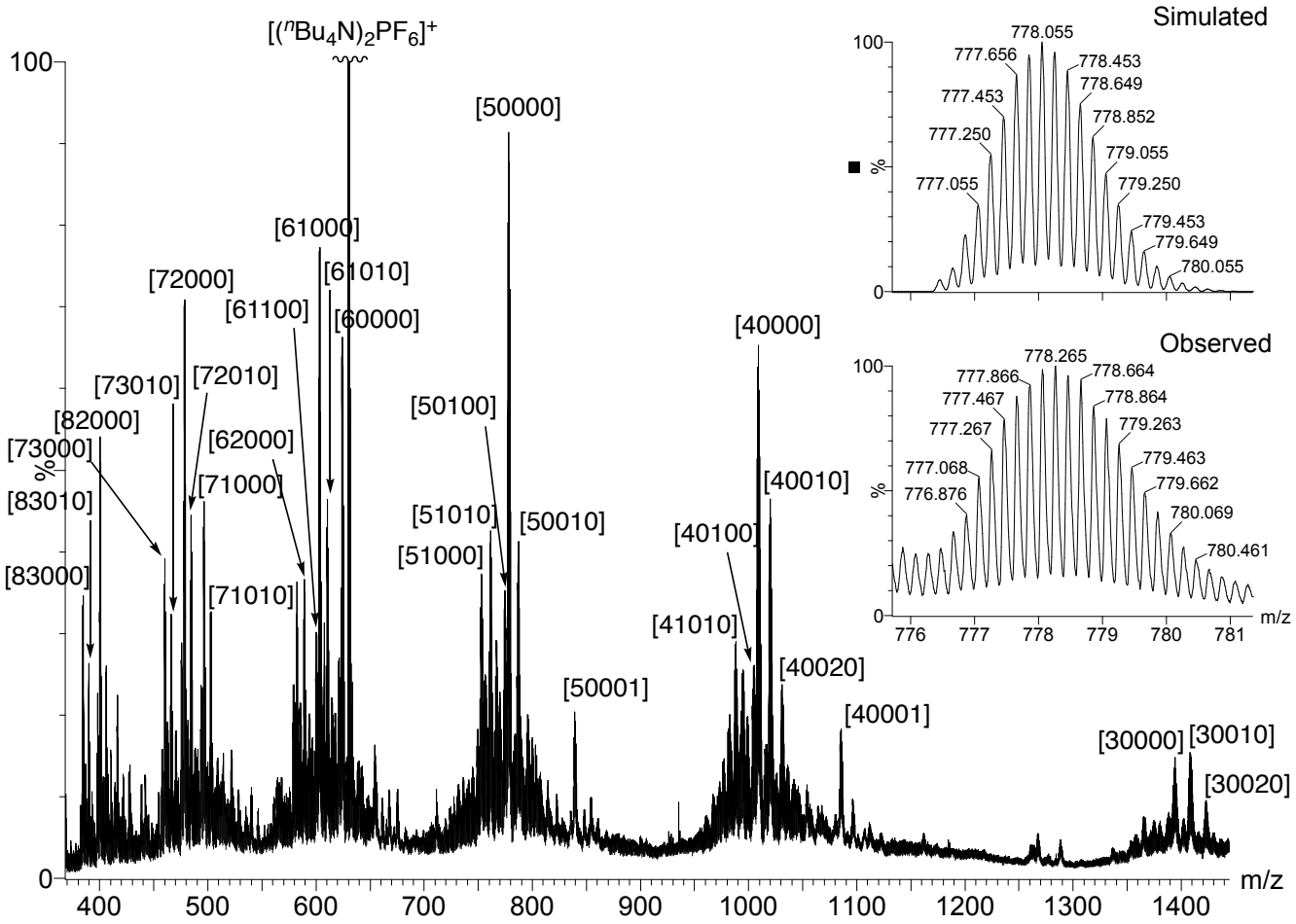

Figure 2-8-22. ESI-MS spectrum of the resultant solution containing **4-$Co^{II}Ni^{II}_3$** in the improved procedure (CD_3CN/D_2O = 20:1, positive, Capillary voltage: 3000 V, Sample cone voltage: 80 V). The right inset shows the comparison of simulated and observed isotope patterns for the signal of $[Co^{II}Ni^{II}{}_3\mathbf{L}_3(PF_6)_6]^{5+}$-$d_1$. The deuteration of the ligand was supposed to occur at the pyridinium *N*-methyl position under the reaction or measurement condition.

Miscellaneous experiments

Stability test of 4-$Co^{II}Ni^{II}_3$

A solution of **4-$Co^{II}Ni^{II}_3$** prepared in the above-mentioned improved procedure (464 μL, starting from 0.431 μmol of **L1**) was heated at 70 °C for 21 h. DMSO-d_6 (51.6 μL) was added to the solution followed by heating at 70 °C for 14 h.

Examination of a one-step strategy

To an NMR tube were added a suspension of **L1**·OTf·3H_2O in CD_3CN (100 μL, 0.500 μmol, 1 eq), D_2O (25.0 μL), a solution of $Co(OTf)_2·6H_2O$ in CD_3CN (5.00 μL, 0.167 μmol, 33.3 mM, 0.333 eq), a solution of $Ni(OTf)_2$ in CD_3CN/D_2O = 9:1 (20.0 μL, 0.500 μmol, 25.0 mM, 1.00 eq), and CD_3CN (352 μL). The reaction mixture was heated at 70 °C for 5 days.

Examination of a transmetalation strategy without redox switching

To a solution of **1-Co^{II}_4** prepared in the above-mentioned procedure was added a solution of $Ni(OTf)_2$ in CD_3CN/D_2O = 9:1 (40.0 μL, 1.00 μmol, 25.0 mM, 2.00 eq). The reaction mixture was heated at 70 °C for 6 days.

Examination of a redox-switching strategy without transmetalation

To an NMR tube were added a suspension of **L1**·OTf·3H_2O in CD_3CN (100 μL, 0.500 μmol, 1 eq), D_2O (25.0 μL), a solution of $Co(OTf)_2·6H_2O$ in CD_3CN (5.00 μL, 0.167 μmol, 33.3 mM, 0.333 eq), a solution of $Ni(OTf)_2$ in CD_3CN/D_2O = 9:1 (20.0 μL, 0.500 μmol, 25.0 mM, 1.00 eq), and CD_3CN (352 μL). The mixture was heated at 70 °C for 5 days. To this solution was added a solution of $(NH_4)_2[Ce(NO_3)_6]$ in CD_3CN (23.0 μL, 0.167 μmol, 7.26 mM, 0.333 eq). The reaction mixture was heated at 70 °C for 4 days.

Single-crystal XRD analyses

1-Co^{II}_4

A single crystal of **1-Co^{II}_4** was not obtained from the sample mentioned above. Crystals suitable for X-ray analysis was obtained as described below.

To an NMR tube were added a solution of **L1**·OTf·3H_2O in $CDCl_3$/CD_3OD/D_2O = 10:10:1 (100 μL, 0.500 μmol, 5.00 mM, 1 eq), a solution containing $Co(NO_3)_2$·6H_2O in the same mixed solvent (30.0 μL, 0.690 μmol, 23.0 mM, 1.38 eq), and the same mixed solvent (370 μL). The reaction mixture was heated at 50 °C for 2 days. The solution contained **1-Co^{II}_4** as the main product as confirmed by the ^{1}H NMR and ESI-MS measurements. To the mixture was added a solution of $La(OTf)_3$·$x$$H_2O$ in CH_3OH (10.0 μL, 0.250 μmol, 25.0 mM, 0.500 eq) to facilitate crystallization. Slow vapor diffusion of Et_2O to this solution afforded some single crystals suitable for X-ray analysis which were found in the powdery crude product.

Crystal data for $[Co_4\mathbf{L1}_3(OH_2)_6(HOCH_3)_3][La(NO_3)_6]_{0.5}(OTf)_{9.5}$: $C_{169.96}H_{113.88}Co_4La_{0.5}N_{36}O_{16.96}Zn_3$, Fw = 3433.04, violet, plate, 0.099 × 0.366 × 0.400 mm^3, trigonal, space group P-3c1 (#165), a = 21.3538(4) Å, b = 21.3538(4) Å, c = 58.2741(18) Å, α = 90°, β = 90°, γ = 120°, V = 23012.1(11) Å^3, Z = 4, ρ_{calcd} = 0.991 g·cm^{-3}, T = 93 K, λ(CuKα) = 1.54184 Å, 2θ_{max} = 136.502°, 65158/14055 reflections collected/unique (R_{int} = 0.0395), R_1 = 0.1058 ($I > 2\sigma(I)$), wR_2 = 0.3319 (for all data), GOF = 1.372, largest diff. peak and hole 1.23 /-0.54 e·Å^{-3}. CCDC deposit number 1896478.

At one of the pyridine rings, thermal parameter restraints (RIGU) were applied to facilitate anisotropic refinement. The zinc atom in the porphyrin ring was modelled as disordered over inside and outside positions. The axial CH_3OH molecule bound to the zinc center was modelled in the same occupancy as the zinc atom, although the axial ligand of the minor disorder component could not be located on a *d*-Fourier map. The NO_3^- ligand and the nearby *N*-methylpyridinium and porphyrin moieties were modelled as disordered over two positions. Due to the close positions of the disordered components, the bond lengths and angles were restrained to be similar to each other (SAME), and thermal parameter restraints (SIMU, RIGU) were applied to facilitate anisotropic refinement. Although 11 anions should be contained as shown in the chemical formula, only 0.5 $[La(NO_3)_6]^{3-}$ ion was found. The remaining anions were supposed to be so heavily disordered that they could not be located on a *d*-Fourier map. After successive trials, solvent accessible voids of 9544.7 Å^3 in total (calculated by solvent mask) were left unfilled, in which anions and solvents ($CHCl_3$, CH_3OH, H_2O, and Et_2O) were supposed to be heavily disordered. At the last stage of refinement, the reflection data modified by solvent mask were used. The solvent accessible void contained 3215 electrons per unit cell. This equates to 10.9 TfO^- (each with 74 electrons) for each molecule of **1-Co^{II}_4**, where Z = 4. This diffuse electron density exceeds well the 9.5 TfO^- anions necessary to satisfy the 11+ charge of

1-Co$^{II}_4$, leaving some room for the contribution of solvent molecules.

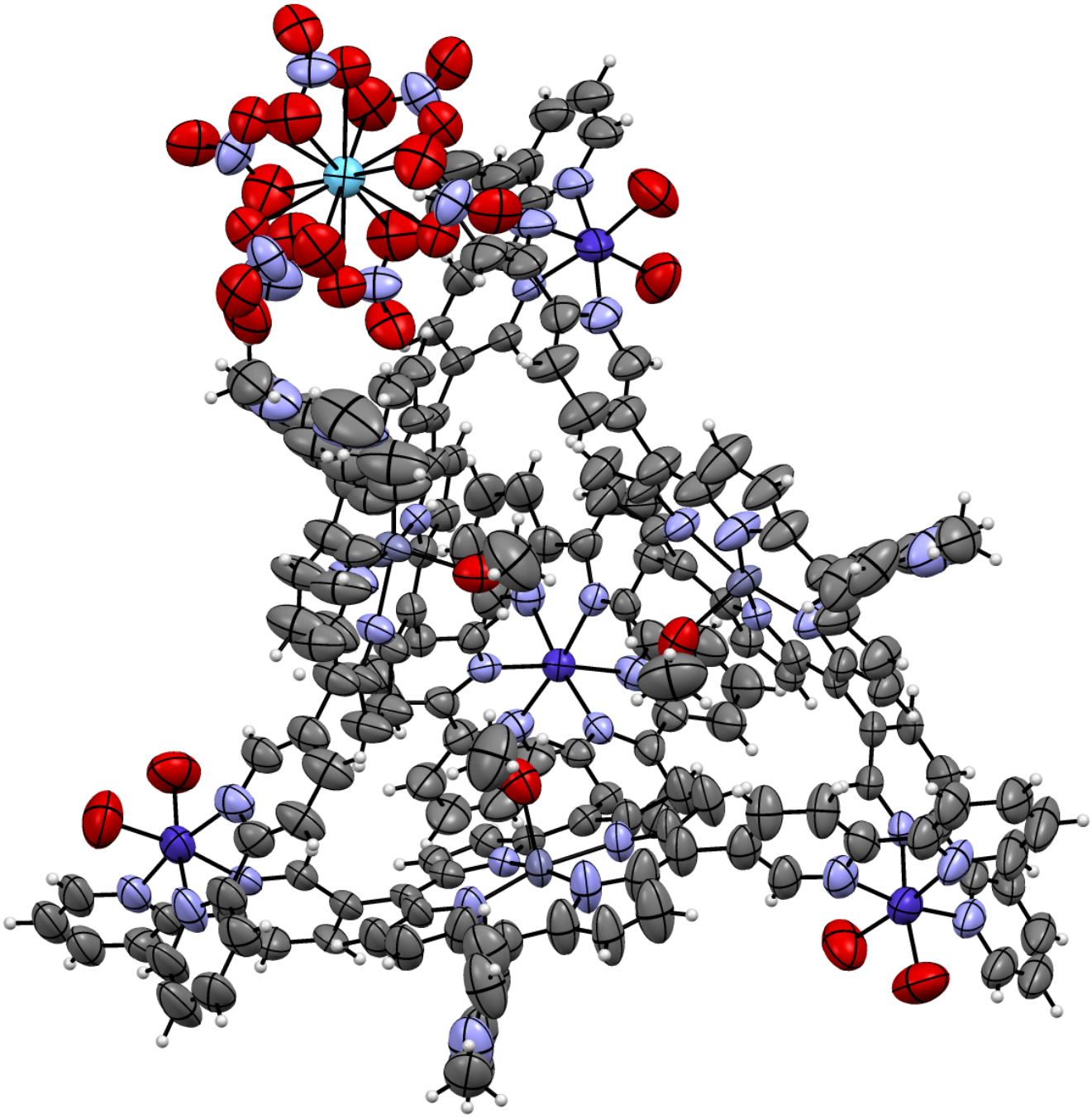

Figure 2-8-23. Crystal structure of $[Co_4\mathbf{L1}_3(OH_2)_6(HOCH_3)_3][La(NO_3)_6]_{0.5}(OTf)_{9.5}$. Thermal ellipsoids set at 50% probability. The atoms are colored based on CPK coloring. Color code; C grey, N blue, O red, Co deep blue, Zn blue-gray, La sky-blue.

2-$Co^{III}Co^{II}_3$

A single crystal of **2-$Co^{III}Co^{II}_3$** was not obtained from the sample mentioned above. Crystals suitable for X-ray analysis was obtained as described below.

To an NMR tube were added a solution of **L1**·OTf·3H_2O in $CDCl_3$/CD_3OD/D_2O = 10:10:1 (100 μL, 0.500 μmol, 5.00 mM, 1 eq), a solution of $Co(NO_3)_2$·6H_2O in the same mixed solvent (30.0 μL, 0.690 μmol, 23.0 mM, 1.38 eq), and the same mixed solvent (370 μL). The reaction mixture was heated at 50 °C for 3 days to obtain a dark green solution. To the mixture was added a solution of $(NH_4)_2[Ce(NO_3)_6]$ in CD_3OD (10.0 μL, 0.167 μmol, 25.0 mM, 0.333 eq). The mixture was kept at room temperature for 5 h. The solution was found to contain the expected complex as the main product as confirmed by the ^{1}H NMR and ESI-MS measurements. Slow vapor diffusion of Et_2O to this solution afforded some single crystals suitable for X-ray analysis which were found in the powdery crude product.

Crystal data for $[Co_4$**L1**$_3(OH_2)_6(HOCH_3)_3][Ce(NO_3)_6]_{0.5}(OTf)_{10.5}$: $C_{170.68}H_{116.03}Ce_{0.5}Co_4N_{36}O_{17.67}Zn_3$, Fw = 3455.80, violet, plate, 0.067 × 0.188 × 0.420 mm^3, trigonal, space group P-3c1 (#165), a = 21.2460(4) Å, b = 21.2460(4) Å, c = 58.2102(12) Å, α = 90°, β = 90°, γ = 120°, V = 22755.4(10) Å^3, Z = 4, ρ_{calcd} = 1.009 g·cm^{-3}, T = 93 K, λ(CuKα) = 1.54184 Å, 2θ_{max} = 136.376°, 54339/13847 reflections collected/unique (R_{int} = 0.0491), R_1 = 0.0994 ($I > 2\sigma(I)$), wR_2 = 0.3230 (for all data), GOF = 1.147, largest diff. peak and hole 0.99/-0.89 e·Å^{-3}. CCDC deposit number 1896498.

At one of the bipyridine moieties, thermal parameter restraints (RIGU) were applied to facilitate anisotropic refinement. The zinc atom in the porphyrin ring was modelled as disordered over inside and outside positions. The axial CH_3OH molecule bound to the zinc center was modelled in the same occupancy as the zinc atom, although the axial ligand of the minor disorder component could not be located on a *d*-Fourier map. The NO_3^- ligand and the nearby *N*-methylpyridinium and porphyrin moieties were modelled as disordered over two positions. Due to the close positions of the disordered components, the bond lengths and angles were restrained to be similar to each other (SADI, SAME), and thermal parameter restraints (SIMU, RIGU) were applied to facilitate anisotropic refinement. Although 12 anions should be contained as shown in the chemical formula, only 0.5 $[Ce(NO_3)_6]^{3-}$ ion was found. The remaining anions were supposed to be so heavily disordered that they could not be located on a *d*-Fourier map. After successive trials, solvent accessible voids of 9360.8 Å^3 in total (calculated by solvent mask) were left unfilled, in which anions and solvents ($CHCl_3$, CH_3OH, H_2O, and Et_2O) were supposed to be heavily disordered. At the last stage of refinement, the reflection data modified by solvent mask were used. The solvent accessible void contained 3352.4 electrons per unit cell. This equates to 11.3 TfO^- (each with 74 electrons) for each molecule of **2-$Co^{III}Co^{II}_3$**, where Z = 4. This diffuse electron density exceeds well the 10.5 TfO^- anions necessary to satisfy

the 12+ charge of **2-$Co^{III}Co^{II}_3$**, leaving some room for the contribution of solvent molecules.

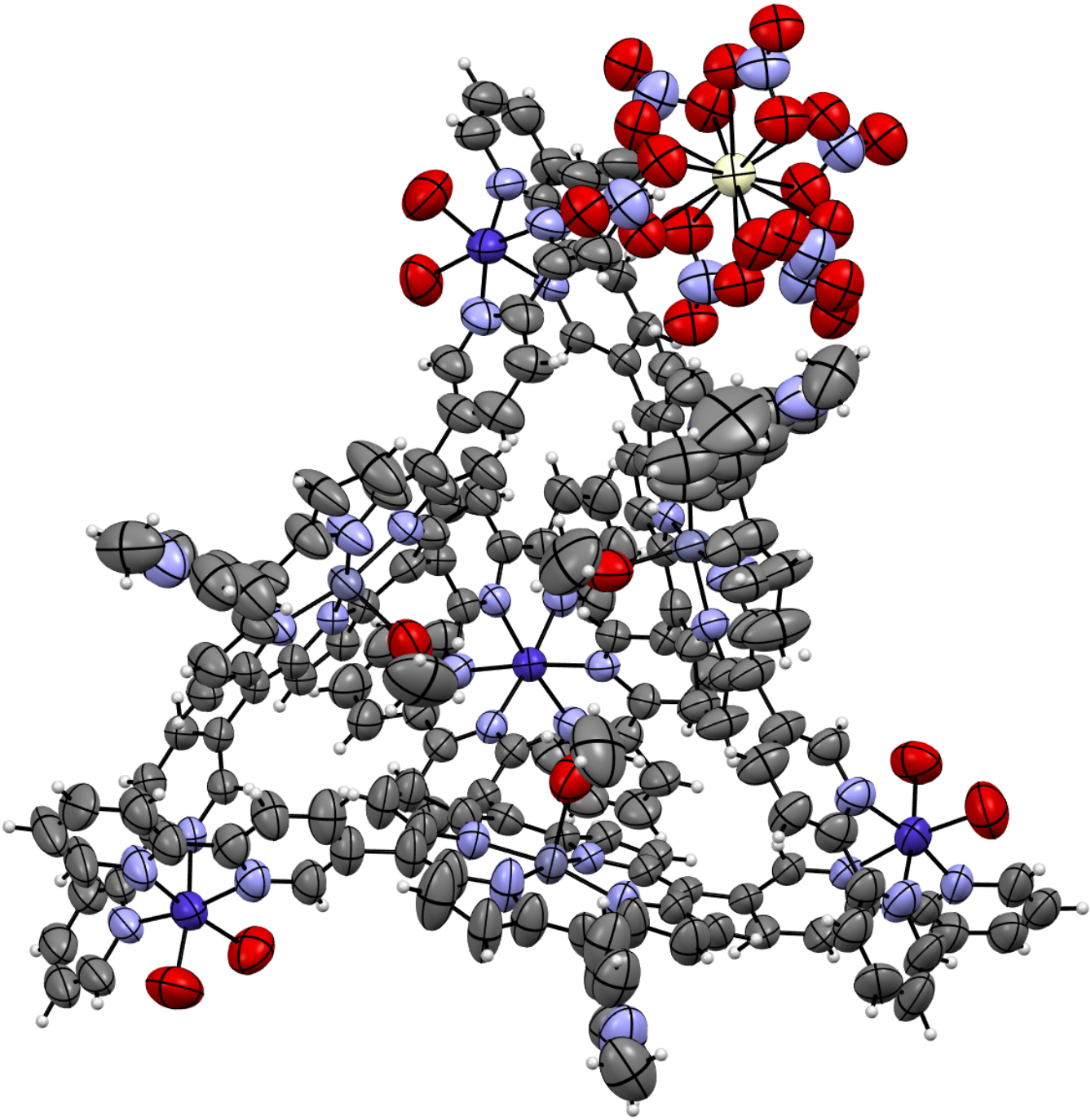

Figure 2-8-24. Crystal structure of $[Co_4\mathbf{L1}_3(OH_2)_6(HOCH_3)_3][Ce(NO_3)_6]_{0.5}(OTf)_{10.5}$. Thermal ellipsoids set at 50% probability. The atoms are colored based on CPK coloring. Color code; C grey, N blue, O red, Co deep blue, Zn blue-grey, Ce pale yellow.

3-$Co^{III}Ni^{II}_3$

A single crystal of **3-$Co^{III}Ni^{II}_3$** was not obtained from the sample mentioned above. Crystals suitable for X-ray analysis was obtained as described below.

To a glass vial was added **L1**·OTf·$3H_2O$ (23.2 mg, 20.5 μmol, 1 eq), CH_2Cl_2/CH_3OH = 5:1 (5 mL) and Bu_4N·NO_3 (65 mg, 0.21 mmol, 10 eq). The solution was filtered and washed with CH_2Cl_2/CH_3OH = 5:1. Vapor of Et_2O was slowly diffused to the combined filtrate. The solid was collected by filtration, washed with Et_2O/CH_2Cl_2 = 5:1 and then CH_2Cl_2, and dried in vacuo to give crude **L1**·NO_3 as a dark violet solid (20.8 mg).

To an NMR tube were added a solution of **L1**·NO_3 in $CDCl_3$/CD_3OD/D_2O = 10:10:1 (250 μL, 0.500 μmol, 2.00 mM, 1 eq), a solution of $Co(NO_3)_2$·$6H_2O$ in the same mixed solvent (18.9 μL, 0.667 μmol, 35.3 mM, 1.33 eq) and the same mixed solvent (231 μL). The mixture was heated at 50 °C for 27 h to obtain a dark green solution. To the mixture were added a solution of $(NH_4)_2Ce(NO_3)_6$ solution in the same mixed solvent (10.0 μL, 0.167 μmol, 16.7 mM, 0.333 eq) and a solution of $Ni(OTf)_2$ in CD_3OD/D_2O = 1:1 (10.0 μL, 0.500 μmol, 50.0 mM, 1.00 eq). The reaction mixture was heated at 50 °C for 3 days. To the solution was added one more aliquot of the same $Ni(OTf)_2$ solution (10.0 μL, 0.500 μmol, 1.00 eq). The reaction mixture was heated at 50 °C for 2 days. The solution contained **3-$Co^{II}Ni^{II}_3$** as the main product as confirmed by ^{1}H NMR spectroscopy and ESI-MS. To the aliquot of the solution (432 μL) was added DMSO-d_6 (100 μL). Slow vapor diffusion of Et_2O to this solution afforded some single crystals suitable for X-ray analysis which were found in the powdery crude product.

Crystal data for $[CoNi_3\mathbf{L1}_3Cl_3(dmso)_6](OTf)_9$·DMSO: $C_{179.77}H_{140.32}Cl_3CoF_3N_{33}Ni_3O_{9.7}S_{6.39}Zn_3$, Fw = 3717.33, violet, plate, 0.1 × 0.1 × 0.02 mm^3, trigonal, space group R-3 (#148), a = 21.5526(5) Å, b = 21.5526(5) Å, c = 83.834(3) Å, α = 90°, β = 90°, γ = 120°, V = 33725(2) Å^3, Z = 6, ρ_{calcd} = 1.098 g·cm^{-3}, T = 93 K, λ(MoKα) = 0.71073 Å , $2\theta_{max}$ = 57.67°, 46042/16339 reflections collected/unique (R_{int} = 0.0485), R_1 = 0.0595 ($I > 2\sigma(I)$), wR_2 = 0.1797 (for all data), GOF = 1.051, largest diff. peak and hole 0.80/-0.71 e·Å^{-3}. CCDC deposit number 1898214.

As Co and Ni atoms have similar electron densities, assignment of these atoms was conducted by consideration of the M–N bond distances as discussed in the main text.

At the methyl group of the *N*-methylpyridinium moiety, thermal parameter restraints (RIGU) were applied to facilitate anisotropic refinement. The zinc atom in the porphyrin ring was modelled as disordered over inside and outside positions. Due to the close positions and the highly biased occupancy of the disordered atoms, the bond lengths and angles were restrained to be similar to typical values (DFIX, DANG), and a thermal parameter constraint (EADP) was applied to facilitate anisotropic refinement. The axial

DMSO bound to the zinc center was modelled in the same occupancy as the zinc atom with disorder over two positions. Due to the close positions of the disordered components, thermal parameter restraints (SIMU, RIGU) were applied to facilitate anisotropic refinement. The axial ligand of the minor disorder component of zinc could not be located on a *d*-Fourier map. One of the ligands coordinating to the nickel center was modelled as disordered over H_2O and DMSO molecules. Due to the diffuse electron densities of the disordered components, the bond lengths and angles were restrained to be symmetric (SAME), and thermal parameter restraints (RIGU) were applied to facilitate anisotropic refinement. The DMSO molecule located inside the complex was modelled as disordered around the 3-fold axis. Due to the severe overlapping of electron density around the 3-fold axis, the bond lengths were restrained to be similar to typical values (DFIX) and the molecular geometry to be symmetric (SAME), and thermal parameter restraints (SIMU, RIGU) were applied to facilitate refinement. Although 9 anions should be contained as shown in the chemical formula, only one TfO^- ion was found. For this ion, thermal parameter restraints (RIGU) were applied to facilitate anisotropic refinement. The remaining anions were supposed to be so heavily disordered that they could not be located on a *d*-Fourier map. After successive trials, solvent accessible voids of 11136 $Å^3$ in total (calculated by SQUEEZE) were left unfilled, in which anions and solvents ($CHCl_3$, CH_3OH, H_2O, DMSO, and Et_2O) were supposed to be heavily disordered. At the last stage of refinement, the reflection data modified by SQUEEZE were used. The solvent accessible void contained 4196 electrons per unit cell. This equates to 9.45 TfO^- (each with 74 electrons) for each molecule of **3-$Co^{III}Ni^{II}_3$**, where $Z = 6$. This diffuse electron density exceeds well the 8 TfO^- anions necessary to satisfy the 12+ charge of **3-$Co^{III}Ni^{II}_3$**, leaving some room for the contribution of solvent molecules.

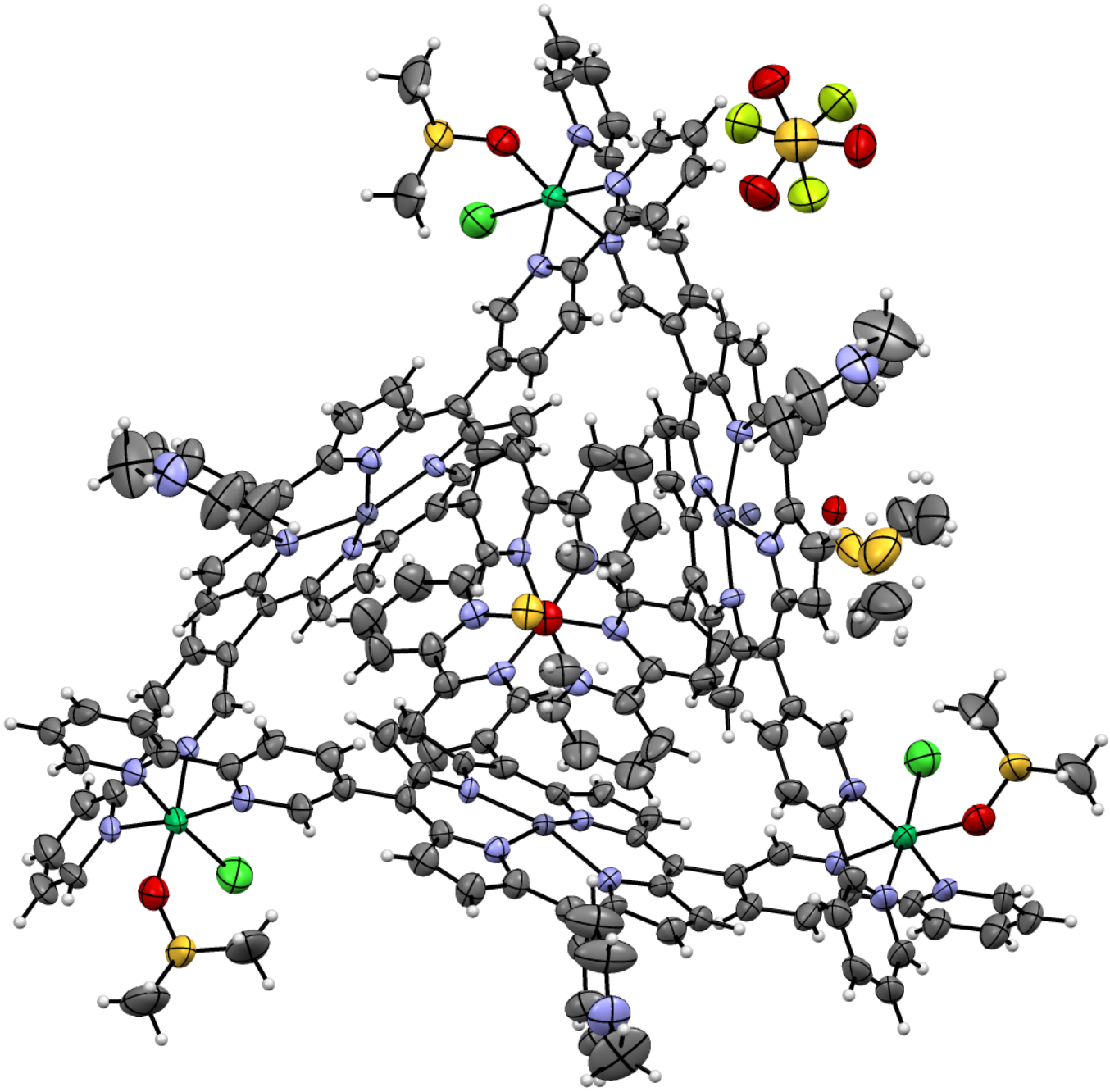

Figure 2-8-25. Crystal structure of $[CoNi_3\mathbf{L1}_3Cl_3(dmso)_6](OTf)_9 \cdot DMSO$. Thermal ellipsoids set at 50% probability. The atoms are colored based on CPK coloring. Color code; C grey, N blue, O red, F yellow-green, S yellow, Cl green, Co deep blue, Ni blue-green, Zn blue-grey.

2-9. References

1. Balzani, V.; Juris, A.; Venturi, M. *Chem. Rev.* **1996**, *96*, 759–833.

2. Iki, N. *Supramol. Chem.* **2011**, *23*, 160–168.

3. Ostrowska, M.; Fritsky, I. O.; Gumienna-Kontecka, E.; Paclishchuk, A. V. *Coord. Chem. Rev.* **2016**, *327–328*, 304–322.

4. Huang, Y.-G.; Jiang, F.-L.; Hong, M.-C. *Coord. Chem. Rev.* **2008**, *253*, 2814–2834.

5. Aboshyan-Sorgho, L.; Besnard, C.; Pattison, P.; Kittilstved, K. R.; Aebischer, A.; Bunzli, J. C.; Hauser, A.; Piguet, C. *Angew. Chem. Int. Ed.* **2011**, *50*, 4108–4112.

uang, Y.-G.; Jiang, F.-L.; Hong, M.-C. *Coord. Chem. Rev.* **2008**, *253*, 281

4–2834.

7. Aboshyan-Sorgho, L.; Besnard, C.; Pattison, P.; Kittilstved, K. R.; Aebischer, A.; Bunzli, J. C.; Hau

ser, A.; Piguet, C. *Angew. Chem. Int. Ed.* **2011**, *50*, 4108–4112.

1732.

9. Buchwalter, P.; Jacky, R.; Braunstein, P. *Chem. Rev.* **2015**, *115*, 28–126.

10. Sasai, H.; Suzuki, T.; Itoh, N.; Tanaka, K.; Date, T.; Okamura, K.; Shibasaki, M. *J. Am. Chem. Soc.* **1993**, *115*, 10372–10373.

11. Que, L., Jr.; Tolman, W. B. (eds.) *Comprehensive Coordination Chemistry II, Vol. 8* (Elsevier, Amsterdam, 2003).

12. Strange, R. W.; Antonyuk, S. V.; Hough, M. A.; Doucette, P. A.; Valentine, J. S.; Hasnain, S. S. *J. Mol. Biol.* **2006**, *356*, 1152–1162.

13. Zhang, Y.-Y.; Gao, W.-X.; Lin, L.; Jin, G.-X. *Coord. Chem. Rev.* **2016**, *344*, 323–344.

14. Li, H.; Yao, Z.-J.; Liu D.; Jin, G.-X. *Coord. Chem. Rev.* **2015**, *293–294*, 139–157.

15. Sun, X.; Johnson, D. W.; Caulder, D. L.; Powers, R. E.; Raymond, K. N.; Wong, E. H. *Angew. Chem. Int. Ed.* **1999**, *38*, 1303–1307.

16. Piguet, C.; Bernardinelli, G.; Williams, A. F.; Bocquet, B. *Angew. Chem. Int. Ed. Engl.* **1995**, *34*, 582–584.

17. Hiraoka, S.; Tanaka, T.; Shionoya, M. *J. Am. Chem. Soc.* **2006**, *128*, 13038–13039.

18. Kumar, G.; Gupta, R. *Chem. Soc. Rev.* **2013**, *42*, 9403–9453.

19. Li, L.; Fanna, D. J.; Shepherd, N. D.; Lindoy, L. F.; Li, F. *Journal of Inclusion Phenomena and Macrocyclic Chemistry* **2015**, *82*, 3–12.

20. Lintvedt, R. L.; Ahmad, N. *Inorg. Chem.* **1982**, *21*, 2356–2359.

21. Davies, G.; El-Sayed, M. A.; El-Toukhy, A. *Chem. Soc. Rev.* **1992**, *21*, 101–104.

22. Carnes, M. E.; Collins, M. S.; Johnson, D. W. *Chem. Soc. Rev.* **2014**, *43*, 1825–1834.

23. Cai, G. Z.; Davies, G.; El-Sayed, M. A.; El-Toukhy, A.; Gilbert, T. R.; Onan, K. D. *Inorg. Chem.* **1986**, *25*, 1935–1940.

24. Mensinger, Z. L.; Zakharov, L. N.; Johnson, D. W. *Acta Cryst.* **2008**, *E64*, i8–i9.

25. Simler, T.; Braunstein, P.; Danopoulos, A. A. *Angew. Chem. Int. Ed.* **2015**, *54*, 13691–13695.

26. Ai, P.; Monakhov, K. Y.; van Leusen, J.; Kögerler, P.; Gourlaouen, C.; Tromp, M.; Welter, R.; Danopoulos, A. A.; Braunstein, P. *Chem. Eur. J.* **2018**, *24*, 8787–8796.

27. Kamunde-Devonish, M. K.; Jackson, Jr., M. N.; Mensinger, Z. L.; Zakharov, L. N.; Johnson, D. W. *Inorg. Chem.* **2014**, *53*, 7101–7105.

28. Givaja, G.; Castillo, O.; Mateo, E.; Gallego, A.; Gómez-García, C. J.; Calzolari, A.; di Felice, R.; Zamora F. *Chem. Eur. J.* **2012**, *18*, 15476–15484.

29. Pittala, S.; Kittilstved, K. R. Cation Exchange in Small ZnS and CdS Molecular Analogues. *Inorg. Chem.* **2015**, *54*, 5757–5767.

30. Echegoyen, L.; Perez-Cordero, E. *Redox Chemistry of Metal Ion Complexes: Preparation of New Materials.* In: *Transition Metals in Supramolecular Chemistry* (Springer, Dordrecht, 1994).

31. Burke, M. J.; Nichol, G. S.; Lusby, P. J. *J. Am. Chem. Soc.* **2016**, *138*, 9308–9315.

32. 遠藤健一, 平成 28 年度修士論文「非対称ポルフィリン配位子と亜鉛イオンに基づく超分子金属錯体コンテナの他刺激応答キラル／アキラル相互変換」(東京大学 大学院理学系研究科 化学専攻 生物無機化学研究室, 2017).

33. Brisig, B.; Constable, E. C.; Housecroft, C. E. *New J. Chem.* **2007**, *31*, 1437–1447.

34. Huang, T. L. J.; Brewer, D. G. *Can. J. Chem.* **1981**, *59*, 1689–1700.

35. Hall, B. R.; Manck, L. E.; Tidmarsh, I. S.; Stephenson, A.; Taylor, B. F.; Blaikie, E. J.; Vander Griend, D. A.; Ward, M. D. *Dalton Trans* **2011**, *40*, 12132–12145.

36. Turega, S.; Whitehead, M.; Hall, B. R.; Haddow, M. F.; Hunter, C. A.; Ward, M. D. *Chem. Commun.* **2012**, *48*, 2752–2754.

37. Riddell, I. A.; Smulders, M. M.; Clegg, J. K.; Hristova, Y. R.; Breiner, B.; Thoburn, J. D.; Nitschke, J. R. *Nat. Chem.* **2012**, *4*, 751–756.

38. Haynes, W. M. *CRC Handbook of Chemistry and Physics, 94th Edition* (CRC Press, Boca Raton, 2013).

39. Sasaki, Y., Kato, H., Kudo, A. *J. Am. Chem. Soc.* **2013**, *135*, 5441–5449.

40. Groom, C. R.; Bruno, I. J.; Lightfoot M. P.; Ward, S. C. *Acta Cryst.* **2016**, *B72*, 171–179.

41. Smith, R. M.; Martell, A. E. *Critical Stability Constants* (Plenum Press, New York, 1976).

42. Nakamura, T.; Kaneko, Y.; Nishibori, E.; Nabeshima, T. *Nat. Commun.* **2017**, *8*, 129.

43. Dolomanov, O. V.; Bourhis, L. J.; Gildea, R. J.; Howard, J. A. K.; Puschmann, H. *J. Appl. Cryst.* **2009**, *42*, 339–341.

44. Sheldrick, G. M. *Acta Cryst. C* **2015**, *71*, 3–8.

45. Nakamura, T.; Ube, H.; Shiro, M.; Shionoya, M. *Angew. Chem. Int. Ed.* **2013**, *52*, 720–723.

46. Gianelli, L.; Amendola, V.; Fabbrizzi, L.; Pallavicini, P.; Mellerio, G. G. *Rapid Commun. Mass. Spectrom.* **2001**, *15*, 2347–2353.

3. Tetrahedral chiral-at-metal Zn^{II} complex

本章については、5 年以内に雑誌等で刊行予定のため、非公開。

4. Conclusions

4-1. Conclusions

Kinetically controlled stepwise synthesis is a useful method for preparation of metal complexes with intricate structures. However, its applicable scope has been limited chiefly to the inert metal complexes. In this thesis, I presented two new strategies to expand the target scope of kinetically controlled stepwise synthesis toward the labile metal complexes. These strategies belong to two distinct fields: a heterometallic complex and a chiral-at-metal complex (Figure 4-1-1).

Heterometallic complexes show interesting properties based on interactions between different metal ions. However, it is difficult to selectively synthesize a heterometallic complex which contains analogous metal ions in desired numbers and positions. In Chapter 2, I proposed "site-selective redox switching and transmetalation" as a new stepwise method to selectively arrange different metals. This method consists of four steps: homometallic complexation, site-selective oxidation, site-selective transmetalation, and reduction. Using this method, selective synthesis of a Co^{II}–Ni^{II} heterometallic complex was achieved, which is normally difficult because of the lability and similarity of Co^{II} and Ni^{II} complexes. This result gives wider access to novel heterometallic complexes, which can exhibit functions specific to the combination of metals.

Chiral-at-metal complexes are useful as enantioselective catalysts or chiroptical materials because of coupling of their chirality and metal-based functions. However, tetrahedral chiral-at-metal complexes without chiral ligands are difficult to synthesize enantioselectively because of their fast stereoinversion. In Chapter 3, I proposed an unsymmetrical tridentate ligand with strong and non-planar coordination ability as a ligand design to kinetically stabilize a metal complex against stereoinversion. Using this ligand in combination with an acidic chiral auxiliary ligand, enantioselective synthesis of a tetrahedral chiral-at-Zn^{II} complex was achieved, which is normally difficult because of the lability of Zn^{II} complexes and tetrahedral complexes. In addition, the utility of the resultant complex was demonstrated in enantioselective catalysis. These results revealed the overlooked utility of the tetrahedral chiral-at-metal complexes composed of achiral ligands.

The expanded scope of kinetically controlled stepwise synthesis will be useful in preparation of metal complexes with new structures, which can be suitable for a particular purpose such as catalysis or material applications.

Chapter 2.
Heterometallic complex

New strategy:

Site-selective redox switching and transmetalation

Stepwise selective synthesis

Co^{II}–Ni^{II} complex

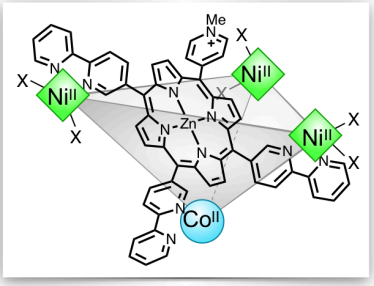

Chapter 3.
Chiral-at-metal complex

New strategy:

Strong and non-planar coordination

Kinetic stability

Tetrahedral chiral-at-Zn^{II} complex

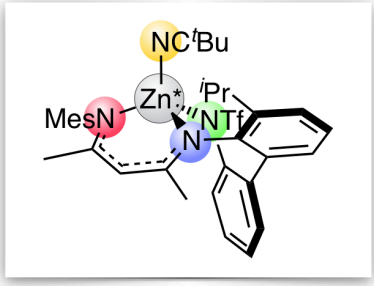

Figure 4-1-1. Summary of Chapters 2 and 3.

List of publications

[Publication related to the thesis]

1. Hitoshi Ube, Kenichi Endo, Hiroyasu Sato, Mitsuhiko Shionoya, "Synthesis of Hetero-multinuclear Metal Complexes by Site-Selective Redox Switching and Transmetalation on a Homo-multinuclear Complex" *J. Am. Chem. Soc.* **2019**, *141*, 10384–10389.

[Publication not related to the thesis]

2. Kenichi Endo, Hitoshi Ube, Mitsuhiko Shionoya, "Multi-Stimuli-Responsive Interconversion between Bowl- and Capsule-Shaped Self-Assembled Zinc(II) Complexes" *J. Am. Chem. Soc.* **2020**, *142*, 407–416.

Acknowledgments

This research was conducted under the supervision of Professor Dr. Mitsuhiko Shionoya (The University of Tokyo) and Assistant Professor Dr. Hitoshi Ube (The University of Tokyo). The single-crystal XRD analysis in Chapter 2 was conducted in collaboration with Dr. Hiroyasu Sato (Rigaku Cooperation). The experiments in Chapter 3 was conducted in collaboration with Mr. Yuanfei Liu (master student) and Project Assistant Professor Dr. Koichi Nagata (The University of Tokyo). I sincerely appreciate their assistance on this research.

Professor Dr. Mitsuhiko Shionoya enthusiastically motivated me with scientific curiosity throughout my PhD course and gave me many fruitful suggestions and corrections on the research. The research target in Chapter 3 originated from his idea of "tetrahedral chiral-at-metal complex." I would like to express my profound gratitude here.

Assistant Professor Dr. Hitoshi Ube advised me so many times in a daily level both on research and on life in this group. The unsymmetrical ligand **L1** used in Chapter 2 was a derivative of a prototype ligand born in a discussion with him. I am deeply grateful to him.

Project Assistant Professor Dr. Koichi Nagata taught me numerous ideas and experimental techniques, especially air-free techniques necessary for Chapter 3. Meanwhile, his devotion to research motivated me a lot. I am deeply grateful to him.

Mr. Yuanfei Liu helped me on the research topic in Chapter 3. His diligence strongly promoted this research. I also learned as many things by teaching him as he learned. I am very thankful to him.

Associate Professor Dr. Shohei Tashiro and Assistant Professor Dr. Yusuke Takezawa suggested me useful advice and maintained the laboratory apparatus. I appreciate their cooperation.

The colleagues in Shionoya Group helped me with daily troubles and cooperatively build up the joyful research environments. I was happy to work as a colleague. Thank everyone!

Professor Dr. Eric Meggers and the colleagues in Philipps-Universität Marburg, Germany kindly accepted my short research internship and gave me a unique opportunity to touch with their research, which was closely related to the topic in Chapter 3. I appreciate them very much.

Advanced Leading Graduate Course for Photon Science (ALPS) program, JSPS Research Fellowship for Young Scientists DC1, and Graduate Research Abroad in Science Program (GRASP) offered me financial supports. I appreciate these programs.

Finally, I would like to show my gratitude to my wife, who supported my daily life and also sometimes even this research.